TÉCNICO LISBOA

Tracing the hydrochemical water types and salinization mechanisms in the great Maputo area as a function of groundwater recharge, hydrogeological properties and human activities

Guilherme Emídio Horta Nogueira

Thesis to obtain the Master of Science Degree in

Environmental Engineering

Supervisors: Doutor Tibor Stigter
Doutora Maria Teresa Condesso de Melo

Examination Committee

Chairperson: Prof. Doutor Luís Filipe Tavares Ribeiro
Supervisor: Doutora Maria Teresa Condesso de Melo
Members of the Committee: Doutor Jasper Griffioen

September 2017

Tracing the hydrochemical water types and salinization mechanisms in the great Maputo area as a function of groundwater recharge, hydrogeological properties and human activities

Master of Science Thesis

by

Guilherme Emídio Horta Nogueira

Supervisors

Doutor Tibor Stigter

Doutora Maria Teresa Condesso de Melo

Examination committee

Prof. Doutor Luís Filipe Tavares Ribeiro

Doutora Maria Teresa Condesso de Melo

Doutor Jasper Griffioen

This thesis is submitted in partial fulfilment of the requirements for the academic degree of

Master of Science in Water Science and Engineering
IHE-Delft, Institute for Water Education, Delft, the Netherlands

Master of Science in Environmental Engineering
Instituto Superior Técnico, Universidade de Lisboa, Portugal

Master of Science in Hydro Science and Engineering
Technische Universität Dresden, Germany

MSc research host institution

IHE-DELFT

September 2017

Acknowledgements

First, I would like to direct my thankfulness and love for my family, Dad, Mom, and Tha. You define for me what life about, what happiness means is, and what love is. Without your support and presence I wouldn't be able to get so far and learn so much. You are part of this. Thank you very much.

I would like to express my sincere gratitude to my mentor Dr. Tibor Stigter for his countless moments of help and brilliant guidance. Your private classes during our meetings, key-points during the discussions and recommendations during the talks and emails were more than helpful. Thank you very much.

I also extend my sincere gratitude to my mentor Dr Diniz Juízo for his support and guidance, especially during the field campaign, and at distance through numerous emails. Your knowledge of the area and insights were fundamental for the advance of the research.
Thank you very much.

I would like to thank Eng. Fátima Mussa for especial help during my initial data collection and during fieldwork. I also thank all the other staff and members from UEM and from ARA-Sul, who were master pieces for the development of the fieldwork in Maputo.

In addition, I thank to Dr. Jochen Wenninger for the great support during isotope analyses and interpretation, making himself available many times for discussion as well. I also thank to all laboratory staff from IHE-Delft, who were crucial during analyses of my samples, and Prof Michael McClain for his smart questions and recommendations.

Last, but not least, I want to express my gratefulness for the new friends I made during the last years of my studies, each one from a different corner of the world, each one representing a whole different world. Thank you for all shared experiences and (very) good times. Especial thanks to my GroundwatCH family, which together with me fought solid battles during hard learning times, but also made the path more pleasant and full of lovely memories.

Resumo

Salinidades elevadas, escassez de recursos de água superficiais, rede pública de disrtribuição ineficaz e o crescimento populacional colocam uma pressão constante nos recursos de água subterrânea de Maputo. Uma metodologia utilizando sistemas de informação geográfica (SIGs) permitiu classificar diferentes zonas de recarga potencial, com base na análise das propriedades hidrogeológicas e do uso/ cobertura do solo. A taxa de recarga foi calculada pelo método do balanço hídrico na zona da raiz das plantas e mostrou que cerca de 30% da precipitação se destina a recarga das águas subterrâneas. As maiores taxas de recarga ocorrem nos sedimentos eólicos cobertos por arbustos; menores taxas ocorrem nas áreas agrícolas, devido principalmente à elevada evapotranspiração. A análise de dados hidroquímicos e isotópicos permitiu a classificação de seis grupos de águas desde doces a salobras/ salgadas. A análise de dados de isótopos estáveis $\delta^{2}H$ e $\delta^{18}O$ em conjunto com razões iónicas de Na/Cl e SO_4/Cl sugere que os processos de evaporação e mistura com a água do mar são os mais determinantes para a salinidade da área de estudo, seguidos pelas interações água-rocha. A razão $\delta^{18}O$/Cl das águas salobras/ salgadas subterrâneas e superficiais (~ -4,0 ‰ e ~ -0,5 ‰, respectivamente) sugerem que: 1) as águas subterrâneas salobres/ salinas resultam da mistura entre águas doces e água do mar, alojada desde o último período de transgressão marinha e permanecendo como lentículas nos níveis aquitardos; 2) águas superficiais salobras/ salgadas resultam da descarga de águas subterrâneas salobras/ salgadas sob evaporação, portanto aumentando a salinidade e $\delta^{18}O$. A origem marinha da salinidade, ao contrário da dissolução de halite, é corroborada por razões de Br/Cl de amostras de água salobra/ salgada ligeiramente abaixo da proporção da água do mar ($1,2x10^{-3}$ ~ $1,4x10^{-3}$).

Palavras chave: hidrogeoquímica, recarga subterrânea, salinização, SIG, Moçambique

Abstract

High salinities, scarce surface water, poor public network supply and increasing population growth place constant pressure on Maputo groundwater resources. A GIS approach was used to classify different recharge potentials zones, based on hydrogeological properties and land use/cover, while calculated recharge rate through a root zone water balance method showed that 30% of precipitation goes to groundwater recharge. Higher recharge occur within aeolian sediments covered by shrubland; lower rates occur in agricultural areas, largely due to high evapotranspiration. Hydrochemical and isotopic data analysis allowed clustering of six water groups, from fresh to brackish/salt waters. Analysis of stable isotopes $\delta^{2}H$ and $\delta^{18}O$ together with Na/Cl and SO_4/Cl ratios suggest that evaporation and mixing with seawater are major processes determining salinity in the area, followed by water-rock interactions. $\delta^{18}O$/Cl of brackish/salt groundwater and surface waters (~ -4.0‰, ~ -0.5‰, respectively) suggest that: 1) inland brackish/salt groundwaters result from mixing between fresh waters and entrapped seawater, emplaced during last transgression period and remaining as lenses within aquitard units; and 2) surface brackish/salt waters result of brackish/salt groundwater seepage undergoing evaporation, hence increasing salinity and $\delta^{18}O$ values. Seawater salinity origin, rather than halite dissolution is corroborated by Br/Cl ratios of brackish/salt water samples ($1.2x10^{-3}$ ~ $1.4x10^{-3}$) slightly below ocean ratio.

Keywords: hydrogeochemistry, groundwater recharge, salinization, GIS, Mozambique

Table of contents

List of Figures

List of Tables

List of Equations

Equation 2.1: $\delta D = 8\delta^{18}O + 10$

Equation 2.2: $z_s = \frac{\rho_f}{\rho_s - \rho_f} z_f$ or $z_s = 40\, z_f$

Equation 2.3: $2Na^+ + Ca\text{-}X \leftrightarrow 2Na\text{-}X + Ca^{2+}$

Equation 2.4: $m_{i,mix} = f_{sea} \,.\, m_{i,sea} + (1 - f_{sea}).\, m_{i,fresh}$

Equation 2.5: $m_{i,react} = m_{i,sample} - m_{i,mix}$

Equation 2.6: $f_{sea} = \frac{m_{Cl,sample} - m_{Cl,fresh}}{m_{Cl,sea} - m_{Cl,fresh}}$ or $f_{sea} = m_{Cl,sample}/566$

Equation 3.1: Qperc = (P - E - R) + Qcap – Sroot

Equation 3.2: $\delta = \frac{R_{sample} - R_{standard}}{R_{standard}} x1000$

Equation 3.3: $\text{Ion balance error } (\%) = (\sum \text{cations} - \sum \text{anions})/(\sum \text{cations} + \sum \text{anions})$

Equation 3.4: $SI = \log({}^{IAP}/_{K_{sp}})$

Equation 3.5: $\text{PI} = \ln \frac{\ln\left\{10 * \left[{}^{NO_3}/_{62} + SO_4^c\right]\right\}}{\ln 2}$, if $\{\ldots\} < 0$, PI=0;

where $SO_4^c = 0.67 * \left(\frac{SO_4}{96} - \frac{0.0232 * Cl}{35.453}\right)$, if $\text{SO}_4^{\text{c}} < 0$, then $\text{SO}_4^{\text{c}} = 0$

Equation 5.1: $RP = (L_w L_r + LU_w LU_r + DF_w DF_r + S_w S_r) * L$

Equation 5.2: $CO_2\,(g) + H_2O \rightarrow H^+ + HCO_3^-$

Equation 5.3: $2NaAlSi_3O_8 + 2H_2CO_3 + 9H_2O \rightarrow Al_2Si_2O_5(OH) + 2Na^+ + 2HCO_3^- + 4H_4SiO_4$

Equation 5.4: $CaCO_3\,(s) + H_2CO_3 \rightarrow Ca^{2+} + 2HCO_3^-$

Equation 5.5: $CaMg(CO_3)_2$ (Dolomite) $+ H_2CO_3 \rightarrow Ca^{2+} + Mg^{2+}\, 4HCO_3^-$

Equation 5.6: $q = \frac{Cl_{rain}}{Cl_{GW}}$

Introduction

1.1. Background

Groundwater is recognized as one of the most important sources of fresh water for human supply and socio-economic development. Especially in developing countries, groundwater is often chosen because it demands less treatment and has a better bacteriological quality (Appelo and Postma, 2005). In coastal areas the pressure on groundwater resources is particularly big due to an ongoing trend of increasing population, attracted by the abundant natural resources and their ease of access, or simply because people want to be closer to the seaside (Ferguson and Gleeson, 2012; Lee et al., 2016; Neumann et al., 2015). Since these areas are an economic and social focal point in most countries, the increasing human activities and high vulnerability to seawater intrusion makes coastal aquifers more exposed to over-abstraction and contamination. Moreover, local climate variations and water-rock interactions can also lead to a non-desired groundwater quality, like high salinities. The causes for high salinities in groundwater vary from place to place and require a good local monitoring network and supplementary studies to ensure which factors contribute and control local water chemistry (Hiscock and Bense, 2014; Nonner, 2015; Werner et al., 2013).

Maputo Province in the south of Mozambique is a deltaic area comprising the most populated portion and the biggest cities of the country, Figure 1.1. This study covers great part of Maputo Province, as the cities of Maputo and Matola, as well as the cities of Manhiça and Xinavane on the north. The city and the metropolitan area of Maputo together have a population of approximately 1.8 million (Census 2007) and growth rates of around 7% per year (Mozambique, 2005). The region has experienced a rapid and unplanned growth, which led to a lack of basic structures and municipal/public services for the population. Sanitation system and access to channelled water and electricity are very limited in the peri-urban areas, while the official service networks still mostly restricted within urbanized areas (FIPAG, 2012; Matsinhe et al., 2008). The rapid increase in population requires water supply from surface water sources to be complemented with groundwater. Thus, the coastal aquifer is under intense pressure from water consuming activities and uncontrolled groundwater pumping may lead to salinization (ARA-Sul, 2011).

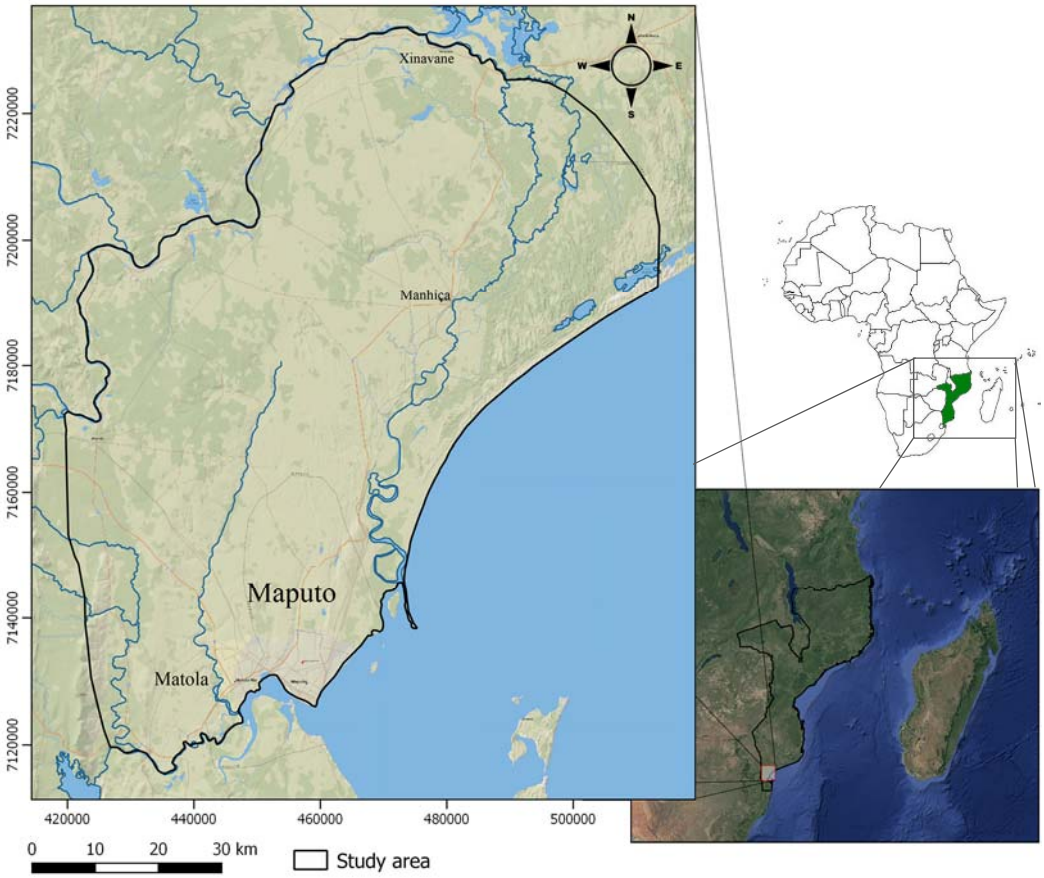

Figure 2-1: Location of the study area in the regional context with the main cities.

Local high salinity values and presence of brackish to saline groundwater limit the exploitation potential of the local aquifer system, while the possible involved salinization mechanisms requests further study to be comprehended (ARA-Sul, 2011; Chairuca, 1997; DNA, 1988; Juizo, 1995; Mozambique, 2005; Muiuane, 2007). Groundwater is managed by the local water agency ARA-Sul, which has the task to monitor and regulate the use of the resource in the area. In 2005 more than 240 groundwater based small pipes systems were found as private Small-Scale Service Provision (SSIPs) especially in the peri-urban area, representing about 30% of the households in the area. (Matsinhe et al., 2008). Small pipe systems from SSIPs refers to households connected to a small private water distribution system, provided by a regulated well owner. Between 2008 and 2014 the number of boreholes for domestic water supply in Maputo increased from approximately 1300 to 2500 (Rosário Dias, 2016).

1.2. Problem statement

Even though with locally high salinity, the aquifer is being largely exploited for water supply due to lack of surface water and poor public water supply network, and uncontrolled exploitation can induce salinization owing to seawater intrusion. However, other mechanisms can explain high salinity in groundwater, as water-rock

interactions, presence of old connate waters and/or high evaporation rates (Appelo and Postma, 2005; Hiscock and Bense, 2014).

Previous studies and technical reports confirmed brackish/saline waters in inner sectors of the aquifer, suggesting but not defining real causes for this occurrence, and recommending further investigations to clarify such questions (ARA-Sul, 2011; DNA, 1988; Juizo, 1995; Smidt, 1990). Due to limited hydrochemical knowledge of local aquifer, together with the different possible factors involved in groundwater salinization, this hydrochemical investigation was carried out aiming the better identification of such factors in Maputo area. The identification of salinization mechanisms requests a multi approach hydrochemical assessment, which has not been executed up to now in the area.

1.3. Research objectives

The overall objective of this dissertation is to differentiate the main hydrochemical water types and groundwater salinization mechanisms under influence of groundwater recharge, hydrogeological properties and human activities in Maputo area. Specific research objectives can be defined as:

- Explain the different hydrochemical water types in the area according to their main physico-chemical characteristics, such as EC and major cations and anions concentrations;
- Use specific tools such as environmental stable isotopes (^{18}O and ^{2}H), SO_4 and Br concentrations to better understand and distinguish processes of water mixing, mineral dissolution and evaporation taking place in the area;
- Refine conceptual groundwater flow models of the area through piezometry, hydrochemistry and isotope analyses;
- Understand the relation between the different hydrochemical water types and their link with the spatial distribution of groundwater recharge;
- Test different hypotheses of salinization mechanisms considering local land uses and hydrogeological properties through hydrogeochemical modelling.

CHAPTER 2

Literature Review

This chapter presents a brief review of topics relevant for the work. The addressed themes comprise hydrochemical facies and water types, environmental stable isotopes and salinization mechanisms.

2.1. Hydrochemical facies and water types

The interest of people in groundwater chemistry is mainly for water supply reasons. Although drinking water can be produced, for example, by desalinization, this process still too expensive. Therefore, the understanding of groundwater chemistry and its controls has a high priority for environmental and water authorities (Appelo and Postma, 2005). The concept of hydrochemical facies and water types, first introduced by Chebatorev (1955), is a useful tool to adopt when interpreting groundwater chemistry/quality and identifying major controlling hydrochemical processes. A hydrochemical facies defines a zone containing cation and anion concentrations within defined ranges (Hiscock and Bense, 2014).

As known, groundwater chemistry varies from place to place due to different reasons and factors, whereas most important can be pointed as water-rock interactions, rainfall and water-level seasonal variations, atmospheric interactions, and human activities (AlSuhaimi et al., 2016; Appelo and Postma, 2005; Hiscock and Bense, 2014). These factors result in different physicochemical signatures in groundwater. In coastal areas, for example, over-pumping can increase seawater intrusion and consequently increasing salinity, denoted by the increase in Total Dissolved Solids (TDS) of previous fresh groundwater. The taking and analysis of water samples from boreholes, wells, springs and rivers can help in understanding the hydrochemical processes and the groundwater flow system in a region (Nonner, 2015).

As water flows through the soil and aquifer material, its chemistry evolves over different water types due to different processes. A hypothetical example of groundwater chemistry changes and evolution due to a number of possible factors is presented in Figure 2.1.

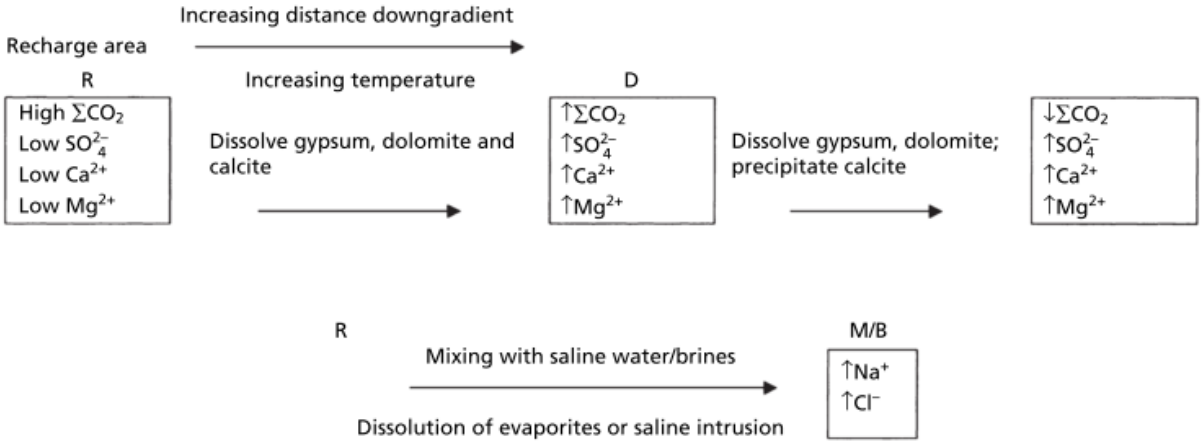

Figure 2-1: Hypothetical evolution of groundwater chemistry from recharge zone (R) with dissolution of carbonate minerals and/or mixing with saline water/brines (source: Hanshaw and Back (1979) in Hiscock and Bense, 2014).

In the example, fresh NaCl water from precipitation infiltrates and reacts with carbonate minerals, as gypsum, dolomite and/or calcite increasing the concentration of total CO_2, Ca^{2+}, Mg^{2+} and SO_4^{2-}. Later mixing with saltwaters, seawater or dissolution of evaporites leads to an major increase of Na^+ and Cl^- concentrations. In the example, calcite starts to precipitate due to the high concentration of Ca^{2+} in the solution (Hiscock and Bense, 2014).

To better understand these processes, analyses of temperature, pH, EC, four major cations (Na^+, K^+, Mg^{2+}, Ca^{2+}) and four major anions (Cl^-, HCO_3 , SO_4^{2-}, NO_3^-), as well as Na/Cl, SO_4/Cl and Ca/Mg ratios are the standard for a groundwater chemical analysis (Appelo and Postma, 2005). These physicochemical parameters are the base for the most common ways to classify different water types in groups. They are widely used in water type classification, hydrochemical studies and seawater intrusion assessment (Adonis, 2007; Appelo and Postma, 2005; Ghesquière et al., 2015; Han et al., 2015, 2013, 2011; Hiscock and Bense, 2014; Mongelli et al., 2013; Narany et al., 2014; Sajil Kumar, 2013; Stigter et al., 1998; Werner et al., 2013). Different ways of grouping water types according to different authors and methods are presented in Table 2.1. In a hydrochemical study the methods are usually simultaneously applied for different purposes.

Table 2-1: Different methods used to support classification and grouping of water samples. Compiled from (Appelo and Postma, 2005; Sajil Kumar, 2013; Stuyfzand, 1989).

Method - Author	Classification base	Purpose
Maucha diagram - Maucha, 1932	Graphical representation of major cations and anions.	Suitable for showing changes in time. Similar to Stiff diagram.
Piper plot - Hill, 1940 & Piper, 1944	Milliequivalent percentages of major cations and anions	Overall character of water and groups of water types

Stiff diagrams - Stiff, 1951	Major cations and anions concentration in meq/L (or meq/kg)	Visual comparison between waters from different sources
Water types - Stuyfzand, 1989	Chloride concentration, alkalinity as HCO_3^-, and predominant ions	Water types in different sub-components – hydrochemical facies analysis
Chadha diagram - Chadha, 1999	Difference between alkaline earths and alkali metals, and between weak acidic anions and strong acidic anions	Variation of Piper plot. It can be drawn in any spreadsheet software packages

The Piper plot and Stiff diagrams are the most applied to assess water samples main characteristics and groups. The classification proposed by Stuyfzand (1989) for hydrochemical facies analysis helps to better understand the evolution of water and possible processes from recharge to discharge areas, and it will be further explained. Additionally, hydrochemical facies analysis supports the understanding about hydrological and hydrochemical maturity of a hydrosystem. The first denotes a system in which flow has reached steady-state condition, while the second refers to a system which has groundwater with the same origin, without presence of relic waters (only one hydrosome is present). Usually, hydrological maturity precedes hydrochemical maturity (Stuyfzand, 1993, 1989).

2.2. Environmental stable isotopes

Stable isotopes of common elements, as Oxygen, Hydrogen and Nitrogen have being widely applied in groundwater investigations (called as environmental stable isotopes). Special application of stable isotopes of water (^{16}O, ^{18}O, ^{1}H, ^{2}H) to trace groundwater origins and processes involved in recharge is seen in diverse studies (Adelana et al., 2015; Clark and Fritz, 1997; Lee et al., 2016; Liu et al., 2015; Mook, 2001; Rozanski et al., 2001).

Seawater chemistry is relatively homogeneous around the world and the ratio between Oxygen and Hydrogen isotopes are near constant in the ocean ($^{18}O/^{16}O$ = 2/1000; $^{2}H/^{1}H$ = 16/1000), but not the same in fresh waters thanks to different fractionation processes (Appelo and Postma, 2005). Fractionation comes as a result of differences in masses of isotopes of the same element, that behave slightly different during physical, chemical and biological processes such as evaporation/ precipitation, exchange reactions resulting in isotopic equilibrium of two substances, and separation (depending on reaction rates) (Hiscock and Bense, 2014). Thus, resulting small changes in isotopic concentrations may lead to information on the climate at the point of infiltration or the origin of the water (Appelo and Postma, 2005; Rozanski et al., 2001).

The analysis of the O and H isotopic ratios can also identify excessive evaporation in an area since evaporation leads to fractionation and consequently enrichment in heavier isotopes in the remaining water pool. Then again, mixing processes does not lead to fractionation and, thus, different isotopic ratios can indicate mixing of different water types (Appelo and Postma, 2005; Clark and Fritz, 1997; Lee et al., 2016; Stigter et al., 1998).

Isotopic changes are presented by means of a δ notation, usually expressed in parts per mil (‰) with respect to a known standard. For water the Vienna Standard Mean Ocean Water (VSMOW) is the international accepted standard. Increasing values in δ imply an increasing proportion of heavier isotopes (^{18}O and/or ^{2}H) in the water,

wherein the sample is said to be isotopically enriched or to have a heavier isotope composition. The opposite gives depleted waters or waters with lighter isotope composition (Appelo and Postma, 2005; Clark and Fritz, 1997; Hiscock and Bense, 2014; Mook, 2001; Rozanski et al., 2001).

As stated before, ocean water is relative constant in the globe, but meteoric waters show a large range of $\delta^{18}O$ and $\delta^{2}H$ due to fractionation processes from continuous cycles of evaporation and condensation of evaporated water. According to Craig (1961), the relation between these isotopes and the related δ values show a linear relation for globally distributed meteoric water samples, known as the Global Meteoric Water Line (GMWL). The equation is usually presented in ^{2}H (or D) excess in relation with ^{18}O present in Figure 2.2 and written as Equation 2.1:

$$\delta D = 8\delta^{18}O + 10 \qquad \text{Eq 2.1}$$

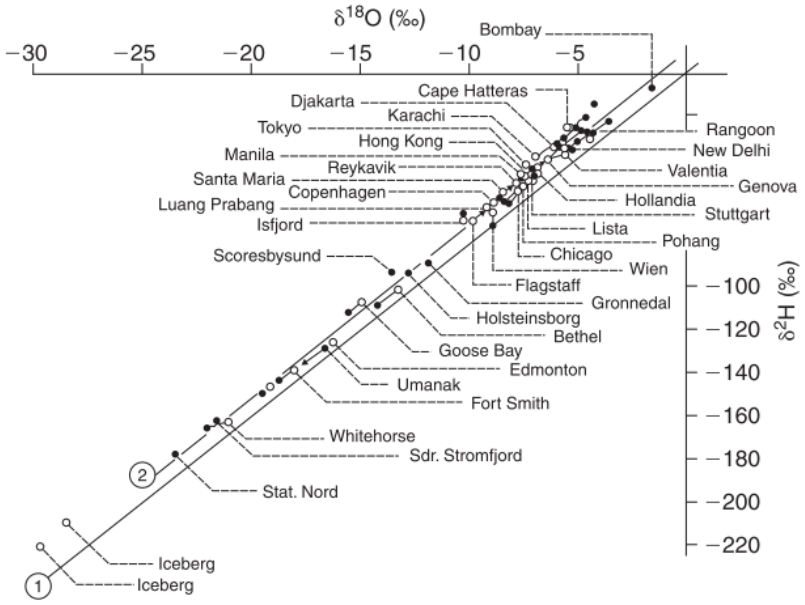

Figure 2-2: Relation of $\delta^{2}H$ and $\delta^{18}O$ from rain of different locations. Line 2 represents the GMWL; line 1 has the same slope but an interception of zero (source: Dansgaard, 1964 in (Appelo and Postma, 2005)).

High latitudes snow and ice samples present generally $\delta^{18}O$ and $\delta^{2}H$ lighter than -22‰ and -160‰ respectively, while low latitude rainwater samples present small deviation from ocean water. A Local Meteoric Water Line (LMWL) can be calculated and presents the relation between $\delta^{2}H$ and $\delta^{18}O$ for a specific area since the isotopic relationship in rainwater can be shifted from the GMWL due to latitude, continental, altitude and amount effects and seasonal variations (Appelo and Postma, 2005; Hiscock and Bense, 2014). Works from authors as (Adelana et al., 2015; Adonis, 2007; Edmunds et al., 2006; Han et al., 2015, 2013, 2011; Lee et al., 2016; Liu et al., 2015; Mollema et al., 2013; Mongelli et al., 2013; Stigter et al., 1998) show the application of environmental isotopes assessment to appraise evaporation and mixing processes in different coastal aquifers. For other elements different

than H_2O, isotope fractionation supports to clarify geochemical processes and reactions which leads to a certain water type composition (Clark and Fritz, 1997).

2.3. Salinization mechanisms

Salinization mechanisms can be defined as the natural and/or human induced process or group of processes, which lead to an increase of Total Dissolved Solids (TDS) of groundwater (Hiscock and Bense, 2014). Hydrochemical assessment and water types classification is being largely applied together with isotope analyses in distinguishing origins of groundwater salinity and different salinization mechanisms (Alcala and Custodio, 2008; Bouchaou et al., 2008; Edmunds et al., 2006; Ghesquière et al., 2015; Han et al., 2015, 2013, 2011; Lee et al., 2016; Liu et al., 2015; Mollema et al., 2013; Mongelli et al., 2013; Stigter et al., 1998; Vengosh et al., 2002; Werner et al., 2013).

Salinization can take years and continuously decreases water quality limiting its application. For instance, human-induced salinization is a hard process to control or to restore. Some known contributing factors for salinization are: 1) seawater intrusion; 2) water-rock interactions; 3) presence of connate waters; 4) agriculture return flow and high evaporation rates. Hydrochemical studies are required to better understand which factor or factors are responsible for salinization in a particular area. This section briefly explains each of the above mentioned mechanisms and how they can contribute to salinization.

2.3.1. Seawater intrusion

The natural intrusion of seawater is one of the major issues to deal with in groundwater management in coastal areas. Because saline water has a higher TDS than freshwater and is denser, it stays beneath freshwater inland forming a natural transition zone. The first approach for assessing this natural interface in coastal areas was given by the Ghyben-Herzberg relation, De Wiest (1965), where the depth of the interface below sea level is approximately 40 times the height of the freshwater above sea level. The relation takes into account the simple hydrostatic equilibrium, and differences between freshwater and seawater densities (ρ_f and ρ_s) of 1000 and 1025 kg/m^3, respectively, Equation 2.2 (Appelo and Postma, 2005; Hiscock and Bense, 2014):

$$z_s = \frac{\rho_f}{\rho_s - \rho_f} z_f \qquad \text{or} \qquad z_s = 40\, z_f \qquad \text{Eq 2.2}$$

where z_s represents the saline water interface below the sea level and z_f represents the water level or potentiometric surface for confined aquifers. The lower density of fresh groundwater allows it to override seawater and, as more water is added through precipitation, the height of water table above sea level increases, plus the thickness of freshwater lens. Under natural conditions, the interface has a near to fixed position, with small changes due to tidal effects, and sea level and seasonal variations. However, uncontrolled groundwater exploitation can induce the progress of the interface towards inland with the drop of the freshwater table resulting in an upconing of the seawater interface, Figure 2.3.

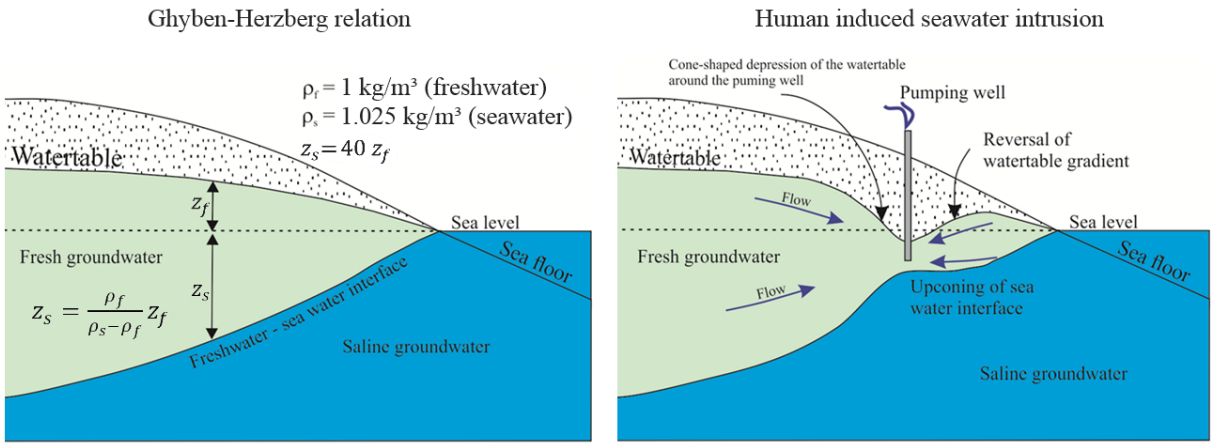

Figure 2-3: (left) Natural relation of freshwater and seawater interface according to Ghyben-Herzberg relation; (right) human induced seawater intrusion due to over pumping near the coastline (modified from: http://www.geological-digressions.com/?p=973).

This human-induced process leads to salinization and it is one of the major causes of high salinities in coastal aquifers with well-documented examples around the world (Appelo and Postma, 2005; Ferguson and Gleeson, 2012; García-Menéndez et al., 2016; Han et al., 2015, 2013; Hiscock and Bense, 2014; Johnson, 2007; Neumann et al., 2015; Werner et al., 2013). In addition, sea level rising due to climate change can also increase salinization with the advance of the interface towards inland and sea transgression over estuarine planes, especially in areas already experiencing salinization due to uncontrolled abstraction (Han et al., 2015; Hiscock and Bense, 2014; Werner et al., 2013).

This sharp interface is in reality a brackish transition zone. This mixing zone can be thicker within highly permeable aquifers under large abstractions and smooth topography. With the advance of the interface, salinization is accompanied by general increase of TDS in groundwater. While a NaCl water type intrudes the aquifer with initial freshwater in equilibrium with the rock material (usually CaHCO3 water types) ion exchange may take place if the cation exchange capacity of the sediment is significant and water types shift towards a $CaCl_2$ type. In these cases, the Na/Cl ratio drops below 0.86 (typical ratio for seawater) due to releasing of Ca from the rock complex and exchange by Na from seawater (Appelo and Postma, 2005)(Hiscock and Bense, 2014), left to right in Equation 2.3:

$$2Na^+ + Ca\text{-}X \leftrightarrow 2Na\text{-}X + Ca^{2+} \qquad \text{Eq 23}$$

where X represents the exchanger complex. The opposite can occur in Equation 2.3 (from right to left) under freshening of a saline aquifer. When freshwater intrudes the aquifer, Na is replaced by Ca leading to NaHCO3 water types. Cation exchange is particularly easy to observe when analyses are plotted in a Piper diagram. Average compositions of seawater and freshwater are plotted and a straight line between them represents different water compositions due to conservative mixing. Deviations from the line can indicate contribution of different processes, for instance, a surplus of Ca^{2+} in coastal waters compared to the conservative mixing can imply in seawater

intrusion, while a surplus of Na^+ suggests freshening. The concentration of any ion *i* by conservative mixing can be written as Equation 2.4:

$$m_{i,mix} = f_{sea} \cdot m_{i,sea} + (1 - f_{sea}) \cdot m_{i,fresh} \quad \text{Eq 2.4}$$

where m_i is the concentration of ion *i* in mmol/L; f_{sea} represents the fraction of seawater in the mixture; and *mix*, *sea*, and *fresh* indicate a conservative mixture, seawater and fresh water, respectively (Appelo and Postma, 2005). Any change in an ion concentration can be attributed to a reaction and its contribution is calculated as Equation 2.5:

$$m_{i,react} = m_{i,sample} - m_{i,mix} \quad \text{Eq 2.5}$$

where m_i is the measured concentration of ion *i* from the sample (in mmol/L). The seawater contribution factor f_{sea} is normally calculated from Cl^- concentration of the sample and written as Equation 2.6, since Cl^- is assumed to be a conservative element (Appelo and Postma, 2005),:

$$f_{sea} = \frac{m_{Cl,sample} - m_{Cl,fresh}}{m_{Cl,sea} - m_{Cl,fresh}} \text{ or } \qquad f_{sea} = m_{Cl,sample}/566 \quad \text{Eq 2.6}$$

where Cl^- concentration is expressed in mmol/L and 566 represents the average composition of Cl^- in seawater (35000 mg/kg). Even though the salinity can vary in seawater, the ratios of major ions remain constant and can be used to calculate compositions of conservative mixtures (Appelo and Postma, 2005; Hiscock and Bense, 2014).

2.3.2. Water-rock interactions

The occurrence of saline groundwater is not restricted only to coastlines. As rainwater infiltrates into the soil, dissolution of highly soluble minerals and contact with clay minerals, organic matter and metal oxy-hydroxides can increase the TDS of groundwater. For instance, in areas where saline formations as evaporites are present, dissolution of halite can result in extreme high values of TDS both in surface and groundwater (Bouchaou et al., 2008; Mongelli et al., 2013). Gypsum ($CaSO_4.2H_2O$), halite (NaCl), fluorite (CaF_2) as well as most carbonate minerals are clear examples of minerals that easily dissolves and are incorporated to the water within relatively short time as compared to groundwater travel time.

For example, in saline water environments, Na/Cl ratios are almost constant and near 0.86 where seawater origin is expected or known. An increase in this ratio can indicate silicate weathering with addition of Na^+ to the water. If this ratio is near 1, halite dissolution can be expected. Likewise, if SO_4/Cl, Mg/Cl and/or Ca/SO_4 ratios are relatively high compared to local fresh and brackish water, mineral weathering can be pointed as contributing factor for water chemistry (Appelo and Postma, 2005; Ghesquière et al., 2015; Han et al., 2013; Mollema et al., 2013; Mongelli et al., 2013). Fundaments of velocity of reactions, equilibria between phases and solubility of minerals can be found at Appelo and Postma (2005), and Hiscock and Bense (2014).

2.3.3. Presence of connate waters

Saline connate waters can be formed in two different process:

1) From past times when sea level was higher and seawater transgressed towards inland, displacing fresh groundwater and successively sinking to the aquifer bottom. A sequence of transgressions can result in accumulated saline water on the bottom of an aquifer, while new infiltrating water dilute the remaining groundwater on shallower levels. This seawater can also be entrapped within clay layers or thick aquitard units existing in aquifer system. The slowly displacement of such waters follows a sequence of cation exchange reactions along time, know as displacement chromatography (Appelo and Postma, 2005);

2) Natural presence of more saline waters at greater depths of poorly flushed aquifer systems. These connate waters formations can be explained by high dissolution of minerals due to water-rock interactions and/or the natural sinking of denser waters (Appelo and Postma, 2005; Hiscock and Bense, 2014; Kansas Geological Survey, 1995; Vengosh et al., 2002). After infiltration, more saline waters tend to sink and lay on the bottom of sedimentary basins due to higher densities. For this reason, many aquifers around the world displays saline water at deeper levels (Appelo and Postma, 2005; Han et al., 2015, 2011; Hiscock and Bense, 2014; Johnson, 2007). In areas with evaporites or halite, resulting brines can show salinities between from five to six times higher than seawater (200 g/L vs 35 g/L). Where evaporites are absent brines can be explained by intense water evaporation before its infiltration and emplacement as interstitial waters, e.g. Hanor and McIntosh (2007) (Hiscock and Bense, 2014).

Although these saline waters are usually laying on the bottom of aquifers, different topographic gradients can push recent freshwater in leading to displacement and dilution. Nevertheless, in areas with smooth topography these gradients are not big enough to flush saline waters out and they are assumed to be mostly stagnant with a very little fluid movement (Hiscock and Bense, 2014). On the other hand, deep exploitation wells and uncontrolled abstraction can disturb the natural layered situation and pull brines and brackish waters up into shallower depths of the aquifer yielding to salinization. A multi-tracer approach combining isotope (stable and radioactive) and hydrochemical data can help in dating and distinguishing connate saline waters from modern seawater intrusion in coastal areas (Bouchaou et al., 2008; Han et al., 2013; Lee et al., 2016; Mongelli et al., 2013; Werner et al., 2013).

2.3.4. Agricultural return flow and high evapotranspiration rates

Agricultural practices as the application of fertilizers by farmers to reach a desired yield is a well-known threat to groundwater quality. Apart from high rates of abstraction for irrigation purposes, which can lead to seawater intrusion, groundwater quality can be largely affected by the misuse of additional agricultural chemicals compounds (Andrade and Stigter, 2011, 2009; Bouchaou et al., 2008; Stigter et al., 1998).

The combination of groundwater overexploitation and large application of fertilizers can result in continued agricultural return flows (nonpoint salinity sources) once they reach pumping wells and are recycled. Additionally high ET of irrigation waters can cause a strong increase of TDS in the return flow. These recycled groundwaters usually present high concentrations of NO_3, K, Ca and/or SO_4 (Andrade and Stigter, 2009; Bouchaou et al., 2008; Hiscock and Bense, 2014; Vengosh et al., 2002). Whenever these incorrect agricultural practices do not cease, water resources in these areas will have their use limited to only agricultural practices due to high levels of undesired chemical compounds for human consumption. The scenario may get worse when climate change is considered with the general increase of temperatures and consequently higher ET rates.

2.3.5. Salinity origin assessment

It is growing the use of minor ions, as Br or Sr and $^{87}Sr/^{86}Sr$, $^{11}B/^{10}B$ ratios together with major ions and isotopes (especially environmental stable isotopes) in distinguishing different sources of salinity. Major ions and their ratios support the identification of mineral dissolution through binary plots and bivariate diagrams. Since Cl^- behaves as a conservative element, they are typically plotted vs Cl^- concentrations (usually in mmol/L or meq/L) (Appelo and Postma, 2005; Hiscock and Bense, 2014). While stable isotopes help in distinguishing evaporation processes from halite dissolution and seawater intrusion, those particular minor ions give insights about seawater-freshwater interaction (Alcala and Custodio, 2008; Bouchaou et al., 2008; Han et al., 2015, 2011; Mollema et al., 2013; Vengosh et al., 2002, 1999; Werner et al., 2013).

Br/Cl ratios, for example, have been near constant for all oceans since the Permian and can be taken as a reference value (Drever, 1997). The ratio is constant ($Br/Cl = 1.5 \times 10^{-3}$) under physical processes until halite precipitates. Since Br^- is less compatible in precipitating salts, it will be relatively enriched to Cl in residual brines - resulting in high Br/Cl ratios within brines; while the precipitated salts are depleted in Br^- leading to low Br/Cl ratios in waters dissolving halite (Han et al., 2011). Therefore, values equal to or above the marine Br/Cl ratio are likely to be originated from marine waters or marine formation waters, while values below the marine ratio may indicate an evaporite source (Alcala and Custodio, 2008; Edmunds, 1996; Han et al., 2013, 2011; Liu et al., 2015), Figure2.4.

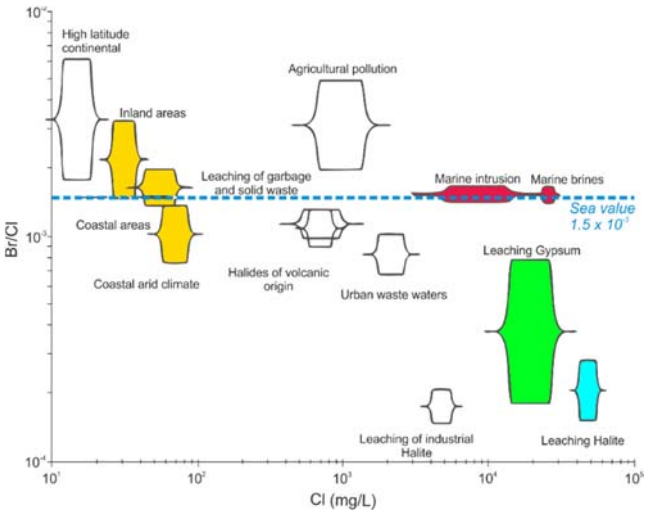

Figure 2-4: Br/Cl ratio vs. Cl (mg/L) and main processes affecting the ratio. The coloured groups are the most relevant to be considered for coastal environments like Maputo (modified from Alcala and Custodio, 2008).

Different authors applied similar method to explain origins of groundwater salinization in coastal aquifers. (Bouchaou et al., 2008) analysed ratios of $^{87}Sr/^{86}Sr$, Br/Cl, B/Cl and $\delta^{11}B$ together with stable isotopes, ^{3}H and Carbon isotopes (^{14}C and $\delta\ ^{13}C$) to explain origins of salinity in a coastal aquifer in Morocco. The authors were able to recognize different salinity sources apart from seawater intrusion, such as recycling of agricultural return

flow, dissolution of evaporites and gypsum, and mixing with connate and entrapped evaporated seawater (Alcala and Custodio, 2008; Bouchaou et al., 2008; Edmunds et al., 2006; Han et al., 2015, 2013, 2011; Mollema et al., 2013; Mongelli et al., 2013; Vengosh et al., 2002, 1999).

CHAPTER 3

Materials and Methods

This chapter present the materials and methods used to achieve proposed objectives. Material and research steps are described under each section: 1) Preliminary Data Collection; 2) Recharge assessment; 3) Field data collection; and 4) Hydrochemical Facies and Water Types. The flowchart in Figure 3.1 illustrates the methodology and some stages of the research.

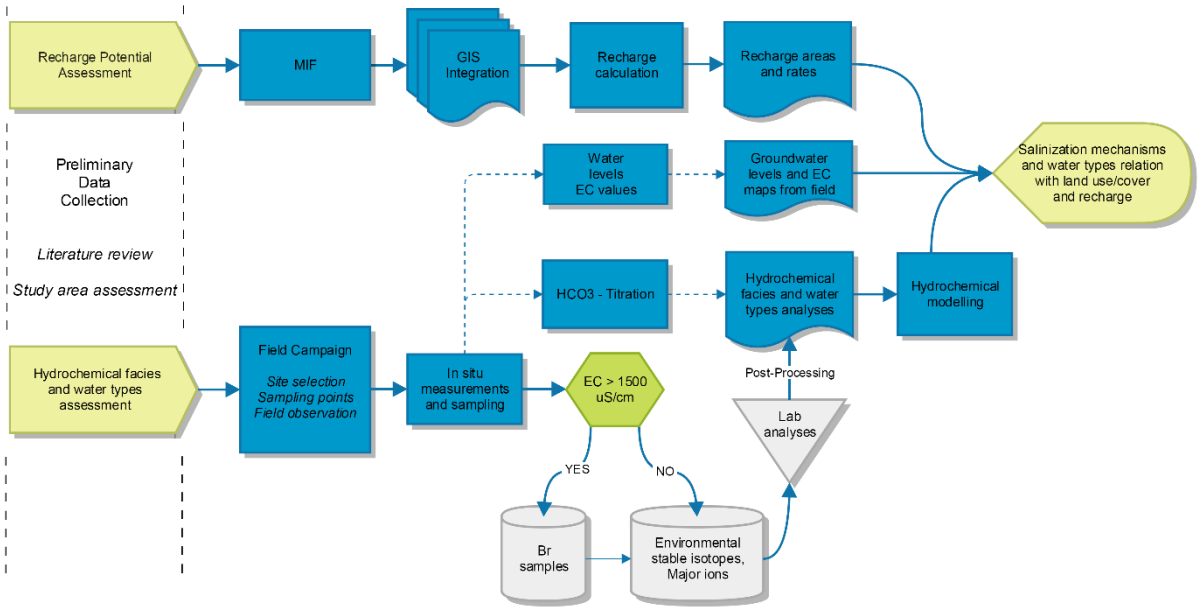

Figure 3-1: Flowchart of the research. Yellowish polygons present main objectives of the research; blue and grey squares represent main stages and steps of the work. Each of the steps are explained in the follow sections.

3.1. Preliminary Data Collection

The preliminary data collection comprises the assembly of existing data of the study area. Information about local hydrology, geology, hydrogeology and land use/cover were acquired through research of relevant topics in papers, thesis and technical reports. Additional data of groundwater levels and quality, and bore log information were acquired from ARA-Sul monitoring database through UEM staffs and collaborators. The main results of this phase are presented in Chapter 4 – Study area description.

3.2. Recharge Assessment

Recharge assessment was divided in two parts: 1) Recharge Potential Areas Assessment; and 2) Recharge Calculation. Among several methods to estimate groundwater recharge, recharge potential areas were qualitatively defined through a GIS approach, and quantitatively estimated with a root-zone water balance method.

3.2.1. Recharge Potential Areas Assessment

A weighting scheme of selected contributing factors for recharge was done through a Multi-Influencing Factor (MIF) method (Bonilla Valverde et al., 2016; Magesh et al., 2012; Yeh et al., 2016). Four factors affecting groundwater recharge were selected for assessment of recharge potential areas: soil type, terrain slope, land-use, and drainage density. In MIF method, relationship between criteria are established in a graphical way, in which each criterion can have a major or a minor effect on the others. A major effect results in 1 point to the criterion, while a minor effect results in 0.5 point. From the total sum of the major and minor effects, relative weights are assigned for each criterion. Figure 3.4 presents a hypothetical criteria relationship under MIF method (Bonilla Valverde et al., 2016; Magesh et al., 2012; Senanayake et al., 2016; Shaban et al., 2006; Yeh et al., 2016).

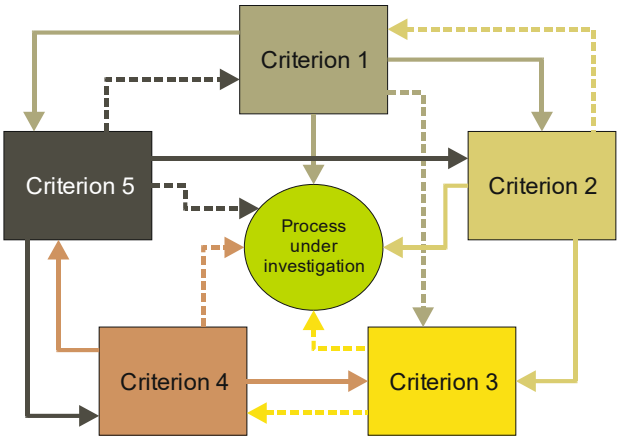

Figure 3-2: Schematic MIF method. Full lines represent major effects, while dashed lines represent minor effects of each criterion (modified from Bonilla et al, 2016; Magesh et al, 2012; and Yeh et al, 2016).

Subsequently, a Weighted Linear Combination (WLC) was used to classify different classes under each criterion. Each class from each different criterion receives a numerical value varying from 0 to 100 according to their influence in recharge where high values represent greater positive effects on recharge. To have aggregated criteria and classes in a common scale, standardized step-wise and linear functions were applied. As highlighted by different authors, weight assignments have to be carried out with precaution since they have great influence on the

results (Bonilla Valverde et al., 2016; Magesh et al., 2012; Senanayake et al., 2016). The obtained maps with their respective assigned weights and classes were prepared and integrated in a GIS environment.

3.2.2. Recharge Calculation

To evaluate groundwater recharge rates and periods, a water budget method was applied. A "Recharge Computation Spreadsheet" (Nonner and Stigter, 2016) was used to compute daily percolation of water in the lower boundary of the root zone taking into account rainfall, run-off and evapotranspiration (ETP), Equation 3.1:

$$Qperc = (P - E - R) + Qcap - Sroot \quad \text{Eq 3.1}$$

where ***Qperc*** represents flux on root zone bottom (recharge), ***P***, ***E*** and ***R***, represent precipitation, evapotranspiration and run-off, respectively, ***Qcap*** represents capillary rise, and ***Sroot*** represents changes in root zone storage. The method requires daily values of precipitation and ETP, as well as soil hydraulic properties and crop information. Due to seasonal variations and meteorological cycles, long-term data are needed for more representative results. Table 3.1 shows the input parameters and their related source.

Table 3-1: Input parameters for recharge calculation and respective sources.

Parameter	Source
Daily precipitation data	Local meteorological stations
Crop type	Land use/cover map (FAO, 2009)
Crop factor; Root zone depth	FAO guidelines (FAO, 1998)
Daily potential evapotranspiration (ETP)	Thornthwaite formula + evaporation from an open pan
Available soil moisture	Borehole descriptions *x* literature (Fetter, 1994)
Run-off threshold	Previous studies (SWECO, 2004)
Depth to groundwater	Piezometers ARA-Sul
Extinction depth	Literature (Nonner, 2015)

Precipitation values were obtained from stations of the study area. Different stations were chosen considering the proximity to the point to be simulated and the availability of data. Stations with more than three months of missing data in a year were disregarded. The location and availability of the data from the meteorological stations are shown in Appendix A. Crop types were obtained from land use/cover map (FAO, 2009). Crop information, as crop factor and root zone depth for each crop type were obtained from FAO guidelines (FAO, 1998), and presented in Appendix B. Potential evapotranspiration was achieved through the Thornthwaite formula using an open pan evaporation daily data. The method is further explained in Appendix B.

Field capacity and wilting point of soil types were acquired through comparison of bore logs and literature references. Available soil moisture (field capacity minus wilting point) is the parcel utilized by plants for transpiration and considered in the spreadsheet. Once available soil moisture is above field capacity, soil water

storage tends to increase and groundwater recharge tends to occur (Fetter, 1994). The values according to different soil types in the area are presented in Appendix B.

Run-off threshold was obtained from previous experiments in the region and assumed as homogeneous for the area (60 mm). The threshold has a big influence in recharge since it splits run-off parcel from soil water available forr evapotranspiration, soil water storage and recharge components. Also, run-off is highly variable and demanding to be estimated, depending on land cover/use, roughness of the surface and slope. Therefore, an estimative is often used based on local knowledge and reference values.

Depth to groundwater table and extinction depth are important parameters especially where groundwater level is shallow (below two metres) and close to the root zone. For shallow areas, average monthly groundwater levels are used to calculate capillary rise using a constant capillary factor. Extinction depth is usually considered a constant value (around two metres) for modelling proposes (Nonner, 2015).

3.3. Field Data Collection

This section presents carried out measurements and collected data during field campaign.

3.3.1. Groundwater levels measurement

Groundwater levels (WL) were measured to depict groundwater flow behaviour in the area, as well as the relation between phreatic and the semi-confined aquifers, whereas it is also important to know WL during sampling procedure. WL were measured in monitoring wells of ARA-Sul and in domestic wells through an acoustic sounding EC meter and water level tape. In some domestic wells the measurement of WL was not possible due to sealing of the borehole, Figure 3.3a.

Figure 3-3: a) Example of sealed domestic well; b) ARA-Sul monitoring well with two piezometers: F – phreatic aquifer, and SC – Semi confined aquifer.

From the 25 ARA-Sul boreholes, 17 present two piezometers, one in the phreatic aquifer and one in the semi-confined aquifer, Figure 3.3b. So that, it was possible to distinguish between phreatic and piezometric levels during WL measurements. Three monitoring wells could not be visited (PZ03 – no key for lock, PZ16 – damaged, and PZ25 – clogged). The distribution of ARA-Sul monitoring wells is presented in Figure 3.4.

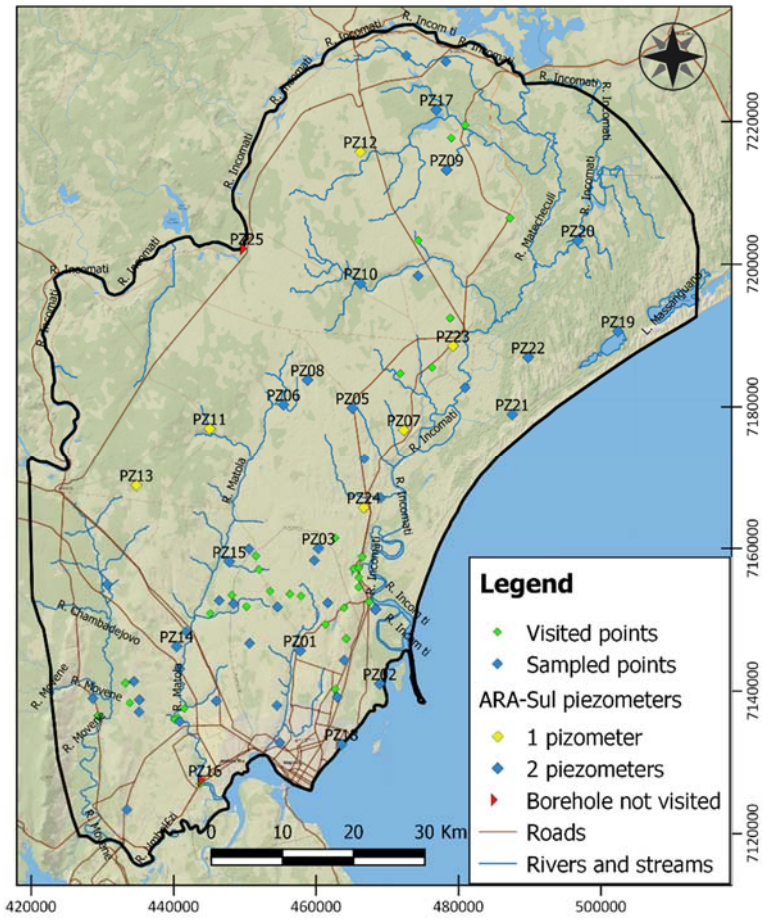

Figure 3-4: Distribution of ARA-Sul piezometers and domestic wells visited during the fieldwork.

Groundwater contour lines maps were produced using geographic information system (Quatum GIS 2.14.6 - Essen). Contour maps were generated using the Multilevel B-spline interpolation method, which was included in the GIS software.

3.3.2. In situ measurements, samples collection and pre-treatment

From visited places, a number of sites were selected for groundwater sampling to improve spatial resolution, Figure 3.4. Samples were collected from monitoring wells, domestic hand dug and pumping wells, and following groundwater sampling procedures as found in IAEA – Sampling Procedures for Isotope Hydrology, Appelo and

Postma (2005), and Hiscock and Bense (2014). Due to local limitations, samples were collected through a passive method using a Teflon bailer. The attempt to reach the well screens were done to improve representativeness of collected samples. During sampling, in situ measurement of EC, temperature and pH were carried out with Greisinger portable digital conductivity meter and WTW pH meter, respectively. In situ NO_3 was estimated via a field Nitrate-test strip. Alkalinity was measured from unfiltered samples via the HACH Digital Titrator titration field kit.

A total of 70 samples were collected for anion and 70 for cation analyses. Anion samples were filtered with a borosilicate glass microfiber filters of 1.2 µm and stored in un-acidified polyethylene bottles of 25 ml. Cation samples were filtered with a cellulose membrane filter of 0.45 µm and stored in pre-acidified polyethylene bottles of 25 ml. The bottles for cation were previously acidified with a few drops of concentrated nitric acid (HNO_3 10%) to preserve sample characteristics until laboratory analysis. Few duplicate samples were collected to check internal consistency of the laboratory. Unfiltered samples for Br analyses were collected in locations where measured EC were above 1500 µS/cm. 17 samples were collected and stored in 100 ml polyethylene bottles with no other added chemical for preservation. All samples were stored below 4°C to reduce biological activity and to conserve sample characteristics.

A total of 70 samples and 04 additional samples from rain events were collected for environmental stable isotope analyses. No filtration nor special preservation are required for stable isotope analyses. Samples were stored in a 1.5 ml glass bottle with double cap and rubber ring to avoid evaporation during storage and transportation.

3.4. Hydrochemical Facies and Water Types

3.4.1. Water sample analyses

Analyses of major ions and stable isotopes were carried out at laboratories of IHE-Deft to obtain required ions concentrations and parameters for hydrochemical facies and water types analyses and classification.

Cations, (Na, Mg, Al, K, Ca and Fe) were determined from *HNO_3* acidified samples with Inductively Coupled Plasma Mass Spectrometry (ICP-MS). Anions (Cl, NO_3, PO_4 and SO_4) were determined from un-acidified samples using Ion Chromatography System (ICS). Samples for Br analyses were sent to ActLabs in Canada, where they were analysed using high resolution Ion Chromatography (IC). Analysis accuracy levels can be found in Appendix D.

Environmental stable isotopes were analysed through a liquid-water isotope analyser (LGR).). The stable isotopic composition of ^{18}O and ^{2}H are reported using the δ notation, expressed in parts per mil (‰) with respect to a known standard, Equation 3.2:

$$\delta = \frac{R_{sample} - R_{standard}}{R_{standard}} x1000 \qquad \text{Eq 3.2}$$

where $\boldsymbol{R_{sample}}$ and $\boldsymbol{R_{standard}}$ represent the isotopic ratios of the sample and the VSMOW standard, respectively. The accuracy of the LGR analyser is around 0.2 ‰ for $\delta^{18}O$ and 0.6 ‰ for $\delta^{2}H$. Results were interpreted in relation with meteoric water lines. GMWL was obtained from Craig (1961), while a regional meteoric water line was obtained from the International Atomic Energy Agency - Global Network of Isotopes in Precipitation (IAEA-GNIP) and represented as the following LMWL-GNIP (Steinbruch and Weise, 2016): $\delta D = 8.7\delta^{18}O + 15.5$.

Chemical results were plotted in diagrams and charts to assist grouping and spatial distribution of water types. "PhreeqC Interactive 3" (Parkhurst and Appelo, 2013) and the spreadsheet "ChemDiagnostics" (Foppen, 2016) were used to calculate ion balance errors (Equation 3.3), molalities, mineral saturation indices (Equation 3.4), pCO_2, and to classify water types using the concept of hydrochemical facies developed by Stuyfzand (1989).

$$\text{Ion balance error (\%)} = (\sum\text{cations} - \sum\text{anions})/(\sum\text{cations} + \sum\text{anions}) \qquad \text{Eq 3.3}$$

$$SI = \log(^{IAP}/_{K_{sp}}) \qquad \text{Eq 3.4}$$

where IAP represents the Ion Activity Product obtained from sample analysis and K_{sp} is the solubility product for a given mineral or solid phase, usually under 25°C and 1 atm pressure.

3.4.2. Water types

The classification of water types was based on the system proposed by Stuyfzand (1989). Water types are presented as a unit with different sub-components: main type, type, subtype and class of water type. Each of the sub-components contributes to the logical codes and name of the water type. The arrangement of the method is presented in Figure 3.5, and each sub-component is explained below.

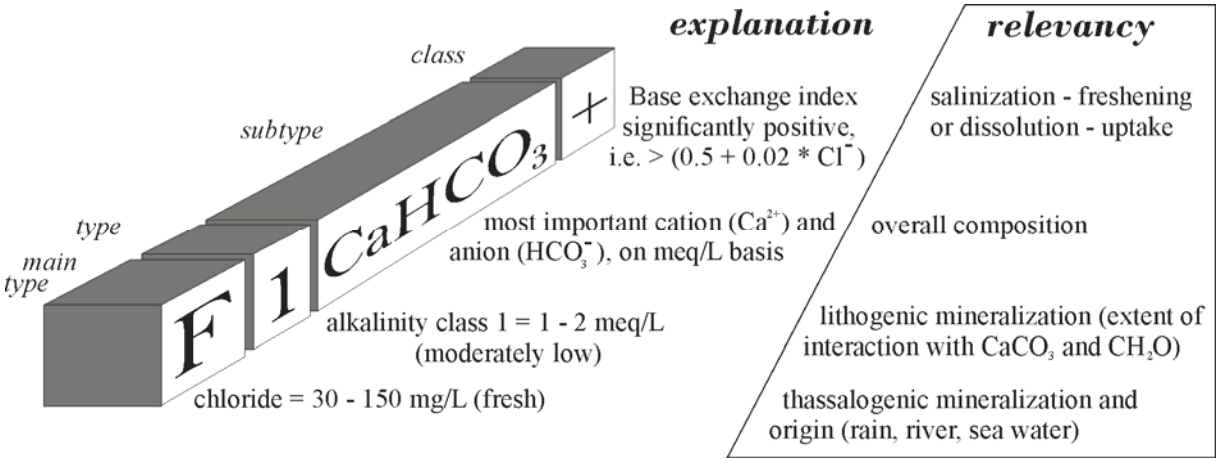

Figure 3-5: Classification of water type in sub-components according to Stuyfzand (1989).

Main Types

The main type is determined by the chlorinity values of the water sample as indicated in Table 3.2, the classified boundaries are based on criteria discussed in (Stuyfzand, 1993, 1989). Chlorinity is important in determining the origin of water and an indicative parameter for thalassogenic mineralization of water.

Table 3-2: Division of main types based on chloride concentration.

Category	Main type	Code	mg Cl/L	meq Cl/L
Fresh	Oligohaline	G	0-5	<0.141
	Oligohaline-fresh	g	5-30	0.141-0.846
	Fresh	F	30-150	0.846-4.231
	Fresh-brackish	f	150-300	4.231-8.462
Brackish	Brackish	B	300-1,000	8.462-28.206
	Brackish-salt	b	1,000-10,000	28.206-282.064
Salt	Salt	S	10,000-20,000	282.064-564.127
Hypersaline	Hypersaline	H	>20,000	>564.127

Types

The main types are subdivided into different groups according to the alkalinity values. The concentration of HCO_3 in water gives the measure for alkalinity and appropriate code is assigned, Table 3.3.

Table 3-3: Subdivision of main type into types based on alkalinity.

		Alkalinity as HCO_3	
Type	**Code**	**mg/L**	**meq/L**
Very low	*	< 31	< 0.5
Low	0	31-61	0.5-1
Moderately low	1	61-122	1-2
Moderate	2	122-244	2-4
Moderately high	3	244-488	4-8
High	4	488-976	8-16
Very high	5	976-1953	16-32
Extreme	6	1953-3905	32-64
Very extreme	7	> 3905	> 64

Subtypes

The predominance of ions was used in determining the subtype. In order to avoid long codes and too much subtypes, the dominant ions is assigned to individual cation and anion which account for more than 50% of total sum of ions in meq/l. Whereas the “MIX” ion family is assigned to water in which no cations or anion makes up more than 50% of the sum of ions.

Classes

The class is defined by the Base Exchange Index (BEX), which identifies ion exchange reactions due to water-rock interactions. Based on that principle, BEX is calculated, Table 3.4: positive values indicate aquifer freshening, while negative values points in the direction of salinization. The classification is even better if temporal resolution is available since it can designates seasonal freshening/salinization trends (Mollema et al., 2013).

Table 3-4: BEX classes based on cations deficit and processes.

BEX class	Process taking place	Code	Equation for BEX calculation
Positive	Freshening	+	
Zero	No base exchange	0	$[Na+Mg+K]_{corr} = Na+Mg+K]_{meas} - 1.0716*Cl$
Negative	Salinization	-	

where 1.0716 equals [(Na+Mg+K)/Cl] in the ocean,
and *corr* and *meas* subscript mean corrected and measured values, respectively

The combination of main types, types, subtypes and classes gives a hydrochemical classification for each analysed groundwater sample. Hydrochemical facies were determined with that.

3.4.3. Hydrochemical facies analyses

Groundwater changes in chemistry as it flows through aquifer material due to dissolution and precipitation of ions, water-rock interactions, and mixing with other water types. Hydrochemical facies is a concept used to group groundwater which belong to same origin, helping in determine groundwater flow path. The determination of groundwater hydrochemical facies is based on the combination of four independent parameters:

- Stuyfzand water type
- Redox index level (RI)
- Pollution index (PI)
- Calcite saturation index (CI)

The spreadsheet "ChemDiagnostics" was used in determining and mapping the spatial distribution of the hydrochemical facies in the subsurface. The spreadsheet combines classification techniques of water types and a deterministic method (PhreeqC) to compute hydrochemical facies from a multi-parameter hydrochemical data set. Hydrochemical data, locations, surface elevation and measuring filter levels of each piezometer were inputted into the spreadsheet. The water types for each piezometer at corresponding filter level and PI were then computed. Determination of PI is based on Equation 3.5 which reflects pollution type from application of fertilizer, manure and infiltration of wastewater.

$$\mathrm{PI} = \ln \frac{\ln\left\{10*\left[{}^{NO_3}/_{62} + SO_4^c\right]\right\}}{\ln 2}, \quad \text{if } \{\ldots\} < 0, \mathrm{PI}=0 \qquad \text{Eq 3.5}$$

$$where \quad SO_4^c = 0.67 * \left(\frac{SO_4}{96} - \frac{0.0232*Cl}{35.453}\right), \quad \text{if } \mathrm{SO_4^c} < 0, \text{then } \mathrm{SO_4^c} = 0$$

RI and mineral saturation indices were computed by PhreeqC. RI follows classification proposed by Stumm (1984) based on redox sensitive components present in groundwater, as O2, NO3, SO4, total Fe, total Mn and SO4, Appendix C. Hydrochemical facies analyses aims to understand the evolution of facies and respective parameters depicting possible natural or human-induced processes controlling groundwater chemistry within a hydrosystem.

3.4.4. Hierarchical Cluster Analysis (HCA)

Further clustering of water groups was done through Hierarchical Cluster Analysis (HCA), a multivariate statistical method for grouping data (frequently hydrochemical) into several groups and sub-groups (clusters). Members of each group are similar to each other and distinct from the others based on the selected variables (Andrade and Stigter, 2009; Güler and Thyne, 2004).

In this study, a Q-mode was applied to group water samples based on their physicochemical variables, as major ion concentrations, pH, EC values, and ratios as Na/Cl and SO_4/Cl (Andrade and Stigter, 2011). The groups were divided with the visual analysis of the HCA dendrogram, where a so-called phenon line is drawn according to sample's levels of similarity together with the interesting for the research. Additional information about HCA is found in (Andrade and Stigter, 2011; Ghesquière et al., 2015; Güler and Thyne, 2004; Swanson et al., 2001).

CHAPTER 4

Study area description

4.1. General information

The study area is located in south of Mozambique, in Maputo Province, and it has approximately 6300 km^2, situated between coordinates 420000 - 520000 mE, and 7110000 - 7230000 mN, WGS84/UTM zone 36S. The maximum elevation is around 230 m close to West boundary, whereas in coastal areas the elevation is close the sea level, Figure 4.1a. The area is near to flat, with slopes between 0 and 10 degrees, with rare exceptions where slopes are greater than 20 degrees in river valleys and close to hills on the western boundary, Figure 4.1b.

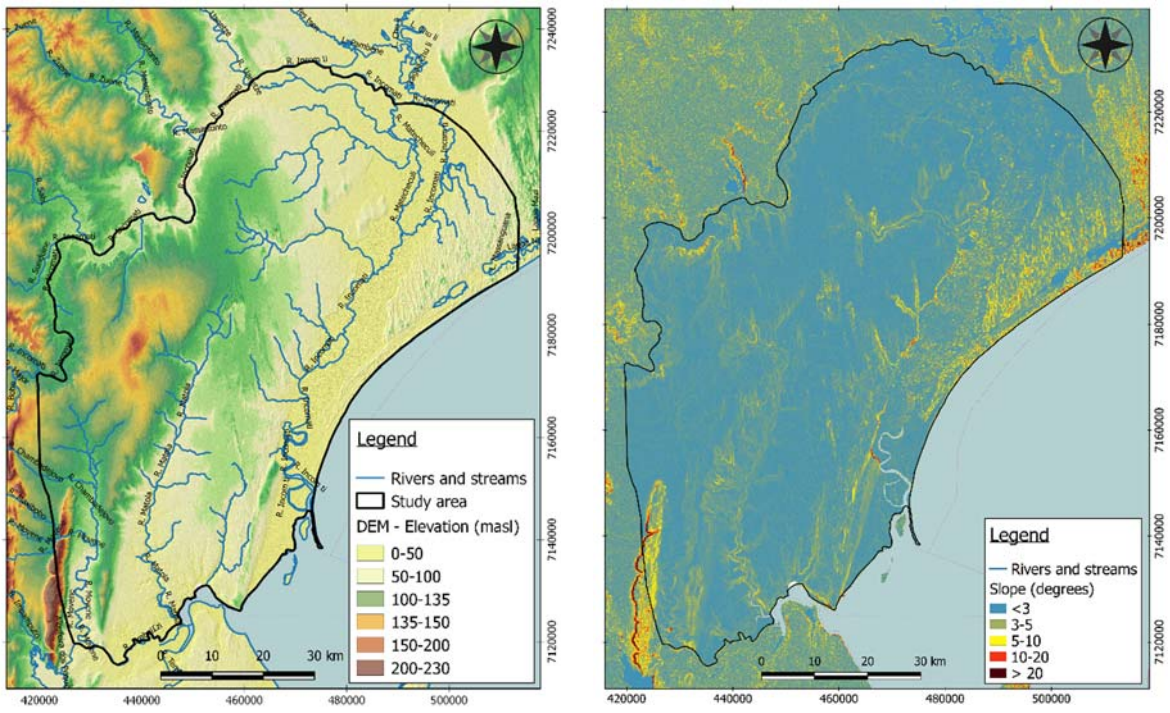

Figure 4-1: a) Digital elevation model (DEM) of the study area; b) Slope map of the study area.

Land use and cover of the area is mainly represented by natural to semi-natural vegetation. Land use/cover map was obtained from the project "*Globcover Regional*" from the Food and Agriculture Organization (FAO) (2009). The digital map has a spatial resolution of 300 m and originally 19 classes classified in relation to the Global Land

Cover Network (GLCN) programme. The classes were reclustered in six bigger classes according to their main properties and similarities, as crop types and density to obtain a better resolution for the study. Notwithstanding, the local land use/cover was checked during fieldwork to confirm FAO remote sensing classification map, with good agreement between the classification and actual land use/cover. The final land use/cover map is presented in Figure 4.2 and summarized in Table 4.1.

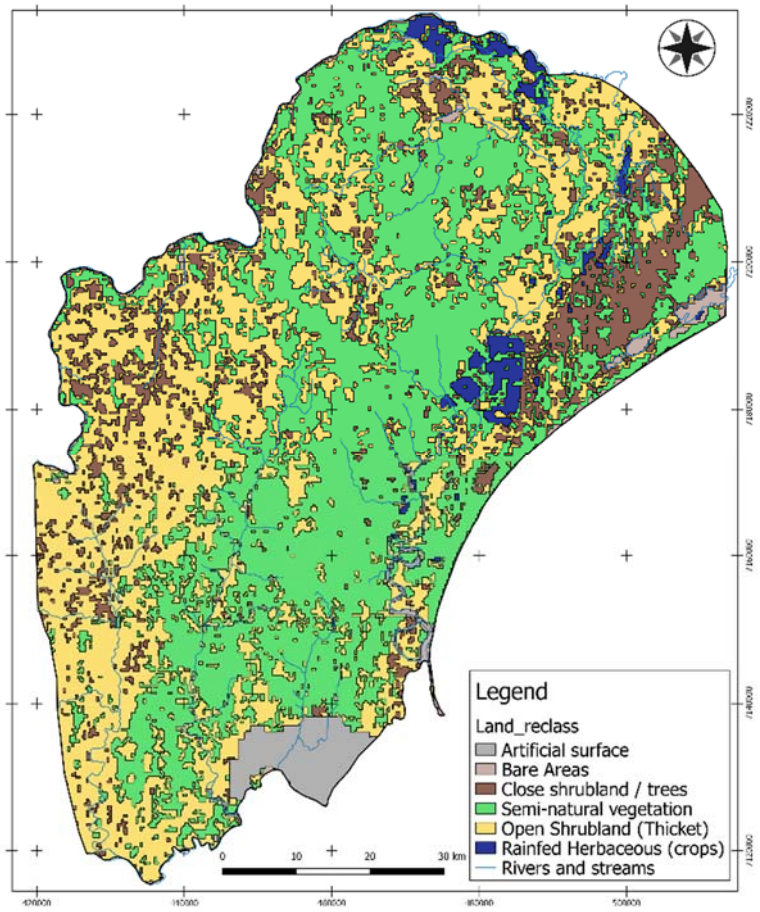

Figure 4-2: Land use/cover map of the study area (source: modified from FAO, 2009).

Table 4-1: Land use/cover of study area and their respectively areas without water bodies.

Land Class	**Area (km^2)**	**% of total area**
Herbaceous or semi-natural vegetation (shrubland, woodland)	2764.7	44.1
Open shrubland (Thicket)	2480.4	39.6
Close shrubland or close to open broadleaved deciduous trees	659.1	10.5
Artificial surface (urban area)	140.8	2.2
Rainfed herbaceous (crops)	119.4	2.0

Bare Areas	102.1	1.6

As observed in Table 4.1, beyond natural vegetation, great part of the study area is covered by deciduous plants (25.3%) and shrubland (thicket) (12.6%). Rainfed herbaceous crops (2%) are composed mainly by vast sugar-cane plantations, usually feed by rain water and additional irrigation from surface waters. Although the total peri-urban area of Maputo is vast (app. 450 km2), only the areas with pavement are considered as artificial surfaces and therefore represent 2.2% of the study area.

4.2. Climate

According to Köppen Geiger classes, the climate in the area is characterized as a savanna climate type (Aw), which resembles to a semi-arid environment but with higher precipitation rates. In the area, the average annual precipitation is highly heterogeneous, varying from 400 to 1000 mm, with an average of about 700 mm, Figure 4.3.

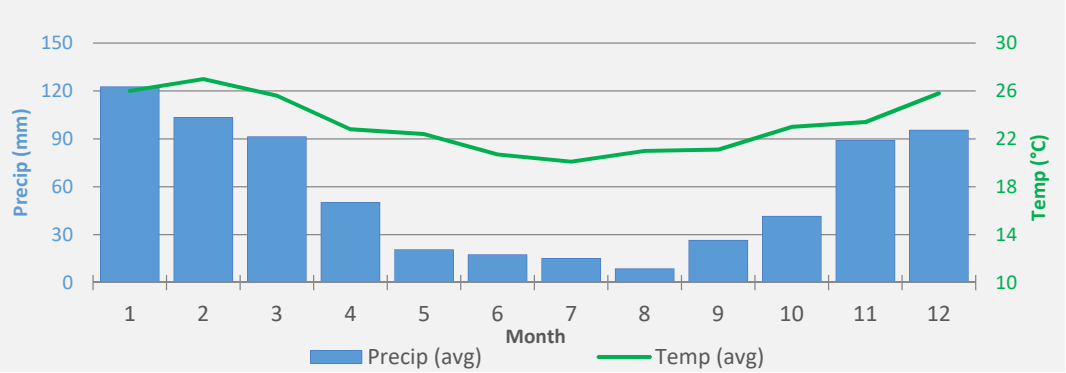

Figure 4-3: Average monthly precipitation and temperature for great Maputo area. Two seasons can be defined: a wet hot summer (Nov-Apr), and a dry cold winter (May-Oct).

From the plot, two seasons are easily defined for the area: a wet summer (Nov-Apr), when approximately 80% of total precipitation tends to occur, and a dry winter (May-Oct). Average low and high temperatures are around 20 and 27 degrees, respectively, with low temperatures during June and July, and high temperatures during January and February. Variations of dry and wet years can be also observed in the area, as well as the general increase of the average temperatures, Appendix A.

4.3. Hydrology

Several small and perennial rivers are present in the area and three main rivers can be highlighted: the Incomati River, the Matola River and the Movene River, Figure 4.1. Incomati River is an international river with a transboundary catchment shared between Mozambique and South Africa.

The Incomati River is the most important river in the region, running from the north of the study area and discharging in the Indian Ocean, on Maputo Bay. The river is the greatest source of water for agriculture and urban supply and it is extensively affected by human activities. The water is well exploited for agriculture, especially for sugar-cane on the surrounding areas of Xinavane and Manhiça (Adonis, 2007). The river forms a flood plain used for agriculture in the area, laterally limited by the sand dunes in the centre of the study area and close to its estuary. No major sources of pollutions were identified along the Incomati River. However, during the rainy season there is a high turbidity. The EC of the river water is generally high and the oxygen level is low (Adonis, 2007; FIPAG, 2012).

The second main river existing in the area is the Matola River. The river has 60 km and runs from the centre of the study area towards south. It discharges in the inner part of the estuary area of Espirito Santo, south of Maputo. The river is perennial, containing water only during the rainy season with great part of its section mainly dry. The river margins are extensively used for pasture and subsidence agriculture. In addition, its downstream area is under threat due to recently urbanization and industrial development (FIPAG, 2012). EC values up to 30000 µS/cm was already observed in the river water due to marine inundations and clayey soils with low permeability (Rosário Dias, 2016).

The Movene River is a perennial affluent of the Umbeluzi River, which discharges in the Maputo Bay and defines the natural boundary of the study area on the south.

4.4. Geology

The study area is located on a sedimentary basin characterized by terrestrial and marine deposits, which occurred under different transgression regimes dated from the Lower Cretaceous to late Palaeozoic. The sedimentation followed the rift sequence between Africa and Madagascar from Jurassic (Muiuane, 2007).

From the bottom to the top, the sedimentary basin is composed by transitional series of transgressive and marine deposits from Tertiary, mainly composed of carbonate units (limestones and calcarenites), followed by aeollian sediments from Quaternary. Both series increase in thicknesses towards the coast, while clay content increases towards inland (ARA-Sul, 2011). Alluvial deposits are well developed along downstream courses of the major rivers, cutting the aeollian sediments in the area. Five main geological groups are observed in the surface, Figure 4.4.

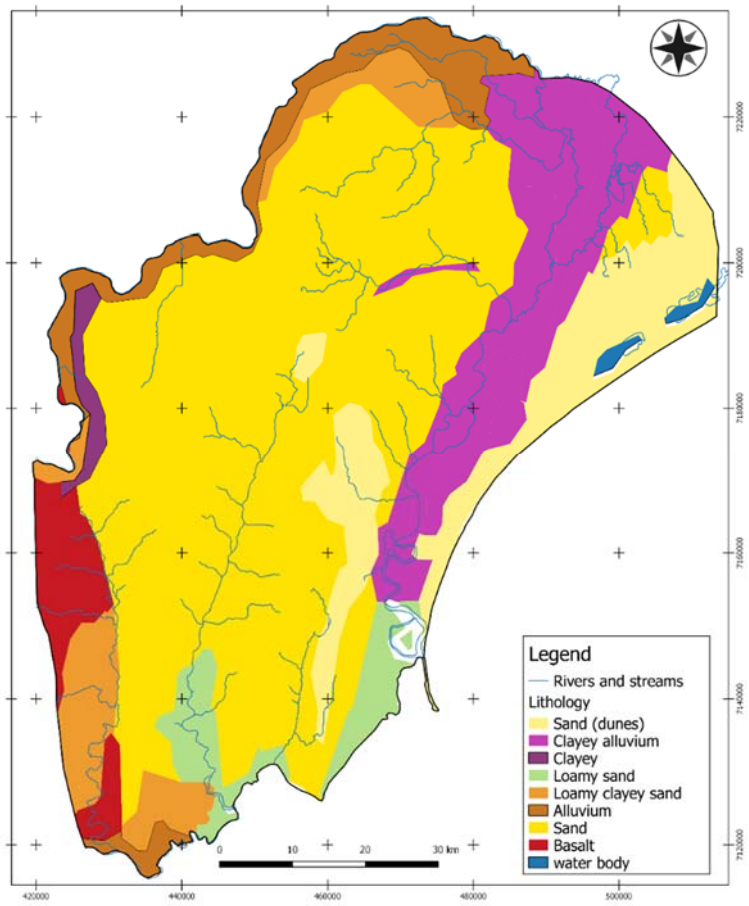

Figure 4-4: Geological map of the study area.

On the surface the main geological group is represented by the Quaternary aeollian sediments, followed by the alluvium deposits and crystalline rocks, the last one appearing only on the western boundary of the study area.

Basalts and rhyolites related to the Jurassic rift sequence form the basement of the system and their outcrops can be observed on the Western boundary of the study area. This unit is characterized by dark brown and loamy-clayey sands, with low permeability.

The Quaternary aeollian sands are composed by coarse to medium sands, sometimes also fine, from red to light-brown and with good sorting. The red colour suggest high content of iron oxide within the unit. The group was mainly deposited in a continental environmental during the Quaternary (Explanatory Notes to the Hydrogeological Map of Mozambique, 1987, in (ARA-Sul, 2011)). This group appears as interior dunes observed especially in the centre of the study area.

On the valleys of recent streams and river, light-brown clayey sands and loamy clayey sands, with localized layers of grey peat are observed - light purple areas in Figure 4.4. The peaty alluvium deposits are related to the Holocene and represent one of the youngest formations in the area. Another similar alluvium deposits with clayey facies are described as containing a deep and dark grey clayey soil with low infiltration rates, surrounding the Incomati River

valley - dark purple areas in Figure 4.4. The light yellow areas in the map are characterized by light-brown loamy sands, representative of estuarine planes. This unit is presented only close to the coast, on the south of Maputo city.

4.5. Hydrogeology

The local hydrogeological context is strongly linked to the geology of the area. Two main aquifers can be defined: an unconfined (or phreatic) aquifer, which is found within the aeollian deposits from the Quaternary; and a semi-confined aquifer underlying the aeollian sediments, and located within the carbonate formations from Tertiary (Smidt, 1990). An aquitard unit varying in thickness and comprising marls and siltstones divides the two aquifers. However, the separation of the two systems is not clearly defined and for large exploitation they can be analysed as one same unit (IWACO, 1985, Juizo, 1995 and SWECO, 2003 apud (Mozambique, 2005)).

Previous studies suggest varying thicknesses from 5 to 50 m for the phreatic aquifer and from 50 to 60 m for the semi-confined aquifer, Figure 4.5. Because of the complex geology, intercalation of clay layers and different grain sizes within the aquifer materials, hydraulic properties of the system vary from well to well, depending on the local lithological settings. Transmissivity values are only available for the East part of the study area, near Maputo city, and reveals values between 200-400 m^2/day, with maximums of 1600 m^2/day in few wells where greater amount of coarse sand is present (ARA-Sul, 2011; IWACO, 1986). Groundwater levels range from 2 to 50 m above sea level, with lower hydraulic heads near the coast. The conceptual model of the system shows that groundwater flows according to hydraulic head gradient of the area, from high values in the West towards the coast in the East. Although, local different flow directions are expected near drainage/discharge areas.

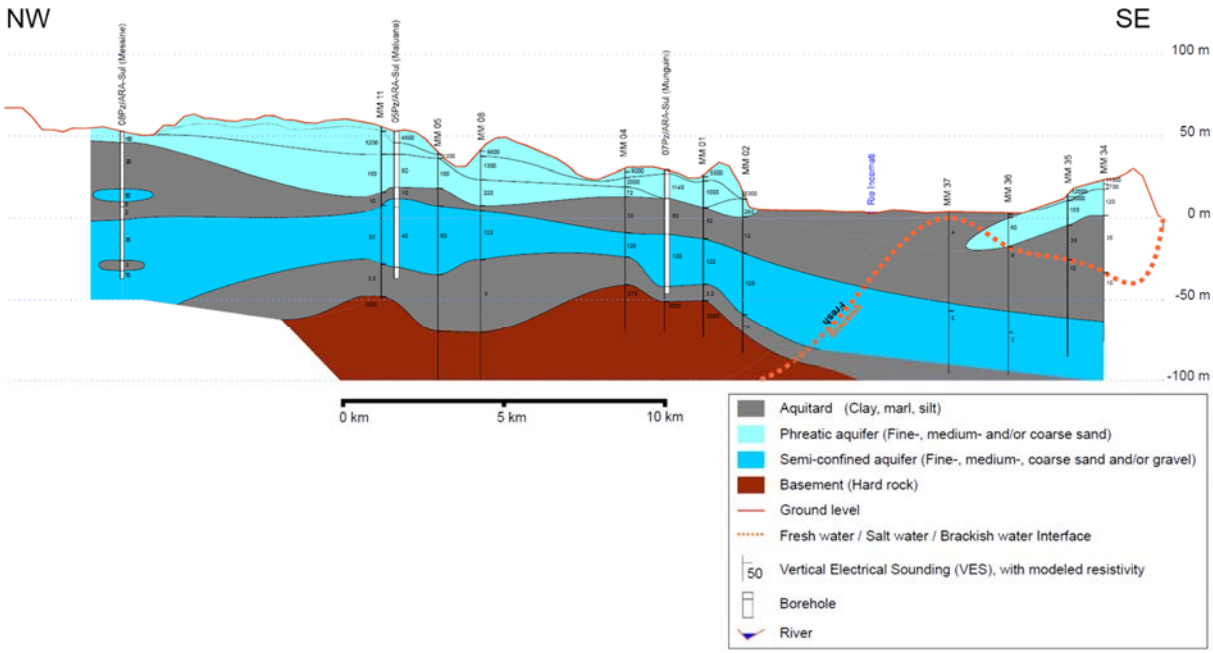

Figure 4-5: NW-SE cross section of the area with two aquifers, aquitard unit and inferred fresh-brackish/saline water interface (source:(ARA-Sul, 2011)).

According to (IWACO, 1986), natural groundwater recharge around Maputo sandy soils was found to be around 140 and 185 mm per year, which represents 20% of total annual precipitation, while in some areas with higher precipitation these values can reach 30% of precipitation. Although, in drier areas with less permeable soils recharge values can be below 10 mm per year, estimated by (DNA, 1988; IWACO, 1986). Sea side and local streams and rivers are the main discharge areas (Mozambique, 2005). Groundwater flow is slow due to the smooth topography of the area (Matsinhe et al., 2008; Muiuane, 2007). In general, hydraulic heads in the phreatic aquifer are higher than in the semi-confined aquifer and a connectivity between the two aquifers is observed, but not well comprehended. Furthermore, the interaction of each river section with the aquifer, in what concerns if a particular branch or section is a gaining or losing river is poorly known (ARA-Sul, 2011).

Groundwater quality assessed in previous studies reveal locally high salinities, especially in the semi-confined aquifer and near the coast, with a strong seasonal variation, however, a more dense monitoring campaign is required to delineate solid conclusions, Figure 4.6.

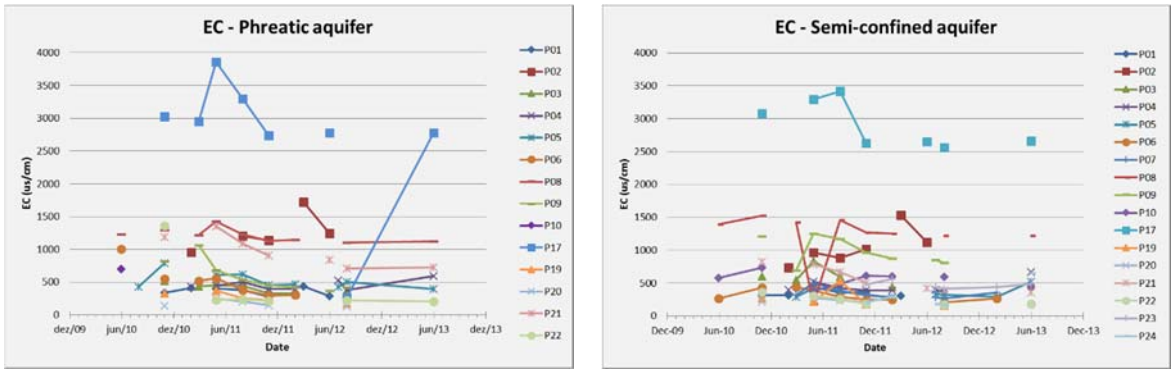

Figure 4-6: Measured EC in different piezometers between 2009 and 2013 in the phreatic aquifer (left) and semi-confined aquifer (right). Although many gaps exist, a seasonal variation of EC can be seen, especially in piezometers showing high EC. Mind the log scale in Y-axis (EC).

In the southern area of Maputo and north of Manhiça EC above 4000 µS/cm were already recorded, Appendix A, but the main cause for the high salinities still indistinct. Reliable information about the salinity origin inland is unclear, while natural seawater intrusion is pointed as main reason in coastal areas (ARA-Sul, 2011; Chairuca, 2016; Mozambique, 2005; Muiuane, 2007). High values of NO_3 (above 200 mg/L) in the phreatic aquifer were documented only near the urban and peri-urban areas of Maputo and Matola mainly due to poor sanitation and disordered new borehole drillings (ARA-Sul, 2011; Muiuane, 2007). Although not measured or monitored, pollution from industrial sites is known to be occurring, near urbanized centres. Similar situation occurs near Gaza Province, where extensive irrigation activities using surface water exist since 1930's (Chairuca, 2016).

Results and Discussion

4.6. Recharge Assessment

Results of groundwater recharge assessment are divided in two parts: Recharge potential zones; and Recharge calculation.

4.6.1. Recharge potential zones

Different criteria govern groundwater recharge, as mainly lithology, slope, land use/cover, and evapotranspiration (ETP). Each criteria influence recharge in a different manner, the spatial combination of two or more factors and their properties defines recharge and its potential. The overall weight of each criterion was assigned through a MIF method, following the scheme presented in Figure 5.1.

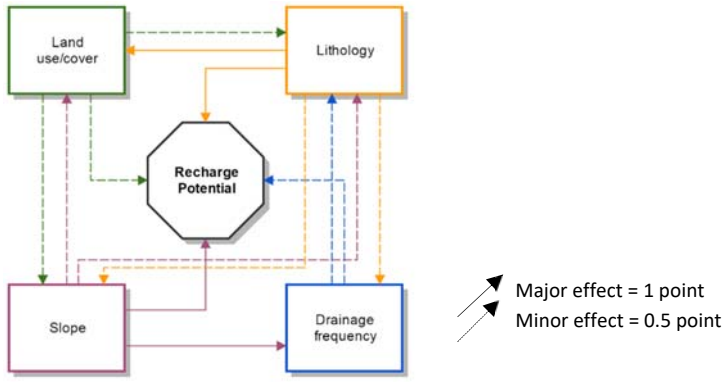

Figure 4-7: Criteria graphical relation following MIF method. Full lines represent major effects, while dashed lines represent minor effects of each criterion on the other(s).

Lithology and slope received the greater scores, 3 points each. Lithology has a major effect on land cover/use and on recharge, and minor effects on slope and drainage frequency. Slope has a major effect on recharge and on drainage frequency, and minor effects on land use/cover and lithology. Land use/cover presents three minor effects, on recharge, slope and lithology since vegetation interaction and presence in the surface plays an important role on recharge processes and on soil. Therefore, land use/cover receives a total of 1.5 point. Drainage frequency presents only minor effects on recharge and on lithology, receiving 1 point in total. The final weights are calculated based on the total score and presented on Table 5.2.

Table 4-2: Criteria scores and weights following MIF method for recharge assessment.

Criterion	Score	Assigned weight (%)
Drainage Frequency	0.5+0.5 = 1	11.75

Land use/cover	0.5+0.5+0.5 = 1.5	17.65
Slope	1+1+0.5+0.5 = 3	35.30
Lithology	1+1+0.5+0.5 = 3	35.30
TOTAL	**8.5**	**100.0**

The classes of each criterion were weighted according to their effect on recharge process. Step-wise functions were used to standardize descriptive classes as lithology and land use/cover, and linear functions were selected to standardize aggregated classes of slope and drainage frequency, as explained below, Table 5.3.

Table 4-3: Weighting factor and classes of each criterion influencing recharge.

Criterion	Classes	Potential effect on recharge	Individual weight	Layer weight % (MIF)	Sources
Lithology	Sand (dunes)	Extremely High	100	35.30	*Bonilla Valverde et al., 2016* *Juizo, 1995* *Magesh et al., 2012* *Shaban et al., 2006* *Yeh et al., 2016*
	Sand	Very High	90		
	Loamy sand	High	80		
	Alluvium	Medium	70		
	Loamy clay	Low	60		
	Clayey alluvium	Very Low	40		
	Clay	Extremely Low	20		
	Basalt	No Potential	0		
Land use/cover	Open shrubland	Very High	100	17.65	*Magesh et al., 2012* *Mahmoud et al, 2015* *Shaban et al., 2006* *Yeh et al., 2016*
	Semi-natural vegetation	High	80		
	Close shrubland/ trees	Medium	60		
	Rainfed herbaceous	Low	40		
	Bare areas	Very Low	20		
	Urban area	Extremely Low	10		
Drainage frequency (seg/km^2)	< 50	High	100	11.75	*Bonilla Valverde et al., 2016*
	50-200	Medium	y=-0.67x+133.34		
	> 200	Low	0		
Slope (degrees)	< 3	Very High	100	35.30	*Bonilla Valverde et al., 2016* *Magesh et al., 2012*
	3-5	High	y=-5x+115		
	5-10	Medium	y=-8x+130		
	10-20	Low	y=-5x+100		
	> 20	Very Low	0		

** y = weight; x= feature (in seg/km^2 or degrees)*

Lithology (L)

Lithological information is crucial for recharge assessment since its properties, as permeability, texture and structure play major roles in infiltration processes and hence recharge. Different soil types result in different permeability, as more clayey the soil, less infiltration tends to occur.

The weight classification was based on local lithological description and references in literature. Eight units were derived from local geological map. Sand units present the highest potential for recharge since their big pores favours rapid infiltration, especially where cross-bedding structures are present, as in dune areas. Therefore, sand units located in dune areas and sand units received a weight of 100 and 90, respectively. The other classes were weighted following a step difference, where clayey units present the smaller potential for recharge (Bonilla Valverde et al., 2016; Magesh et al., 2012; Shaban et al., 2006; Yeh et al., 2016), Figure 5.2a. Areas with basalts were considered not suitable for recharge, since local rock is not well fractured for infiltration, and because the aquifer is mostly absent in those areas (ARA-Sul, 2011; Juizo, 1995; Smidt, 1990).

Land use/cover (LU)

Considering groundwater recharge aspects, characteristics as vegetation type and density, interception, ETP, run-off and imperviousness have to be considered on land use/cover units. Among other factors, these parameters directly affect run-off and infiltration, and hence groundwater recharge. The weights were established considering the cited parameters and distributed respecting a stepwise function, Figure 5.2b. Six classes were defined from the land use/cover map of the area. Open shrublands present higher potential for groundwater recharge, since this is normally a sparse vegetation, with low interception and ETP rates, as well as with a low run-off component associated. Semi-natural vegetation is represent mainly by woodlands and shrublands, usually denser than open shrublands, therefore they have a smaller potential for recharge. Close shrublands and trees are considered in the same group, medium potential for recharge: close shrublands present high interception and high ETP as a unit as a result of high density; trees present deep roots, which can decrease recharge potential due to their high transpiration rates, as well their considered interception. Rainfed herbaceous crops are mainly composed by sugar-canes, well-known negative contributor for recharge thanks to high water consumption and high ETP, resulting in a low potential for groundwater recharge. Bare areas present a high run-off rate, decreasing infiltration and increasing overland flow and erosion, therefore considered as very low for recharge potential. Urban areas were not considered zero due to the fact that artificial recharge can occur from leakages from urban pipes system, for example, as well as minor rainfall infiltration (Magesh et al., 2012; Mahmoud and Alazba, 2015; Shaban et al., 2006; Shah et al., 2007; Yeh et al., 2016).

a) b)

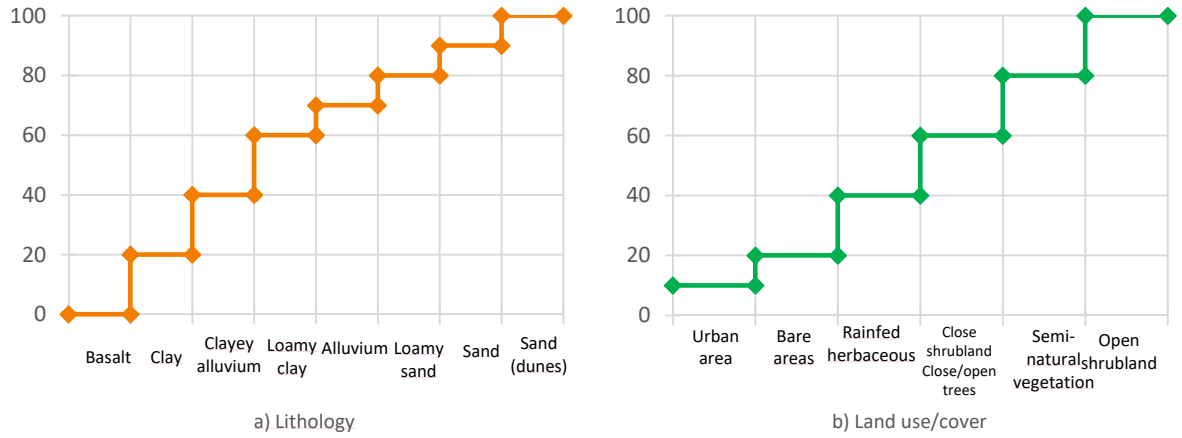

Figure 4-8: Individual weights for different classes according to their potential effect on recharge: a) lithology; b) land use/cover.

Drainage frequency (DF)

The distribution and number of streams and rivers in a basin is a natural indicator of infiltration characteristics of the area. For example, a higher drainage frequency (DF) - number of stream/river segments per unit area – is a suggestion of high run-off and hence low infiltration. Therefore, areas with a high DF are usually considered as with low potential for groundwater recharge (Bonilla Valverde et al., 2016). Drainage network was obtained from local DEM (90 m resolution) and DF was calculated in number of segments per square kilometres, Figure 5.3a. Higher the DF, smaller the weights assigned for groundwater recharge potential. Areas presenting DF between 0 and 50 seg/km^2 received the highest weight, while areas presenting more than 200 seg/km^2 were considered as null potential. Values in between 50 and 200 seg/km^2 were distributed following a linear function (Appendix B), Figure 5.3b. In Maputo province few rivers are present, and they are frequently perennial rivers presenting clayey beds, which can also leads to a small recharge potential.

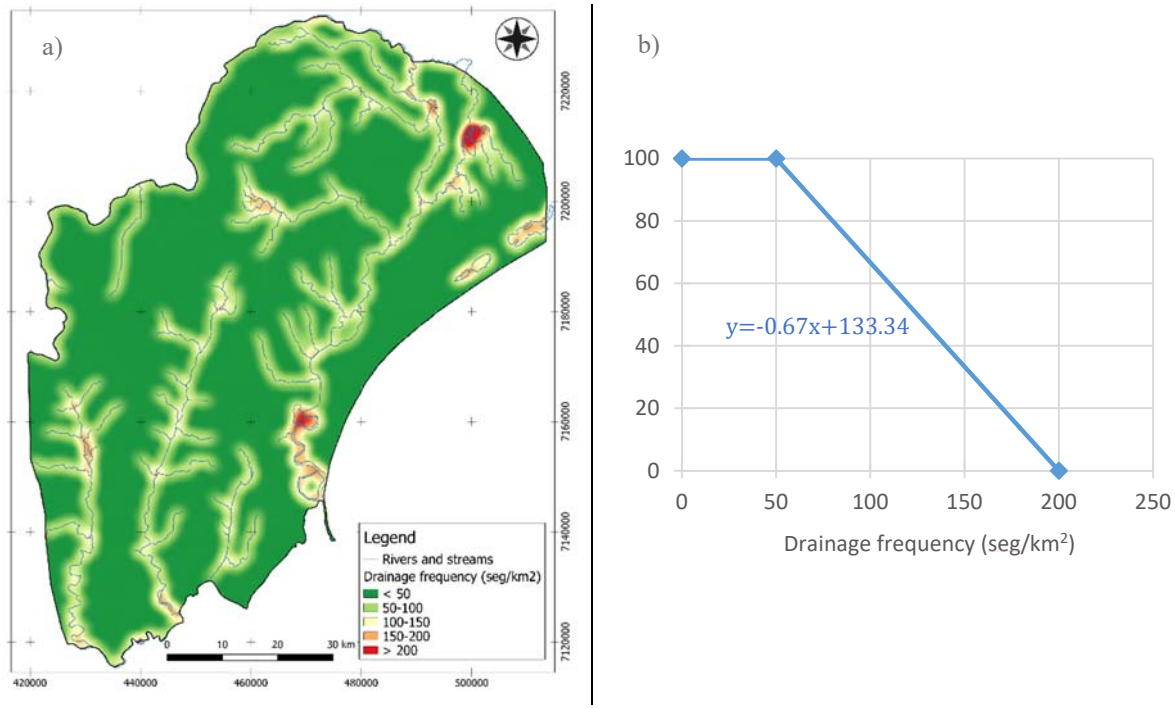

Figure 4-9: a) drainage frequency map; b) distribution of weights for different classes: y =weight; x = number of segments per square kilometre.

Slope (S)

The inclination of the terrain in relation to the horizontal plane is defined as slope. This gradient is usually expressed in degrees (angle with horizon) or in percentage (also known as grade – vertical rising per horizontal distance walked). Slope plays a major role in groundwater recharge since it controls the ratio infiltration/run-off. Steeper slopes result in a rapid water flow, hence, minor or no infiltration thanks to high run-off rates and small or no time for water to infiltrate the soil. Generally, areas presenting slope above 10 degrees (17.6 % grade) are considered to have a very low potential for recharge. Local slopes were derived from DEM and classified in five classes according to their angles (in degrees), Figure 5.4a. Higher slopes received smaller weights and vice-versa. The area is mostly flat, presenting mostly slopes between 0 and 10 degrees, with rare exceptions where this value reaches 35 degrees, within river valleys and in the western region with outcropped crystalline rocks. Slopes between 0 and 3 degrees are considered optimum for groundwater recharge and received therefore the maximum weight. Values between 3 and 5 degrees, 5 and 10 degrees, and 10 and 20 degrees were distributed according to linear functions (Appendix B), Figure 5.4b. Values above 20 degrees were considered null for recharge potential since run-off is the dominant processes in these surfaces (Bonilla Valverde et al., 2016; Magesh et al., 2012; Yeh et al., 2016).

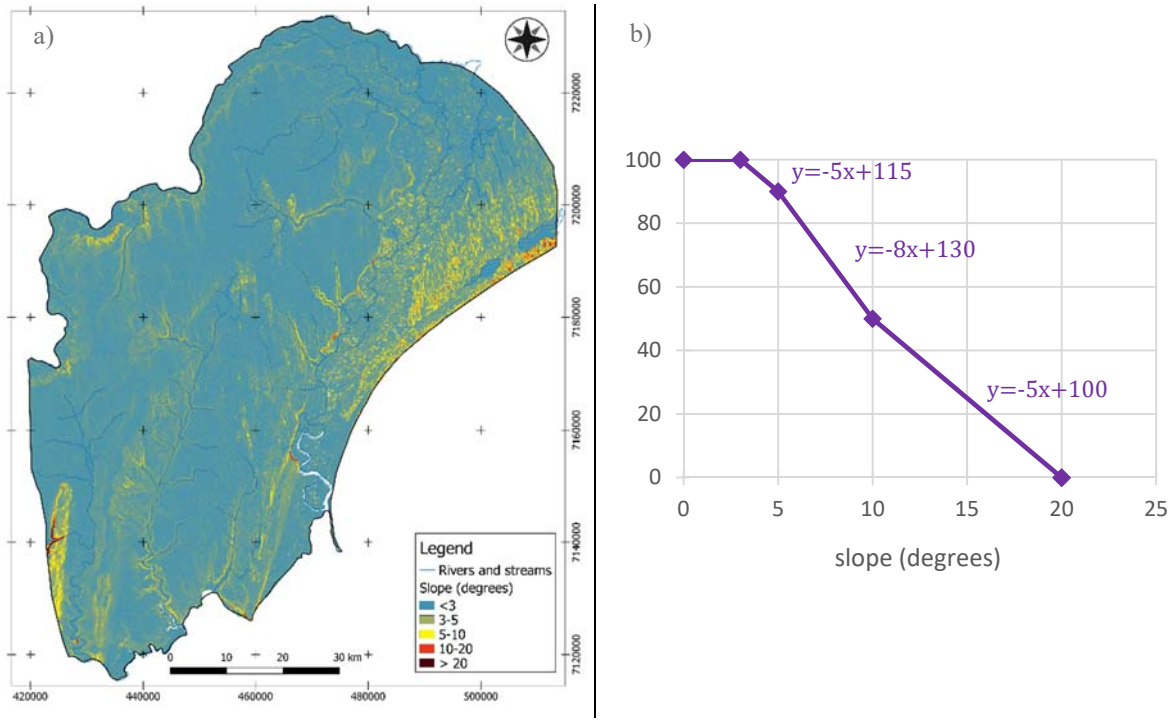

Figure 4-10: a) slope map; b) distribution of weights for different classes: y =weight; x = slope value in degrees.

Demarcation of Groundwater Recharge Potential Zones

Recharge potential (RP) zones were achieved through a GIS integration of thematic layers and their respective weighted classes. The layers integration can be mathematically expressed as Equation 5.1:

$$RP = (L_w L_r + LU_w LU_r + DF_w DF_r + S_w S_r) * L \qquad \text{Eq 5.1}$$

where ***L*** is lithology class, ***LU*** is land use/cover, ***DF*** is drainage frequency, ***S*** is the slope, ***w*** is the weight of criteria (obtained from MIF), and ***r*** is the individual weight of each class under each criterion. The multiplication by ***L*** at the end was done to constrain regions not suitable for groundwater recharge as areas presenting basalt. Figure 5.14 presents groundwater recharge potential map after the integration of the four thematic layers.

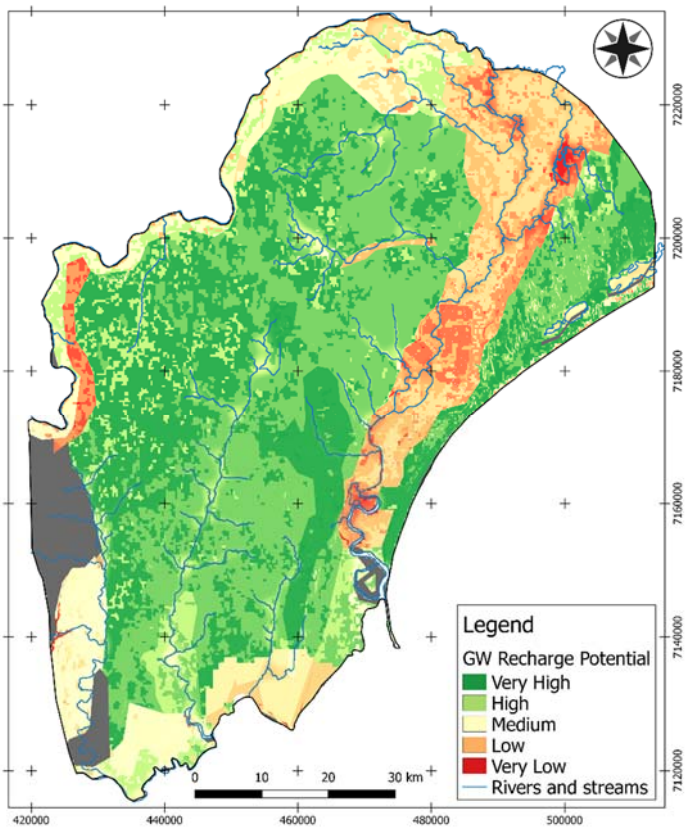

Figure 4-11: Groundwater recharge potential map resulted from the integration of four thematic layers (lithology, land use/cover, slope, and drainage freq.)

RP was classify in five categories, from very high to very low. From the map it is clear that lithology is the main controlling factor on RP, followed by land use/cover. Great part of the study area presents high or very high RP. As expected, sand dune areas covered by open shrublands present the highest RP, while smaller RP are found within agriculture fields and clayey valleys. However slope has weight greater than LU in MIF method, the criterion does not show a great influence on results due to general small slopes in the area.

Even so RP is low within drainage areas, this is not always true since riparian aquifers existing underneath rivers can greatly contribute for groundwater recharge. This fact has been extensively discussed by many authors and different views are defended (Bonilla Valverde et al., 2016; Magesh et al., 2012; Yeh et al., 2016). For that reason, drainage criterion shall be evaluated according to local conditions in what concern its direct or inverse relation with groundwater recharge. The same should be pondered for outcropping crystalline rocks, which can show characteristics for good infiltration and hence groundwater recharge. For a better assessment, evaluation of some factors should be well-adjusted with field observations and measurements whenever possible. For a quantitative evaluation of recharge, climate variables have to be considered too and, therefore, recharge calculation shall be carried out. In addition, RP map supports MAR site selection depicting optimum places with higher potential for groundwater recharge (Bonilla Valverde et al., 2016).

4.6.2. Recharge calculation

Natural groundwater recharge is strongly dependent on climate conditions and seasonal variations since its main source is precipitation. For a quantitative appraisal, rates and periods of recharge were assessed through calculation of water budget in the root zone. The limitation of the method was the availability of precipitation data, since daily values are required and many gaps exist in the available records. For that reason, the application of the method was not possible in the whole area. Ten years, between 2000 and 2010 were selected to run the simulations in order to achieve a better view of yearly precipitation variations.

Daily evaporation values of an open pan were obtained from a meteorological station close to the region, because no data was available within the study area. The values were converted to potential evapotranspiration (ETP) through the Thornthwaite formula, Appendix B. The resulted monthly ETP is shown in Figure 5.6 in association with monthly average temperatures and monthly precipitations.

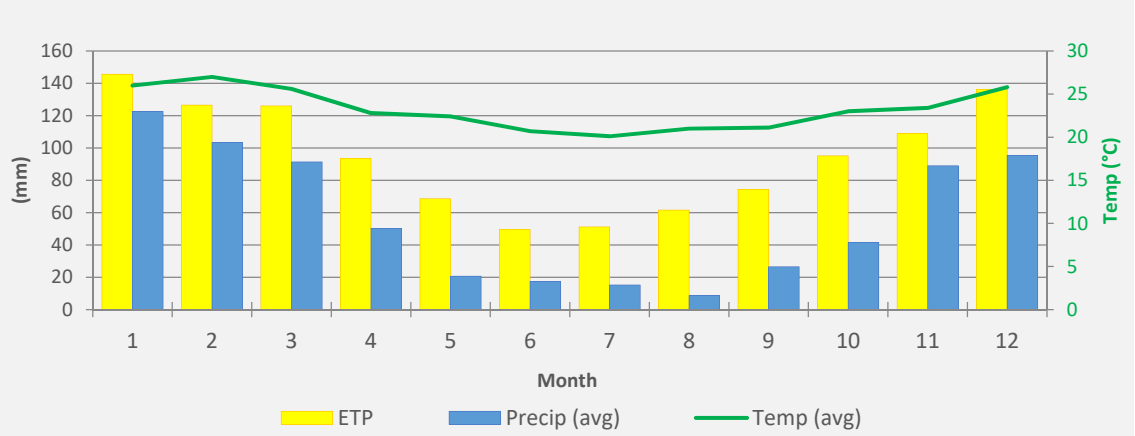

Figure 4-12: Monthly average values f ETP (yellow bars), precipitation (blue bars) and mean temperature (green line). Each number corresponds to a month in the year.

In consequence of local high temperatures, monthly ETP is higher than monthly precipitation, following temperature variations along the year. ETP ranges between 50 and 150 mm/month. ETP values were converted to actual evapotranspiration (AET) following the crop factor of each crop type. Average monthly groundwater levels were obtained from ARA-Sul observation wells, while extinction depth was kept constant and equal to two metres for all simulations. Run-off threshold was defined as 60 mm and homogenous for the whole area. Average recharge estimation and water balance resulted from the recharge spreadsheet are summarized in Table 5.3 and shown in Figure 5.7. Appendix B presents recharge result and water balance for the different piezometers.

*Table 4-4: Results from spreadsheet recharge for different piezometers. Values for 10 years of simulation (2000-2010). Values represent **Minimum – Maximum (Average)**.*

Piezometer	Characteristics	Rainfall (mm)	ET (mm)	Recharge (mm)	Recharge/ precipitation

PZ05	Sand with semi natural vegetation	4.5 – 74.2 (44.2)	14.3 – 72.6 (39.5)	0 – 15.9 (5.5)	12.4%
PZ15	Sandy loam with broadleaved trees	10 – 163 (66.3)	18.4 – 97.8 (53)	0 – 22.3 (4.7)	7.0%
PZ16	Fine sand with open shrubland	2.9 – 171.5 (59.3)	10.2 – 89.7 (41.4)	0 – 32.2 (10.9)	16.4%
PZ17	Clayey sand with closed shrubland	5.5 – 130.6 (64.4)	23 – 97 (53)	0 – 26.1 (7)	12.0%
PZ23	Sand to silt with broadleaved trees	4.5 – 74.2 (44.2)	15.9 – 74.6 (42.2)	0 – 11.3 (2.5)	5.6%
PZ25	Sand with open shrubland	1.4 – 172.4 (67.3)	13.4 – 89.9 (42.7)	0 – 60.3 (19.7)	29.0%

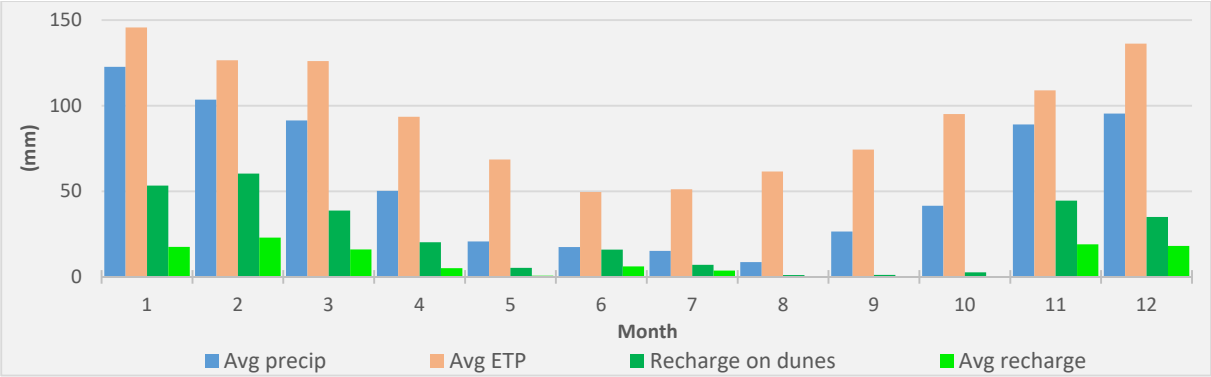

Figure 4-13: Monthly average values of water balance for simulated years (2000-2010). Values expressed in mm.

Recharge shows great variation in the area, mainly from 7 to 29% of monthly precipitation depending on the different geological aspects, land use/cover, rainfall and AET. Coarse and pure media, as sand deposits present highest recharge rates, while fine texture soils present lower rates. This is mainly resulted from higher values of available soil moisture in finer textures compared to coarser texture soils, more water available for ET and less for recharge. Highest average recharge rates are observed in PZ25 and PZ16, 29% and 16.4% respectively. Despite the rate differences, a general pattern of recharge is observed, mainly between November (11) and March (3) coinciding with the wet season in the area. Nevertheless, the method does not consider travel time between root zone bottom and top of saturated zone, and different methods of recharge calculation can result in different recharge periods.

It is also important to highlight the occurrence of recharge even in months when AET is higher than monthly precipitation. This happens because in a particular day of that month, precipitation exceeds AET rates and percolation of water from the root zone occurs. This shows the importance of daily based recharge assessments instead of monthly based. In the area, extreme events seem to have great importance for recharge, especially during dry months. This can be observed in Figure 5.7, especially in months from May to July when a minor recharge takes place in some locations.

Recharge assessment through root zone water balance, in agreement with RP zones shows recharge strongly linked not only to lithology and land use/cover, but also to climate variations of the area. Groundwater recharge is higher in western areas, where higher precipitation rates and coarse textures soil exist. Nevertheless, to overcome low groundwater recharge, managed aquifer recharge (MAR) techniques, as runoff attenuation through infiltration basins and check dams can be a potential measurement for improving recharge since in extreme events great part of rainfall goes to run-off component of water balance.

4.7. Field Data Collection and Measurements

This section presents the data collected during the fieldwork and carried out in situ measurements.

4.7.1. Groundwater levels

Groundwater levels (WL) give insights of the aquifer system dynamics, helping in identifying flow directions, recharge areas and discharge areas. Different measurements were carried out for the phreatic aquifer, and for the semi-confined aquifer. Water levels were transformed into hydraulic head values according to topographic referred piezometers elevations and their respective head-heights for the construction of WL contour maps.

Two different interpolations were used for phreatic water levels. In the first, only GWL were used for the interpolation; while in the second, rivers and streams heads, as well as sea level on the coast were used to constrain water levels in these locations. That imposes that such rivers and streams are directly connected to the aquifer, resulting in assumptions concerning gaining and losing river sections while avoiding WL above local topography. However, the general pattern of groundwater flow is similar for both cases, as shown in Figure 5.8.

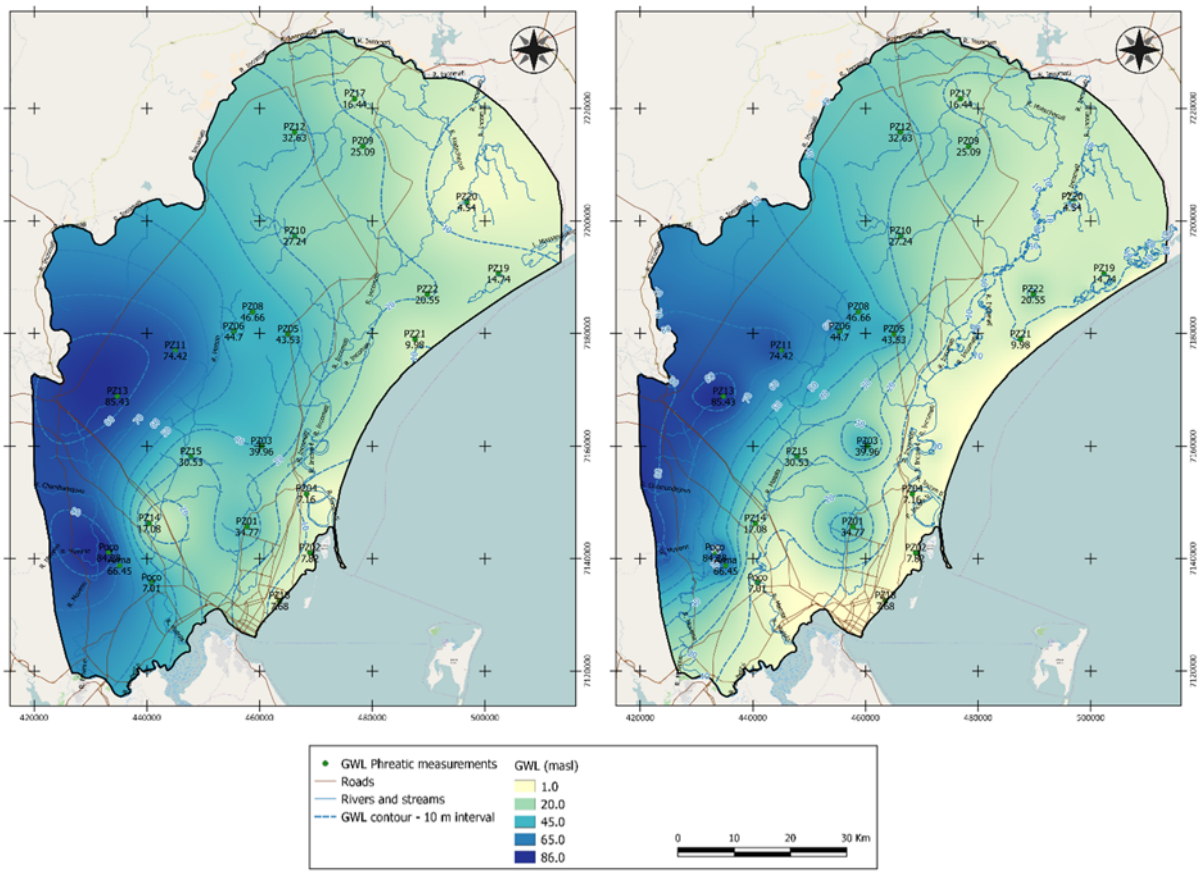

Figure 4-14: (right) Water level contour map for the phreatic aquifer without constrain of river and streams heads. (left) Water level contour map for the phreatic aquifer with constrain of rivers and streams heads, as well as sea level on the coast.

It can be clearly seen that groundwater flows from West towards the coast, from higher to lower hydraulic head values. The total hydraulic gradient of the area is around 80 m, with high values in the western portions of the aquifer and lower values near the coast. Main recharge areas are located around piezometers PZ11 and PZ13 (74.42 m and 85.43 m, respectively hydraulic heads), while the coast is the main discharge area. Local rivers and streams discharges are observed in both interpolations, as, for example, Matola and Incomati Rivers. Main differences among interpolation methods rely on: 1) non-extrapolation of water levels in drainage areas with the constrain streams; 2) on dune areas, where recharge cells are easily observed; and 3) in the north of the area, where groundwater flows northeast vs towards the coast in the second case.

Semi-confined groundwater flows follow similar pattern of phreatic aquifer, from West towards the coast, Figure 5.9. However, a depression cone can be observed in the northeast, where hydraulic head values are below sea level (PZ20 = -0.06m) resulting in a local opposite flow pattern. Nevertheless numerical modelling is required to support flow patterns, WL are the first approach to understand local flow system.

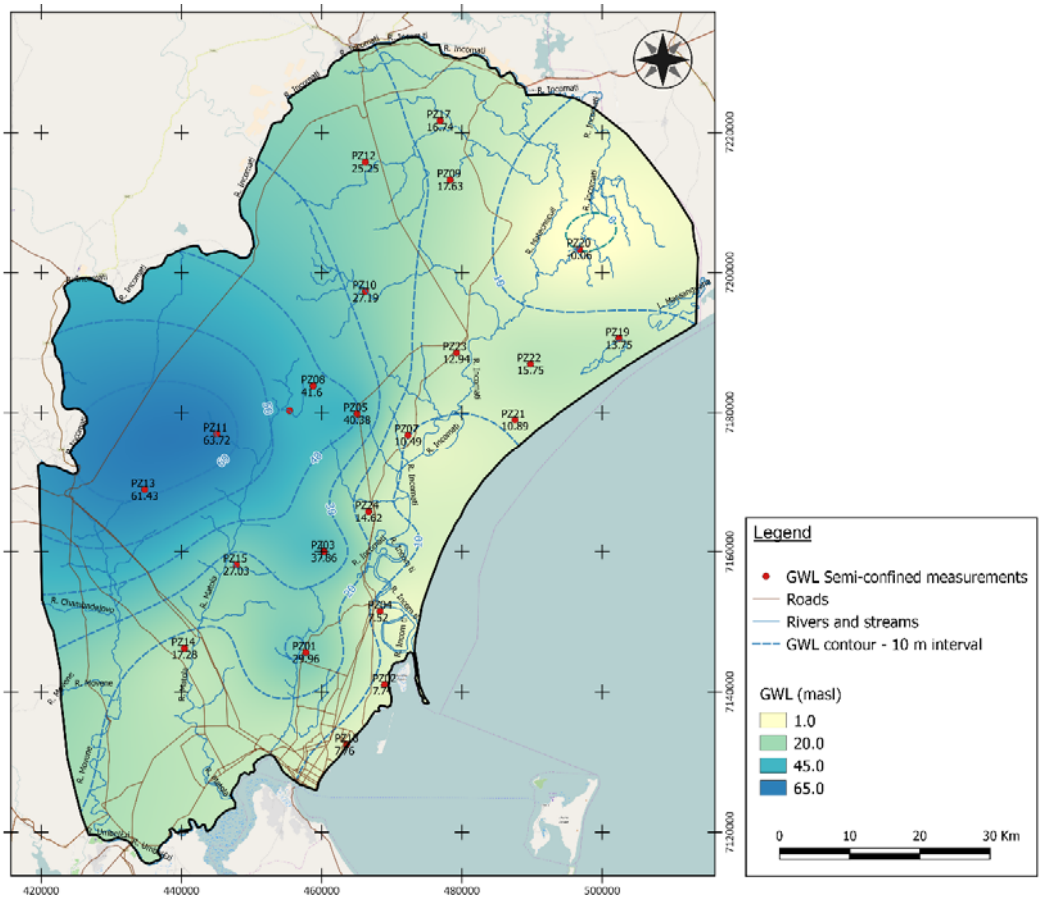

Figure 4-15: Water level contour map for the semi-confined aquifer.

Recharge and discharge zones were delineated using differences between measured phreatic and piezometric levels. In observation wells with two different piezometers it was possible to check whether groundwater flows downwards, from the phreatic aquifer to the semi-confined (recharge areas), or upwards, with leakage-up from the semi-confined aquifer to the phreatic aquifer (discharge areas). Figure 5.10 presents the interpolated map obtained with measured water levels.

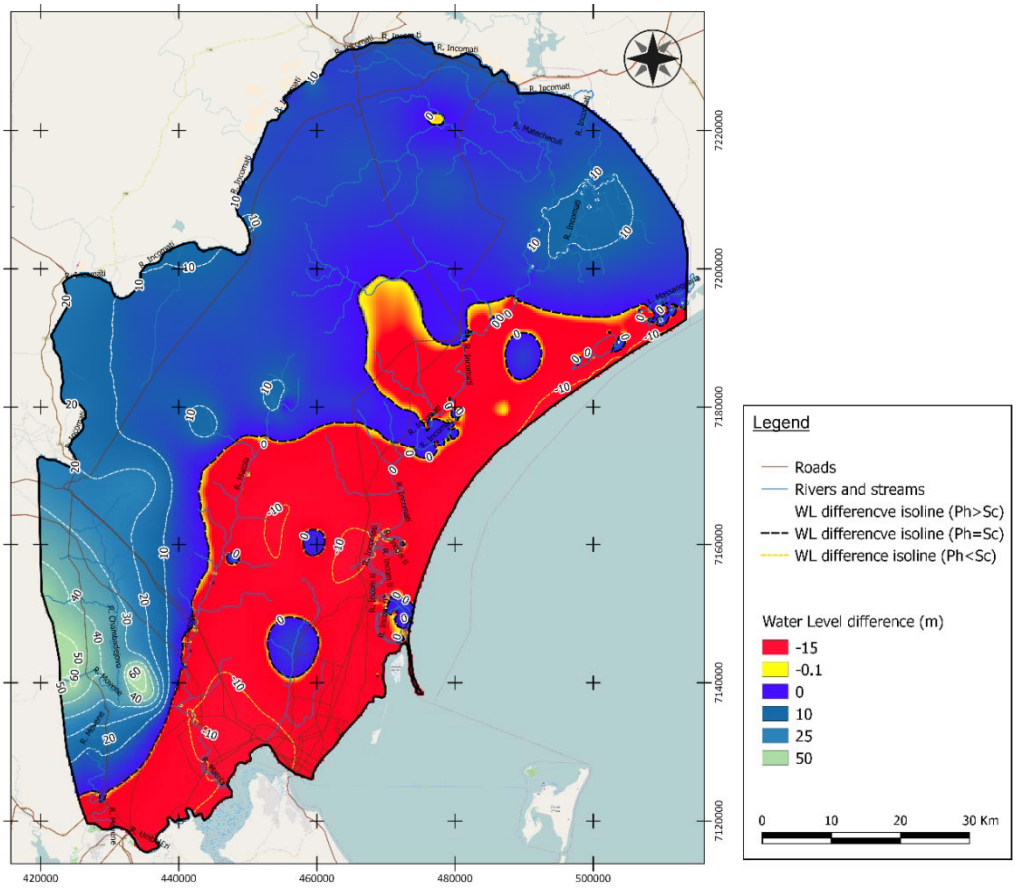

Figure 4-16: Groundwater level difference map. Areas in blue represent zones where groundwater flow downwards (recharge areas); areas in red represents upward flow (discharge areas).

The biggest difference between water levels are located on recharge areas on the East, around 25 m near PZ13. In extrapolated regions (without semi-confined water level data) even 50 m difference is observed. Due to sparse information and interpolation limitations, rivers in the North (Matecheculi River, for instance) appear inside recharge areas although they are expected to act as discharge points from the aquifer. This can be observed in the PZ17, where a very small difference between phreatic and semi-confined water levels is seen (10 cm). Small recharge spots are located especially in the dune areas, which could be greater in reality if more spatial information were available. It is interesting to note that Matola River works as a barrier, where beneath it, groundwater flows upward from the semi-confined aquifer and probably contribute to river discharges together with surface waters and water from the unconfined aquifer.

4.7.2. In situ measurements

Electrical conductivity (EC), HCO_3 and pH should be measured in situ whenever possible due to their easiness of alteration with temperature and time. These parameters also supports initial understanding of water quality and types distribution in the area.

Electrical Conductivity (EC)

The EC is the first indicator of saline waters since it results from the presence of dissolved ions in the water, as mainly Cl and Na. Thus, groundwater presenting high EC values indicate presence of saline waters. In this study, a threshold of 1500 µS/cm was set as a reference value for dividing fresh and saline waters. EC measurements were carried out during sampling. Figure 5.11 presents EC distribution on both aquifers.

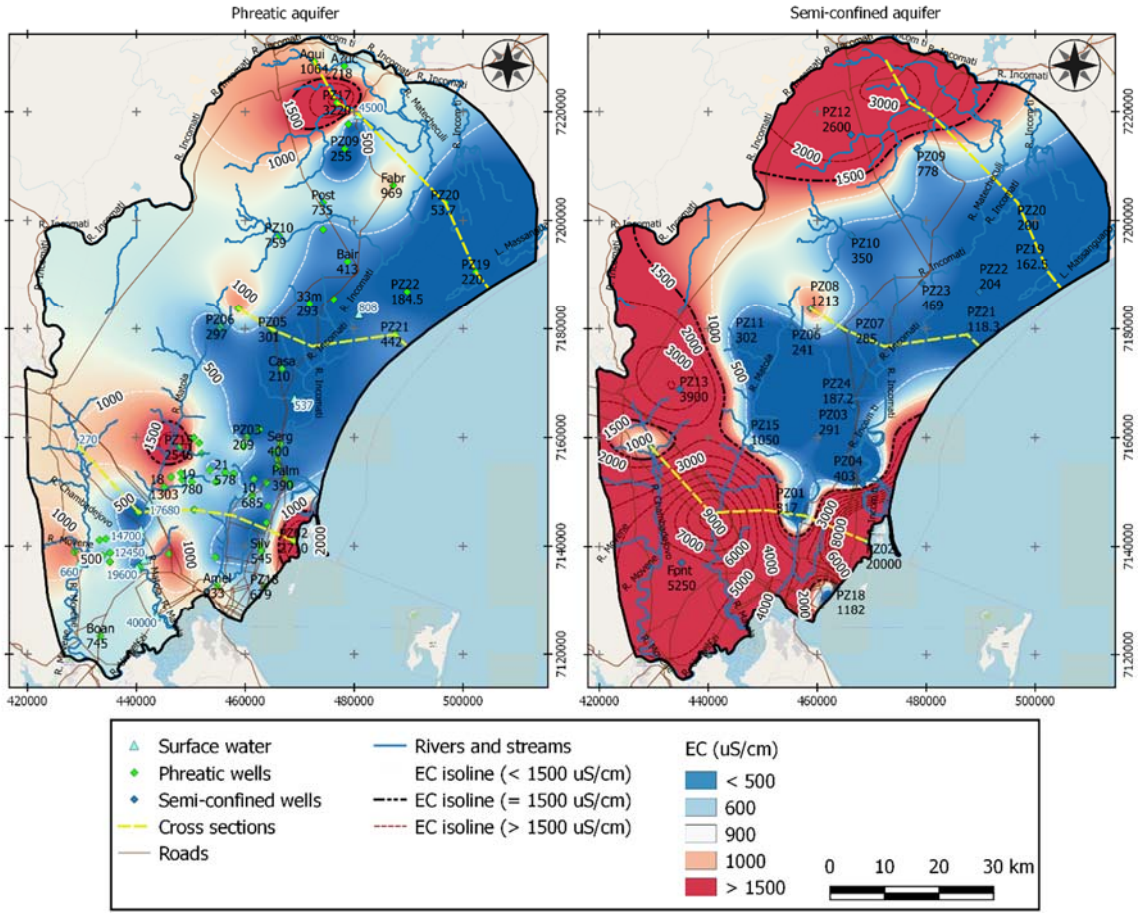

Figure 4-17: EC distribution on both aquifers. Blue colours = fresh groundwater; red colours = brackish groundwater. Yellow lines represent location of EC and WL profiles. Surface water points are presented in blue triangles, together with the phreatic aquifer measurements, although they were not considered for the interpolation.

Two areas inland with EC above 1500 µS/cm are observed in the phreatic aquifer: around south of Matola River (PZ15 = 2546 µS/cm); and in the North, on PZ17 (3220 µS/cm), near Xinavane. Big portion of the study area presents fresh groundwater in the upper levels of the aquifer, as along Incomati valley where measured EC values were below 500 µS/cm. The absence of high EC values in the coast is resulted of shallow wells, which do not reach the interface fresh/saline groundwater, as well as the lack of information in such areas.

In the semi-confined aquifer many inland places present EC above 1500 µS/cm. Areas around Maputo and Matola cities and in the North (near PZ17) present EC up to 9200 and 3200 µS/cm, respectively. It is believed that in the coastal zone the presence of high EC values is a result of natural and human-induced seawater intrusion, but the

high values inland require deeper chemical assess for better understanding, see section 5.3.3. Again, the absence of high EC values in the coast can be explained by the lack information and due to the shallow location of wells. A lens of fresh water is observed on the Southwest of the area (1000 µS/cm) in the semi-confined aquifer, which is believed being linked to the lake at the surface and possible good connection between aquifers in this region allowing fresh waters to reach deeper levels.

Fresh/salt water interface depths were check using a probe to create EC vertical profiles along piezometers. The available ARA-Sul probe (Solinst 107 TLC meter) was currently not-calibrated and required calibration was not possible to be carried out in the field. Therefore, a manual calibration using the hand EC-meter was done. Samples measured with the probe and with the hand EC-meter were used to build a calibration curve. A linear relationship was the best fit among the values ($R^2 = 0.969$), Appendix C. However not accurate, this approach allows at best a qualitative assessment of the position of fresh and saline water interface. The interface is shown in cross section views distributed along the study area, Figure 5.12-5.14. The location of each cross section is shown in Figure 5.11.

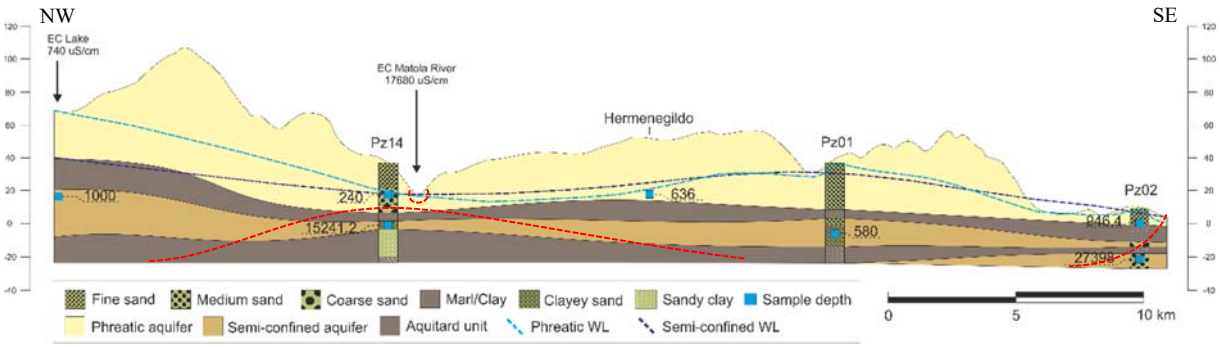

Figure 4-18: Cross section view of EC (µS/cm) and WL from "Lake-well" to PZ02. Dashed light blue line= phreatic WL; dashed dark blue line = semi-confined WL; Measurements shown in blue squares with EC. Dashed red line represents inferred fresh/brackish watetr interface.

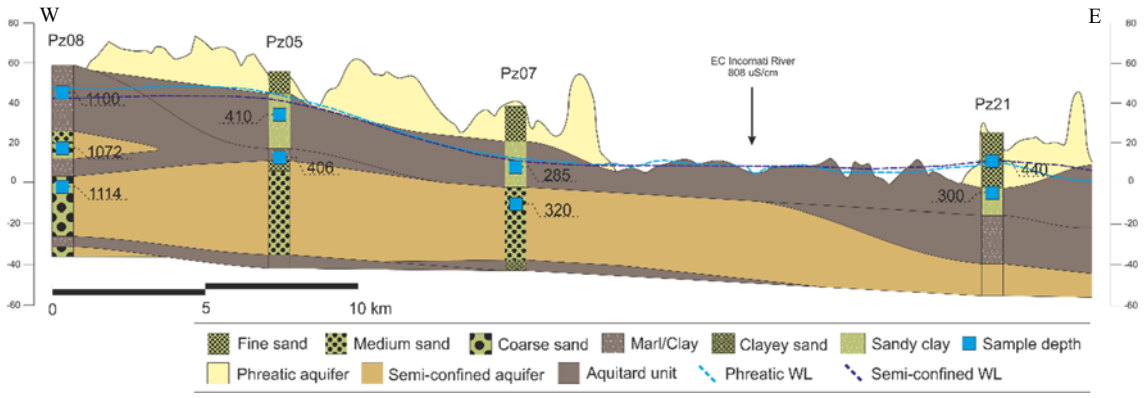

Figure 4-19: Cross section view of EC (µS/cm) and WL from PZ08 to PZ21. Dashed light blue line = phreatic WL; dashed dark blue line = semi-confined WL; Measurements shown in blue squares with EC.

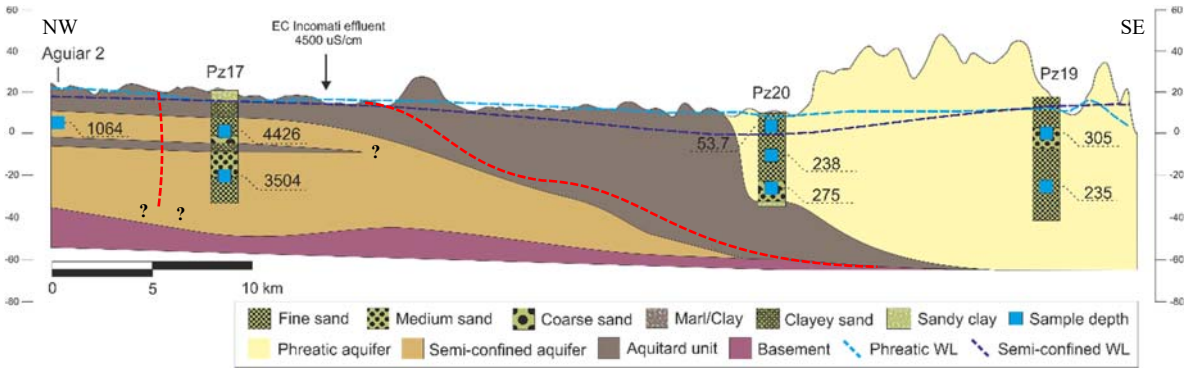

Figure 4-20: Cross section view of EC (µS/cm) and WL from "Aguiar 2" to PZ19. Dashed light blue line=phreatic WL; dashed dark blue line=semi-confined WL; Measurements shown in blue squares with EC. Dashed red line represents inferred fresh/brackish watetr interface.

Like observed in the maps, East portions of both aquifers appear with low EC values in comparison with the West side Stratification of fresh and saline waters is clearly seen in piezometers PZ02 and PZ14. The high values in PZ02 can be linked to seawater intrusion. High EC is persistent in inland regions, as observed in PZ08, PZ14 and PZ17, as well as in surface waters, which probably represents groundwater that seepages from the aquifer. The same can be depicted from the stream water near PZ17. Further discussion of salinity origin is presented in section 5.3.3.

Bicarbonate (HCO3)

The presence of bicarbonate (HCO_3^-) in groundwater can be explained by reactions between water and CO_2 in the soil, and weathering of sodic silicate mineral and/or carbonate minerals existing in the aquifer material, for example, Equation 5.2 – Equation 5.5, respectively:

$$CO_{2\,(g)} + H_2O \rightarrow H^+ + HCO_3^- \quad \text{Eq 5.2}$$

$$2NaAlSi_3O_8 + 2H_2CO_3 + 9H_2O \rightarrow Al_2Si_2O_5(OH) + 2Na^+ + 2HCO_3^- + 4H_4SiO_4 \quad \text{Eq 5.3}$$

$$CaCO_{3\,(s)} + H_2CO_3 \rightarrow Ca^{2+} + 2HCO_3^- \quad \text{Eq 5.4}$$

$$CaMg(CO_3)_2\ (\text{Dolomite}) + H_2CO_3 \rightarrow Ca^{2+} + Mg^{2+}\ 4HCO_3^- \quad \text{Eq 5.5}$$

So that, HCO_3 is an indication of two aspects: dissolved CO_2 and dissolved calcite in water, where higher values of HCO_3 indicate a higher mineralization, hence longer groundwater residence time in the aquifer. Figure 5.15 shows the HCO_3 distribution on phreatic and semi-confined aquifers.

High HCO_3 concentrations in the south of the study-area are clearly seen in both aquifers (around 400 mg/L), while in the North, lower concentrations are observed in dune areas and areas with high recharge potential (around 50 mg/L and below) apart of small pockets of moderately high values in the coast and around Xinavane (PZ17). Furthermore, the high values in the south can indicate higher presence of Ca-minerals, while low values suggest a low mineralization, usually related to a rapid downward flow.

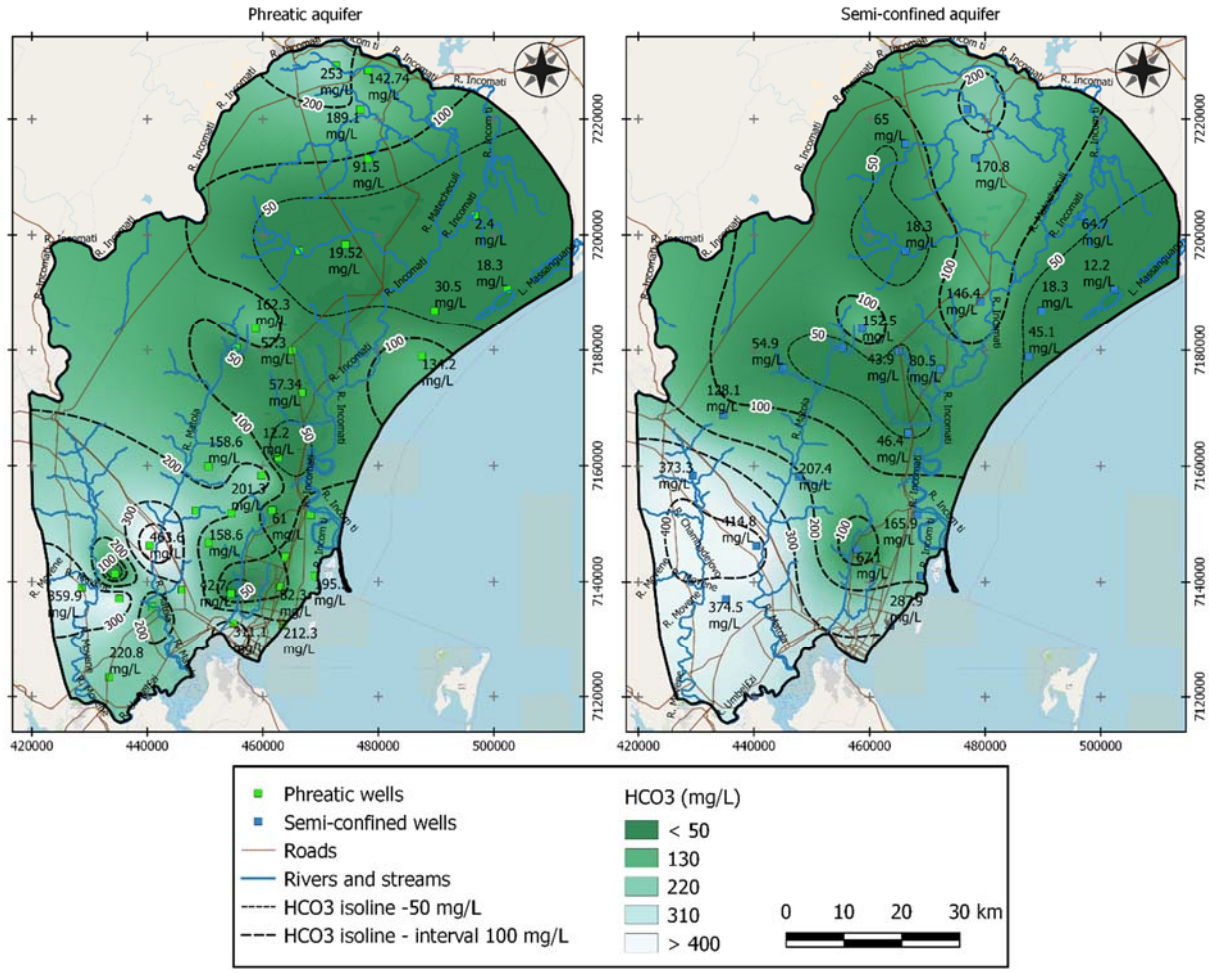

Figure 4-21: Bicarbonate (HCO_3) distribution in the phreatic and in the semi-confined aquifer. Areas with high HCO_3 show in lighter colours, and areas with low HCO_3 show in dark greener colours.

Despite of the separation of both aquifers in North (low HCO_3) and South (high HCO_3), the North section of the semi-confined aquifer can also be subdivided in East and West portions: The first shows very low values of HCO_3 (around and below 50 mg/L), indicating a preferential vertical flow from the phreatic aquifer and good connection with it in this region; while in the West, higher values are observed around Incomati river and its effluents. This pattern can be related to the thick aquitard unit existing in the region and below Incomati River, which splits the system in two unconnected hydrosystems and avoids mixing of coastal groundwater and inland groundwater to

happen, as apparent in cross section view in Figure 5.14. However, no information concerning hydraulic conductivity of the aquitard unit is currently available for the area to support further discussion.

4.8. Hydrochemical Facies and Water Types

This section presents the results and discussion concerning classified water types and hydrochemical facies of Great Maputo area. First sub-sections present resulting water types groups, and following sub-section discuss obtained results and hydrochemical facies analyses.

4.8.1. Water samples post-processing

Collected samples were analysed to obtain physicochemical parameters for water type classifications and hydrochemical facies analyses. Lab results accuracy were checked through samples ion balance error (Equation 3.3). Only three samples presented absolute ion error between 20 and 25% and their results were carefully considered, while majority of samples showed acceptable absolute ion error below 5% (Hiscock and Bense, 2014), Figure 5.16. PZ14C sample initially presented an error of 68%, but its re-analysis resulted in an error below 2%. For isotopes, each sample was analysed at least two times, and until a deviation of less or equal 2 ‰ between different runs was achieved for $\delta^{18}O$ and $\delta^{2}H$, personal communication (Wenninger J., 2017).

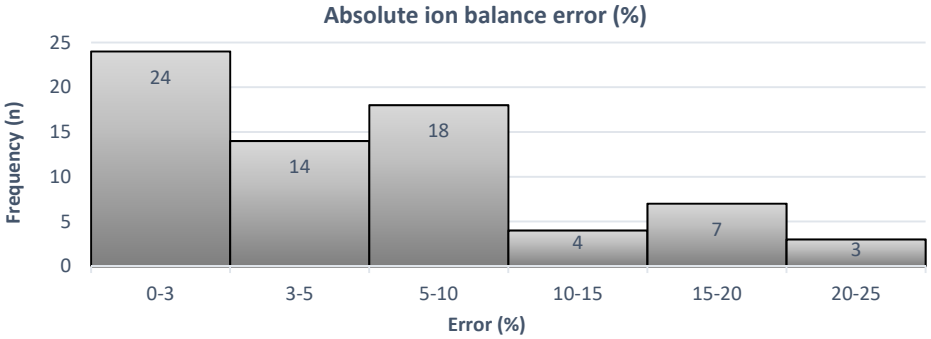

Figure 4-22: Histogram of ion balance error of collected samples. Numbers inside bars represent number of samples within the range.

4.8.2. Results of the grouping into water groups

Water types were defined according to their main physicochemical parameters and Stuyfzand (1989) scheme. Water groups were further achieved based on a hierarchical cluster analysis (HCA) for a better understanding of sample relations and similarities. After different try-outs, 13 variables were considered for cluster analysis - EC, pH, Na, K, Mg, Ca, Cl, HCO_3, SO_4, NO_3, Na/Cl, SO_4/Cl, $\delta^{18}O$. Different parameters selection and combinations showed similar results and the later combination (13 variables) was selected for the research purpose. Only

parameters common for all samples are considered for clustering and, therefore, Br/Cl ratios, for instance, were not selected. Ward's method for linkage was applied in accordance with other authors methods (Andrade and Stigter, 2011; Ghesquière et al., 2015; Güler and Thyne, 2004). A City Block Distance (CDB) as similarity measurement was chosen instead of Euclidean distance because CDB can damp big differences existing between variables, which makes other parameters play a bigger role in the clustering. This derives similar results to Euclidean distance while avoiding excessively relevance to a parameter. Also, definition of water groups above drawn phenonline were done facing the similarity of samples (WT-4 and WT-6 originally derived two clusters). The full cluster analysis and descriptive statistic of physicochemical parameters are presented in Appendix D.

Table 5.4 presents main parameters and characteristics of six major water groups (WT) defined in the area. Figure 5.17 presents a Piper plot of the water samples, and Stiff diagrams with mean values of each water group. Figure 5.18 covers some of main plots and binary charts for the water groups. The location of water samples labelled according to their respective groups is shown in Figure 5.20 at the end of this sub-section. The plots and tables are discussed below for each water group.

Table 4-5: Main physicochemical parameters of major water groups.

WT groups	**WT-1**	**WT-2**	**WT-3**	**WT-4**	**WT-5**	**WT-6**
Number of samples	*32*	*12*	*13*	*6*	*2*	*1*
EC (µS/cm)	53-300	640 - 740	930 - 1460	2600 - 5250	14700 - 17680	9200
Type *(Stuyfzand - Cl conc)*	Fresh (g-f)	Fresh (F-f)	Fresh-Brackish (F-f)	Brackish (B-b)	Brackish-salt (b)	Brackish-salt (b)
Cl (meq/L)	< 4	1 – 5	2.8 – 7.5	18 – 35	150 – 185	59
Alkalinity *(HCO3 meq/L)*	Low - moderately high (<0.5 - 7.7)	Low - moderate (0.1 - 4.1)	Moderately high (2.3 - 6.2)	Moderately high (1.1 – 6.2)	Moderately high (6.4 – 7)	Moderately high (3)
SI calcite	Undersaturated	Undersaturated in HCO3 and NaCl types; In equilibrium in other water types	In equilibrium	Varying	In equilibrium	Slightly supersaturated
Na/Cl	High (1.08)	Very high (1.48)	Very high (1.37)	Low (0.73)	Very low (0.51)	Low (0.78)
Cl/HCO3	Moderately Low (2.6)	Moderate (5.7)	Low (1.4)	High (7.6)	Very high (26.3)	High (8.5)
Br/Cl	0.0377	0.0018	0.0013	0.0013	0.0012	0.0015
Dominant water types	NaCl, Na-CaHCO3	NaCl, NaHCO3	NaCl, NaMIX	NaCl, $CaCl_2$	NaCl, MgCl	NaCl
Other characteristics and remarks	Low SO4, bimodal Ca	High Na, Ca and SO4; High NO3 near Matola	High Mg/Ca ratios	Depleted and constrained $\delta^{18}O$	High negative BEX; (Matola River)	Only one sample (PZ14C)

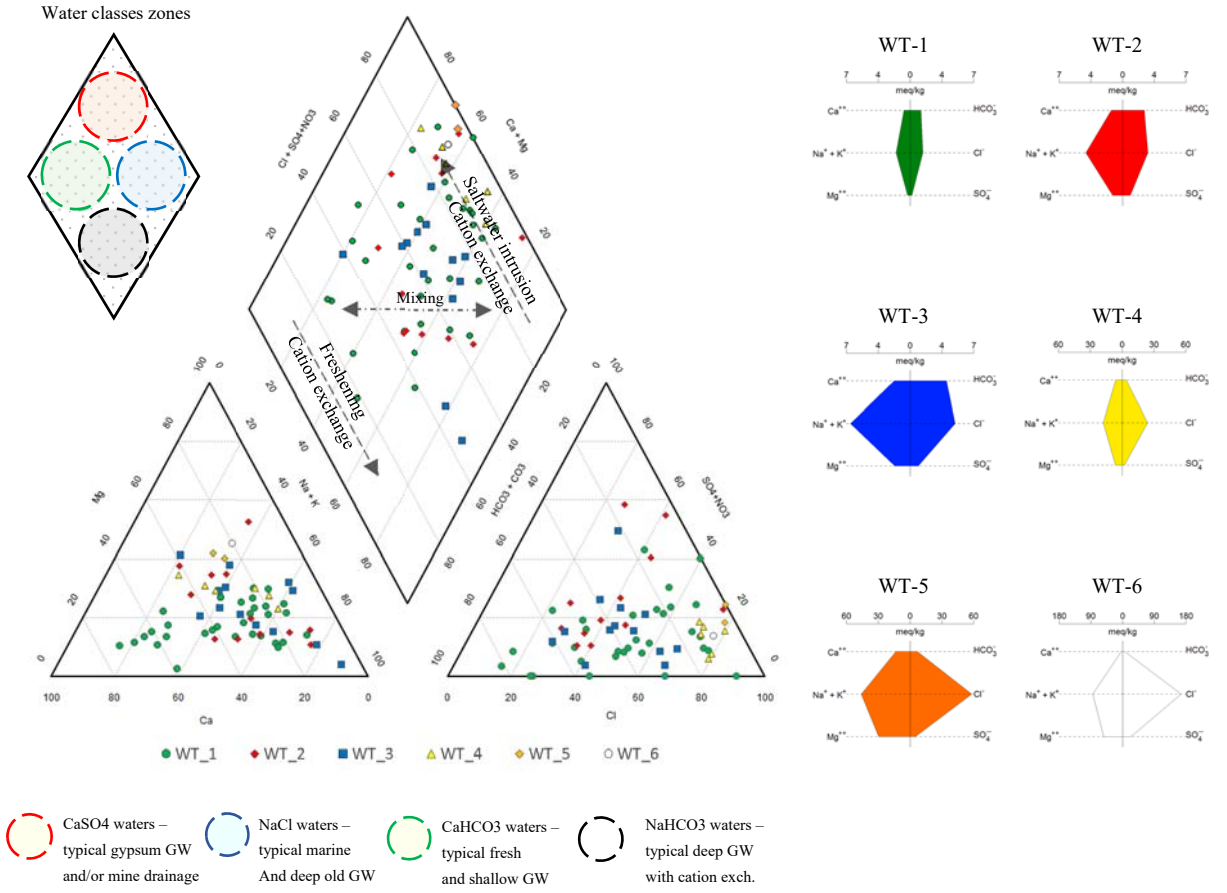

Figure 4-23: Piper plot of groundwater samples labelled as water groups (values in % of meq/L); and Stiff diagrams with mean values from each water group (values in meq/kg – note varying scales).

Major proportion of samples are classified as NaCl-subtype (51.5%), varying from fresh to brackish-salt according to Cl concentration. 82.3% of samples are fresh (Cl < 8.4 meq/L), and 17.6% are brackish/salt (8.4 meq/L < Cl < 282 meq/L), Appendix D. 6.7% of samples are $NaHCO_3$ subtype, 12.1% are Na/Ca/MgMIX, and 9.1% are $CaHCO_3$, all presenting Cl < 8.4 meq/L. 7.6% of samples are classified as $CaCl_2$ subtype, among fresh and brackish-salt waters.

The Piper plot does not show all water groups as clearly since samples are spread with different compositions and proportions, even within defined water groups. This is especially true for WT-1, WT-2 and WT-3 since brackish/saline waters (WT-4, WT-5 and WT-6) plot around NaCl/$CaSO_4$ water classes. Moreover, Table 5.4 and Stiff diagrams (Fig 5.16) show two main distinguished: fresh waters, low TDS (WT-1, WT-2 and WT-3) and brackish-salt waters, high TDS (WT-4, WT-5 and WT-6). Water groups show a big range in SAR diagram, Appendix D, with WT-1, WT-2 and WT-3 showing a low, WT-4 a medium and WT-6 a very high sodium hazard. WT-5 has a relatively extreme high EC, which can be classified as extreme high hazard. None of the samples presented NO_3^- concentrations above 50 mg/L, threshold for potable drinking water (WHO, 2011), while higher values were measured Matola peri-urban area (20 - 40 mg/L) in the unconfined aquifer, Appendix D.

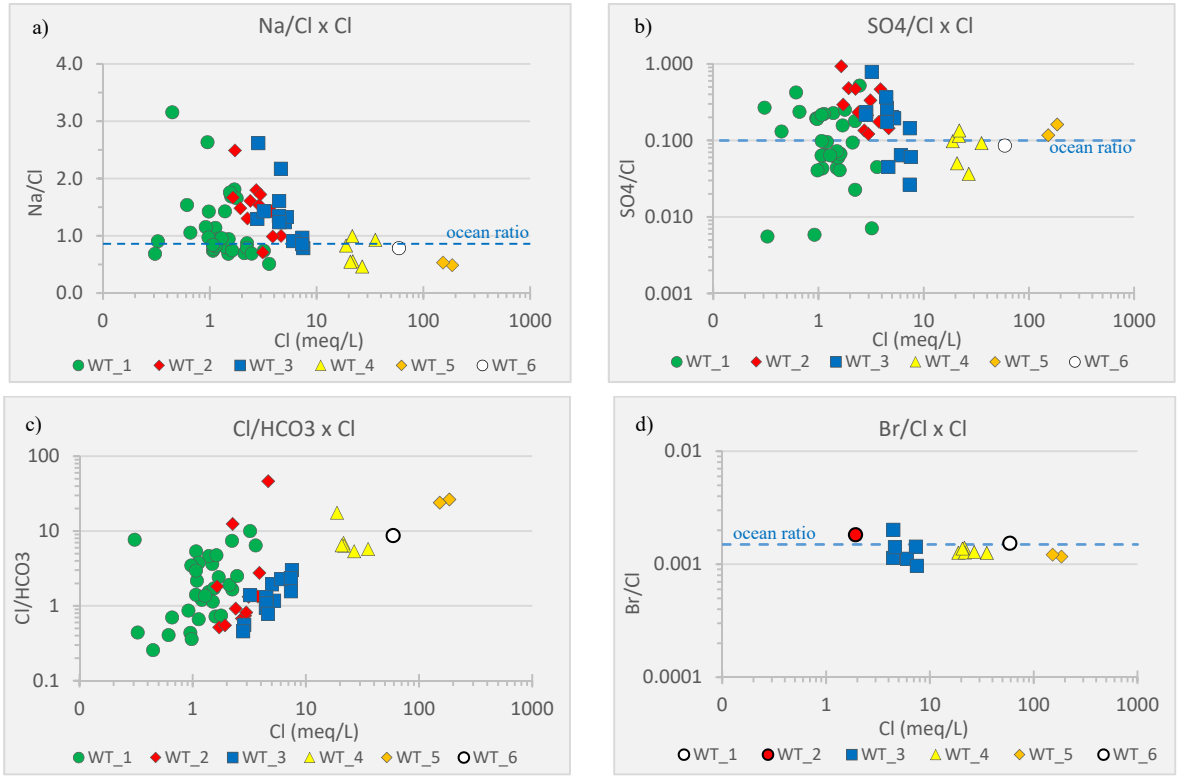

Figure 4-24: Main chemical components and binary charts for water groups labelled according to WT; Dashed blue lines represent mean ocean value for different ratios.

Figure 5.19 shows δ^2H vs $\delta^{18}O$ plot, together with rainfall samples, LMWL, GMWL (Craig, 1961) - Equation 2.1, and LMWL-GNIP (Steinbruch and Weise, 2016). Regarding isotopic data, samples show a wide range of values: δ^2H between -26.5‰ and +4.4‰, and $\delta^{18}O$ between -4.6‰ and +0.2‰. Groundwater samples are mostly isotopically depleted and falling above meteoric lines, while surface water samples (WT-5) fall below meteoric lines, and around rainfall samples and VSMOW (Vienna Standard Mean Ocean Water). Rainfall samples show an enriched isotopic average composition of $\delta^{18}O$ = -0.8‰ and δ^2H = +8.4‰. LMWL ($\delta^2H = 9.2*\delta^{18}O + 16.34$, $R^2 = 0.69$) was obtained through linear regression of four collected rainfall samples. Although with small R^2 and small spatial-temporal representativeness, LMWL is in agreement with LMWL-GNIP showing similar slope and interception (9.2 and 8.7, and 16.34 and 15.5, respectively), equally greater than GMWL values. The distribution of samples is further discussed in section 5.3.3.

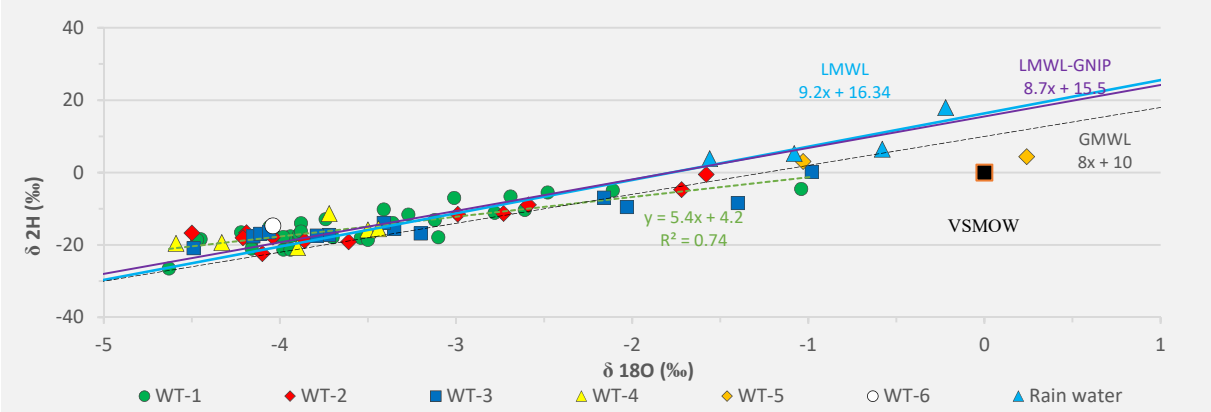

Figure 4-25: δ^2H vs $\delta^{18}O$ plot. Samples labelled according to WT groups. GMWL (black dashed line), LMWL from this study (blue line), LMWL-GNIP (purple line) and their respective equations, and VSMOW are also presented. Green dashed line represents regression line of groundwater samples, with slope equal to 5.4 (further discussed in section 5.3.3). Blue triangles represent collected rainfall samples.

Water Group WT-1

WT-1 represents the vastest group of waters in the area (32 samples). These samples are fresh waters (g-f), with a low mean EC of 299 µS/cm. Mean Na/Cl ratio is 1.137, above ocean ratio, but with a big range (0.7 – 1.137).However, these waters present a high standard deviation in Cl/HCO_3, 2.46 meq/L (Appendix D), showing a wide range in HCO_3, Ca and SO_4 concentrations, as well as in isotopic signature (-26.5‰ < δ^2H< -4.5‰, and -4.6‰ < $\delta^{18}O$ < -1.0‰). Further subgrouping of WT-1 is discussed in next sections. WT-1 samples are mainly located in dune areas in both the phreatic and semi-confined aquifers, Figure 5.20.

Water Group WT-2

WT-2 consists of 12 groundwater samples, presenting a small range of EC, between 640 and 740 µS/cm, and Cl between 1 and 4.6 meq/L, fresh waters class (F-f). Mean Na/Cl ratio is very high (1.479) with few samples below ocean ratio and decreasing with increasing Cl concentration, Figure 5.17. This group shows high SO_4/Cl and low Ca/SO_4 ratios, and as in WT-1, it also shows a great range in HCO_3 and SO_4, as well as in Mg and Ca concentrations. A big range in isotopic composition (-22.4‰ < δ^2H< -0.5‰, and -4.5‰ < $\delta^{18}O$ < -1.5‰) is observed for this water group. WT-2 samples are mainly located around peri-urban areas of Maputo and Matola cities. The samples differ from WT-1 samples due to their higher EC, and higher Cl, Mg, and Na concentrations.

Water Group WT-3

WT-3 is characterized by fresh-brackish waters (F-f), with EC between 930-1460 µS/cm and Cl between 2.8-7.5 meq/L. Na/Cl ratio is generally above ocean ratio, with mean value of 1.368. The 13 groundwater samples show high HCO_3 concentrations (2-6 meq/L). Due to high alkalinity, Cl/HCO_3 ratio is not higher than that of WT-1 and WT-2 (on average even lower), Figure 5.18. Mg and SO_4 concentrations are also higher than previous water types. Ca shows a concentration range close to other WT's, Appendix D, and SI in respect to calcite is around equilibrium

for samples of WT-3, different from WT-1 and WT-2 (generally undersaturated). The Br/Cl ratio shows a big range, from above to below ocean water ratio (3E-04 to 2E-03). WT-3 samples show a bimodal isotopic composition, with samples mostly depleted (-20.9‰ < δ^2H< -16.8‰, and -4.5‰ < $\delta^{18}O$ < -3.2‰), and some isotopic enriched (-6.9‰ < δ^2H< +0.2‰, and -2.2‰ < $\delta^{18}O$ < -0.1‰). Samples of WT-3 are mainly found along the Matola River in both aquifers (southwest of study area), and near Maputo coastal zone, Figure 5.20.

Water Group WT-4

WT-4 represents a group with six samples, represented by brackish/salt waters with EC ranging between 2600-5250 µS/cm and Cl concentration between 18 and 35.4 meq/L. Na/Cl ratio is usually below ocean ratio and mean value equals 0.72, Figure 5.18. The samples present a moderate alkalinity (between 1.1 and 6.1 meq/L), with a high standard deviation, Appendix D. Br/Cl ratio of WT-4 samples plots slightly below ocean value and mean value equals 0.0013. The samples are isotopically depleted and constrained between -19.5‰ and -15.5‰ for δ^2H and -4.6‰ and -3.4‰ for $\delta^{18}O$. WT-4 differs from previous WT's due to higher Cl and Na concentrations, as well as somewhat higher Ca, Mg and SO_4 concentrations. The samples are located near the western border of the study area in the North and near Matola River in the South in the semi-confined aquifer, as well as close to the coastal zone of Maputo (PZ02F) and near Xinavane (PZ17F) in the unconfined aquifer, Figure 5.20.

Water Group WT-5

WT-5 consists of two surface water samples. EC is the highest among samples, 14700 and 17680 µS/cm, the same is true for Cl concentrations (152.3 and 185.2 meq/L), Figure 5.18. Moderate-high alkalinity (around 6 meq/L) and low Na/Cl and Br/Cl ratios are observed in water samples from this group, 0.51 and 0.0012, respectively. SO_4 concentrations are high compared to other samples, as well as SO_4/Cl ratios, being slightly above ocean ratio, Appendix D. Water samples of this group show enriched isotopic composition, ranging from +3.1‰ to +4.4‰ for δ^2H, and from -1.0‰ to +0.2‰ for $\delta^{18}O$, close to rainfall samples and VSMOW. Samples of WT-5 were taken from Matola River, in the southwest of the study area.

Water Group WT-6

WT-6 is represented by only one water sample, showing singular characteristics in comparison with other WTs, therefore, being in a separate group. EC is 9200 µS/cm and Cl equals 59 meq/L. Na/Cl, SO_4/Cl and Br/Cl ratios are near ocean value (Fig 5.17), while Mg and Na concentrations are rather high, Appendix D. The sample shows depleted isotopic composition (δ^2H = -14.7 ‰ and $\delta^{18}O$ = -4.0‰) and is located in the semi-confined aquifer (PZ14C), near Matola River (southwest of study area).

From Figure 5.20 it is clear that fresh waters dominate in the unconfined aquifer, mainly NaCl and $NaHCO_3$ subtypes, except for a small area in the north and in the coast with a pocket of brackish water (PZ17 and PZ02). Near urban areas, mostly WT-2 group is observed with MIX in the anion part, followed by $NaHCO_3$ subtype. However, MIX water subtypes present at max Cl = 5.2 meq/L, Appendix D, and are classified as freshwaters.

For the semi-confined aquifer NaCl is the dominant subtype. Fresh waters (WT-1) are observed in dune areas, while another great portion of samples are brackish/saline waters, like in the trench to West of Matola River until

PZ17 (Cl between 26 and 59 meq/L -WT-4 and WT-6). $CaCl_2$ water subtypes are the second dominant group in the semi-confined aquifer, which occurrence will be further discussed in next sections.

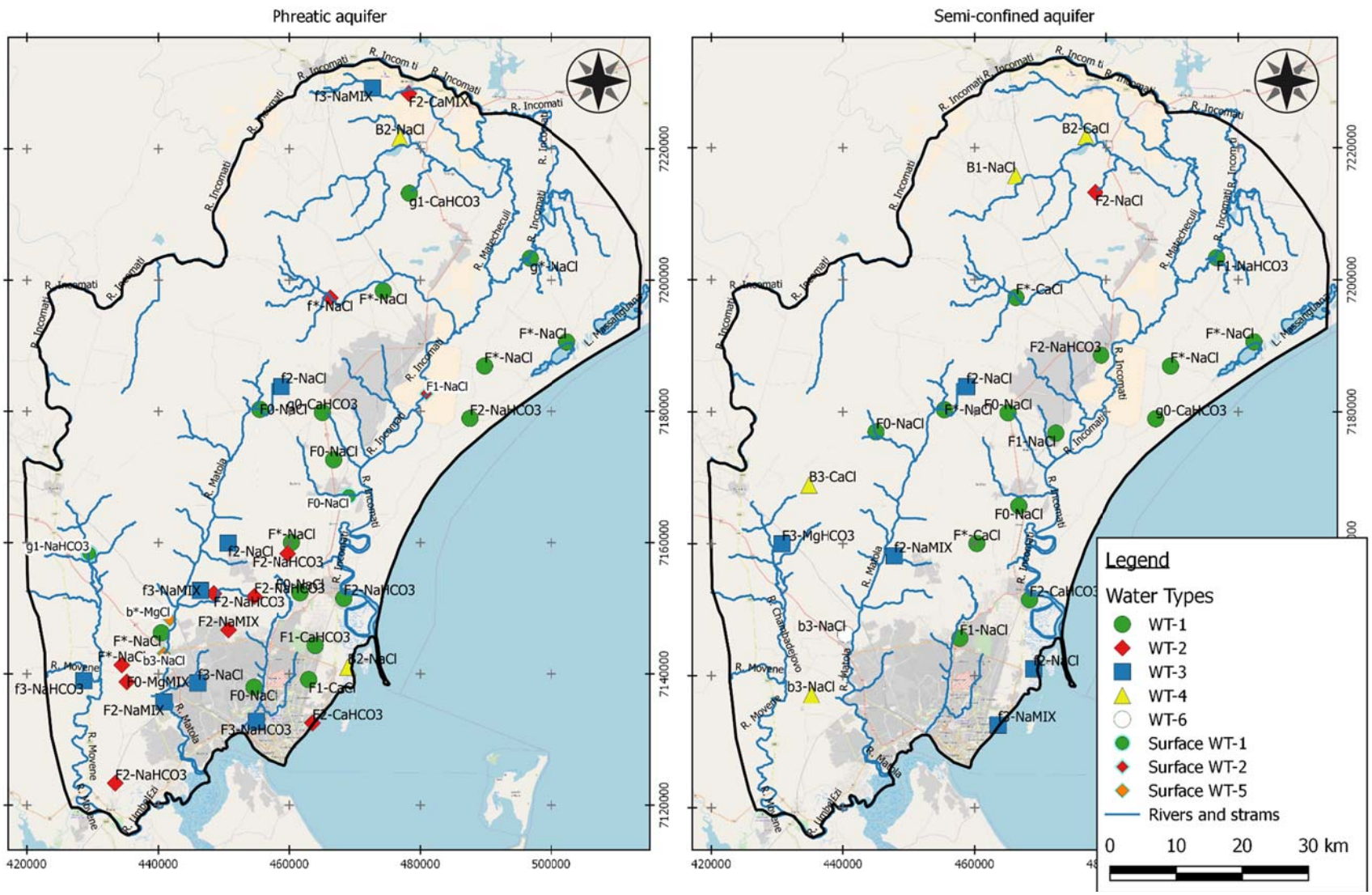

Figure 4-26: Distribution of water types on phreatic and semi-confined aquifers. Surface water samples are presented with highlighted polygons and buffered labels together with phreatic aquifer samples.

4.8.3. Discussion of hydrochemical processes for classified water groups

Upon infiltration and subsurface flow, different processes and factors influence groundwater chemistry. Rock weathering/dissolution is the main sources for ions in groundwater, followed by mixing and evaporation, the last one leading to an overall increase in TDS. These processes are better depicted and differentiated through hydrochemical and isotopic data examination, and corroborated by additional modelling. Mixing models are generally based on conservative elements (as Cl and/or δ18O) and do not account for reactions changing other ions concentrations, as, for example, cation exchange, which result in deviations from purely mixing lines. So that, hydrogeochemical modelling through PhreeqC was carried out aiming the identification of such reactions leading to observed WT compositions.

The Gibbs diagrams (Gibbs, 1970) are widely applied for assess dominant natural effects on groundwater chemistry in arid and semi-arid regions (Feth and Gibbs, 1971; Naseem et al., 2010; Marghade et al., 2012; Yang et al., 2012b; Xing et al., 2013 *apud* (Liu et al., 2015)). The diagrams present $Cl^-/(Cl^-+HCO_3^-)$ and $Na^+/(Na^++Ca^{2+})$ ratios vs TDS, within domains of precipitation, rock and evaporation/seawater as hydrochemical controlling processes. The $Cl^-/(Cl^-+HCO_3^-)$ ratio refers to mineralization degree, while the $Na^+/(Na^++Ca^{2+})$ ratio expresses cation characteristics of the sample, either more Na or Ca dominant. Figure 5.21.

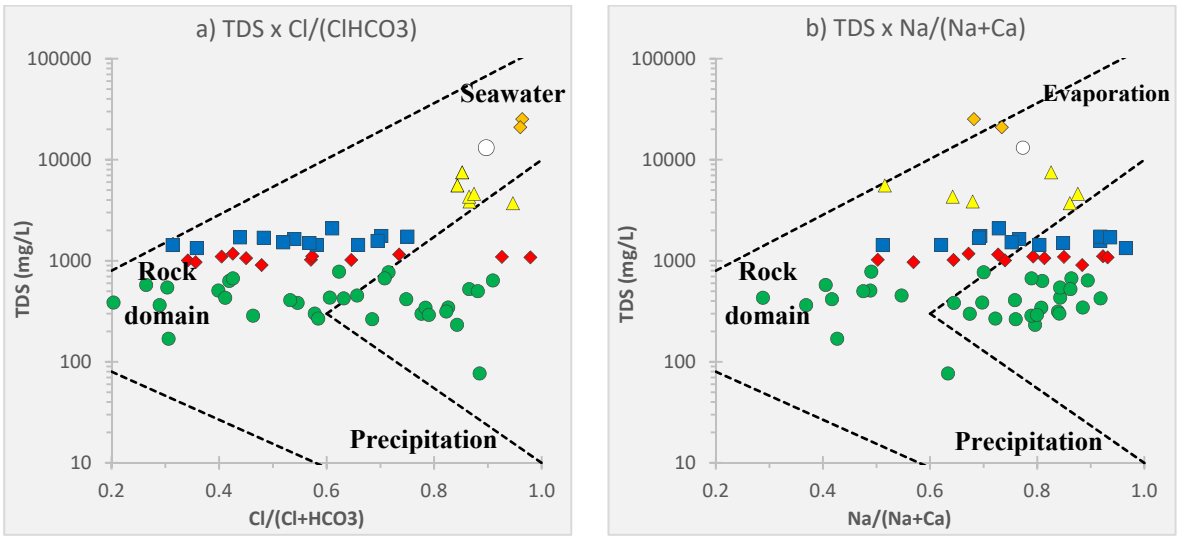

c) Gibbs diagrams:

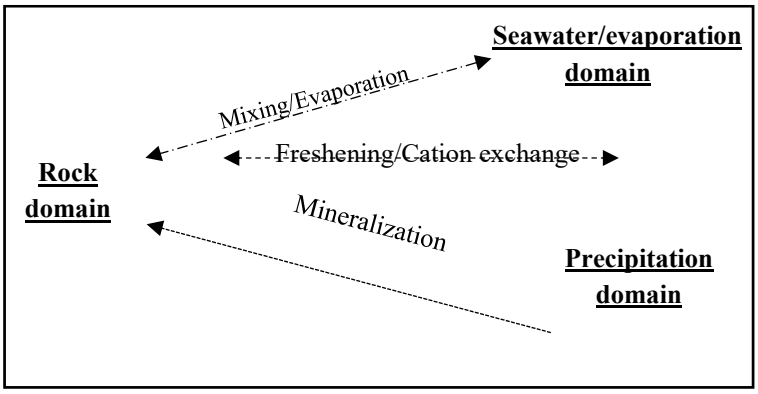

Figure 4-27: Gibbs diagrams of groundwater samples classified as water types groups. a) TDS vs $Cl/(Cl+HCO_3)$; b) TDS vs Na/(Na+Ca). Colours and symbols are the same as previous figures; c) Gibbs diagrams processes and domains.

The spread of samples in both diagrams indicates that more than one factor influences their hydrochemistry. Fresh waters (WT-1, WT-2 and WT-3) plot around rock domain, suggesting rock weathering/dissolution as dominant mechanism controlling hydrochemistry of these groups (Ghesquière et al., 2015; Narany et al., 2014). Evaporation and mixing with seawater begin to influence water chemistry with increasing TDS as observed for the brackish/salt water samples (WT-4, WT-5 and WT-6).

Further, the large range in ratios with small changes in TDS, especially in freshwaters indicates that they can have different origins, influenced by local land user/cover, geology or source. Therefore, two subgroups can be defined in WT-1: WT-1a) samples with strong Na character, representing recently infiltrated waters with a minor rock interaction, hence low TDS and high $Cl^-/(Cl^-+HCO_3^-)$ and $Na^+/(Na^++Ca^{2+})$ ratios, between 0.6 and 1 in both cases. These samples present δ18O slightly below recent rainwaters, are greatly under saturated in respect to calcite, and are mainly located in the dune areas showing a NaCl or $NaHCO_3$ water subtypes class; WT-1b) freshwaters somewhat influenced by mineralization, with calcite saturation index near equilibrium and with higher values of HCO_3 and Ca derived from minor water-rock interaction, and weathering processes resulting in $CaHCO_3$ or $CaCl_2$ water subtypes. However, no other characteristic is clear to further sub-group WT-1 samples and they are treated as one major group. WT-4, WT-5 and WT-6 groups present higher $Cl^-/(Cl^-+HCO_3^-)$ in comparison with $Na^+/(Na^++Ca^{2+})$ ratios, indicating influence of salinization from mixing and/or evaporation accompanying rock weathering/dissolution.

Moreover, the great variation of $Na^+/(Na^++Ca^{2+})$ without big changes in TDS also indicates that cation exchange takes place in the system, as TDS remain near constant whereas Na exchanges for Ca (Aghil et al., 2017; Ghesquière et al., 2015). Water subtypes as $NaHCO_3$ and $CaCl_2$ supports occurrence of cation exchange, as explained in section 2.3.1. Simultaneous freshening ($NaHCO_3$ subtype) and salinization ($CaCl_2$ subtype) in different parts of the aquifer can be linked to changing in groundwater levels and flow directions at local scale, as well as mixing of different waters with different origins (Han et al., 2011). For example, cation exchange upon salinization results in decreasing of Na/Cl ratio due to uptake of Na by the complex (Appelo and Postma, 2005; Ghesquière et al., 2015), which can be expected for WT-4 and WT-5, Figure 5.22, and it is further discussed in next sextions.

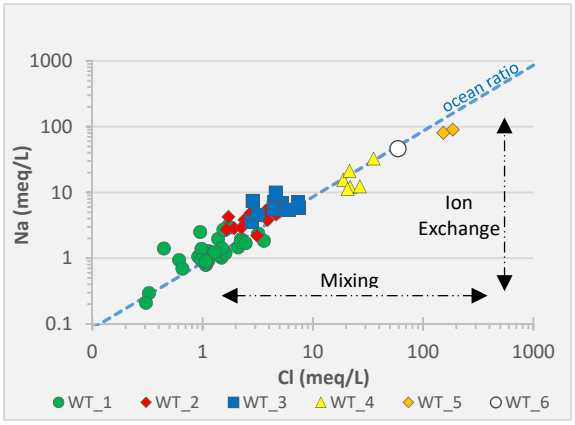

Figure 4-28: Na vs Cl log-plot, together with Na/Cl ocean ratio. Ion exchange upon salinization reduces Na/Cl towards below ocean ratio, as seen in samples of WT-4 and WT-5 in the plot.

The samples spread in the Na vs Cl plot indicates they can result from cation exchange and somewhat influenced by mixing (Ghesquière et al., 2015). High Na/Cl ratios in fresh waters support that silicate weathering plays an important role on controlling hydrochemistry, further discussed in next sections. Saturation indices in respect to calcite, dolomite, gypsum and halite are mainly below zero, suggesting that dissolution of these minerals is an ongoing process whenever they are present in the aquifer, Figure 5.23.

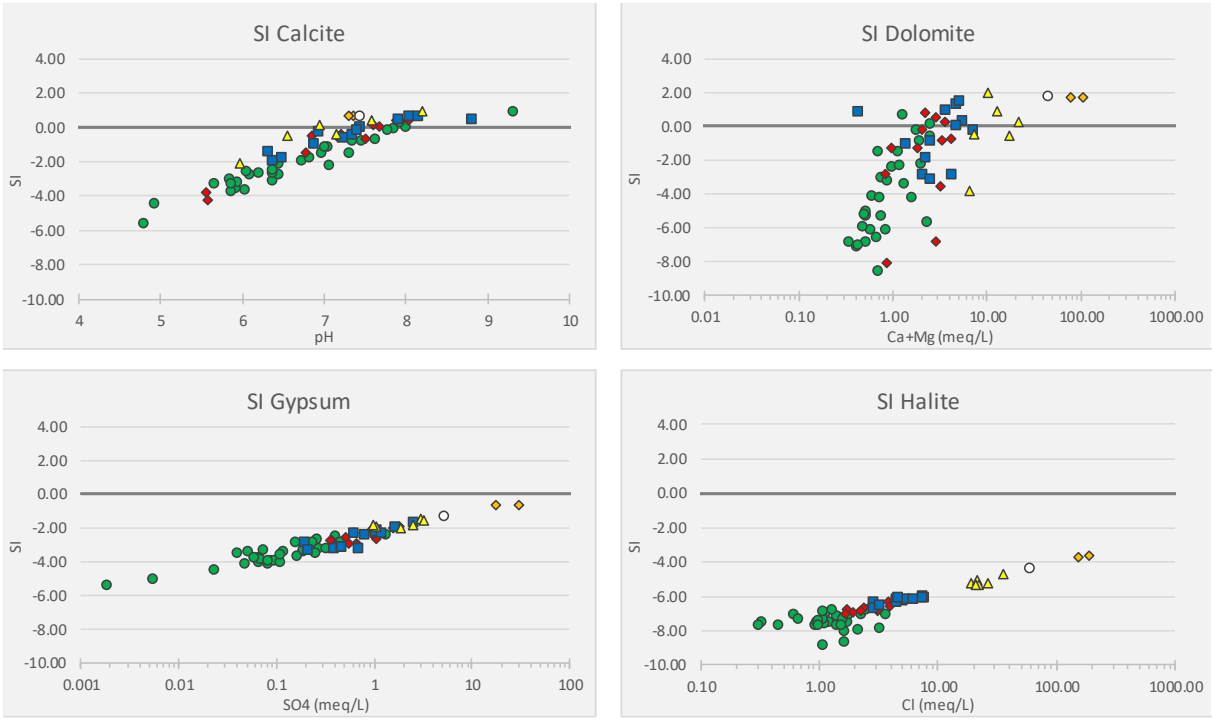

Figure 4-29: Saturation indices of different minerals for samples labelled as water groups. Symbols and colours are the same as previous figures.

Rainfall, evapotranspiration and recharge

Following ETP and subsequent percolation/infiltration, rain water recharges the local aquifer system. Evapotranspiration, which leads to an overall increase of TDS in groundwater can be quantified through Cl mass balance once Cl behaves conservatively (Andrade and Stigter, 2011; Appelo and Postma, 2005; Eriksson and Khunakasem, 1969; Stigter et al., 1998). Here, Cl is assumed as a conservative element given that saturation indices with respect to halite are below zero in all samples (no halite precipitates). So that, comparing Cl concentrations in groundwater and rainfall, recharge rates can be estimated (Eriksson and Khunakasem, 1969; Wood, 1999), Equation 5.6:

$$q = \frac{Cl_{rain}}{Cl_{GW}} \qquad \text{Eq 5.6}$$

where $\boldsymbol{q}$ is recharge rate, $\boldsymbol{Cl}$ is average Cl concentration of rainfall ($\boldsymbol{Cl_{rain}}$) and groundwater ($\boldsymbol{Cl_{GW}}$) in meq/L, respectively. As average rainwater Cl concentration was not currently available for the area, the most pristine water sample (PZ20F – 53 $\mu S/cm$, Cl = 0.3 meq/L, located on the dunes) was adopted as an end-member and assumed as average rainwater composition for Cl mass balance, already considering the Cl added by dry deposition (Appelo and Postma, 2005). For WT-1, Cl concentrations between 1.41 and 3.6 meq/L, recharge rates result in 8.3% and 21.5%, and ETP consequently 91.7% and 78.5%, respectively. Different Cl values in groundwater are linked to different ETP due to more clayey soils, hence less infiltration and more evaporation, or other reasons as finer character of sand sediments, shallow water levels, and/or a combination of uptake and interception by local vegetation. So that, WT-1 origin can be explained almost exclusively by ETP processes, Table 5.5. Within PhreeqC simulations, WT-1 mean ion concentrations could be reproduced using optimal ETP of 78%, leading to a recharge rate of 22%, which is concordant with recharge calculation through water balance method on this study (up to 29%), and values assessed in earlier researches, between 20% and 30% (DNA, 1988; IWACO, 1986). In a similar way, a simulated ETP of 90% could explain the WT-2 mean composition.

Table 4-6: Observed and computed parameters of water group WT-1 taking into account evapotranspiration processes. Solutes in mg/L.

	pH	Na	Cl	K	Ca	Mg	SO_4	Na/Cl	Mg/Ca
Observed	*6.6*	33.4	49.8	4.2	14.0	3.3	6.8	1.04	0.36
Calculated	*6.6*	21.9	49.6	3.4	13.9	2.5	3.0	0.68	0.30

The small differences in Na and K concentration, as well in Na/Cl ratios can be explained by minor silicate weathering, which was not considered in the model. For instance, WT-1 exhibits a high std dev for Na (17.3 mg/L), linked to different silicate weathering degrees within the system, and/or different cation exchange capacities of local clays, also not considered in the simulations. The same could be pondered for K (std dev = 1.7 mg/L). On the other hand, calculated values match most of ions concentrations for WT-1, Appendix D.

Figure 5.24 shows the δ18O vs Cl plot, in which many samples scatter from the seawater-rainwater purely mixing line. The deviation and the strong increasing trend in $\delta^{18}O$ with increasing Cl concentrations suggest that

evaporation, rather than halite dissolution or mixing with seawater, is important in increasing salinity in fresh water groups (Han et al., 2013, 2011; Mongelli et al., 2013; Mook, 2001; Rozanski et al., 2001). Brackish/salt water samples plot close to the mixing line, indicating a greater contribution of mixing with seawater in these groups, about 5% for WT-4 and up to 40% in WT-5.

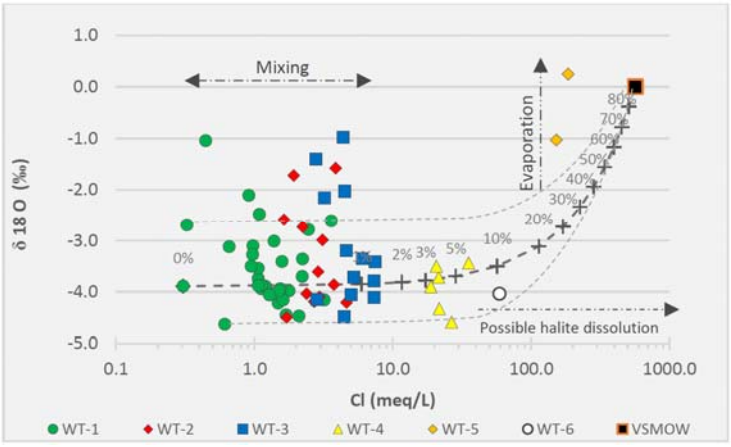

Figure 4-30: Cl vs $\delta^{18}O$ plot along with conservative mixing line between seawater (VSMOW) and rain water end-members. Dashed-dot lines indicate possible processes of mixing, evaporation and/or halite dissolution taking place in the area.

WT-5 samples (Matola River), show an enriched isotopic composition ($\delta^{2}H$ = +4.4‰ and $\delta^{18}O$ = +0.24‰), indicative of high evaporation that can lead to high salinity (Mongelli et al., 2013; Mook, 2001; Rozanski et al., 2001). Additionally, groundwater samples plotted along a line with slope of 5.4 in $\delta^{18}O$ vs $\delta^{2}H$ plot (green dashed line in Fig 5.19), smaller than that from meteoric lines, indicating evaporation effects or mixing (Rozanski et al., 2001).

From samples distribution in plots $\delta^{18}O$ vs Cl and $\delta^{18}O$ vs $\delta^{2}H$, two main hypothesis can be pinched for groundwater origins: 1) precipitation waters undergoing strong evaporation and derived from previous re-evaporated rainwater, which results in enrichment of heavy isotopes in the remaining water and subsequent depleted rain event (Mook, 2001; Rozanski et al., 2001); 2) waters from wetter climate periods, with a depleted isotopic composition in comparison with modern meteoric waters (Appelo and Postma, 2005; Han et al., 2013; Hiscock and Bense, 2014; Tekleab et al., 2014). Furthermore, in fresh waters, evaporation seems to play a significant role in increasing salinity, while mixing with small fractions of seawater cannot be disregarded as an important salinization mechanism in brackish/salt waters, further discussed in next sections. Notwithstanding, seasonal isotopic variation of rain events, and groundwater ages are required to strength the interpretations.

Rock weathering/dissolution

Rock weathering/dissolution increases groundwater mineralization, usually accompanied by increase in HCO_3 concentrations. This is linked to the presence of high soluble carbonate minerals (e.g. calcite, dolomite), most abundant in soils and aquifers, which rapidly dissolve when in contact with CO_2 from atmosphere and from soil

(Equations 5.3 - 5.5) (Appelo and Postma, 2005; Hiscock and Bense, 2014). Figure 5.25a shows the plot (Ca+Mg) vs HCO_3, in which the good fit of samples around the 1:1 line suggests that calcite/dolomite dissolution are most likely responsible for influencing chemical composition of waters in the area, strongly observed in WT-3, which shows samples with SI in respect to dolomite above saturation.

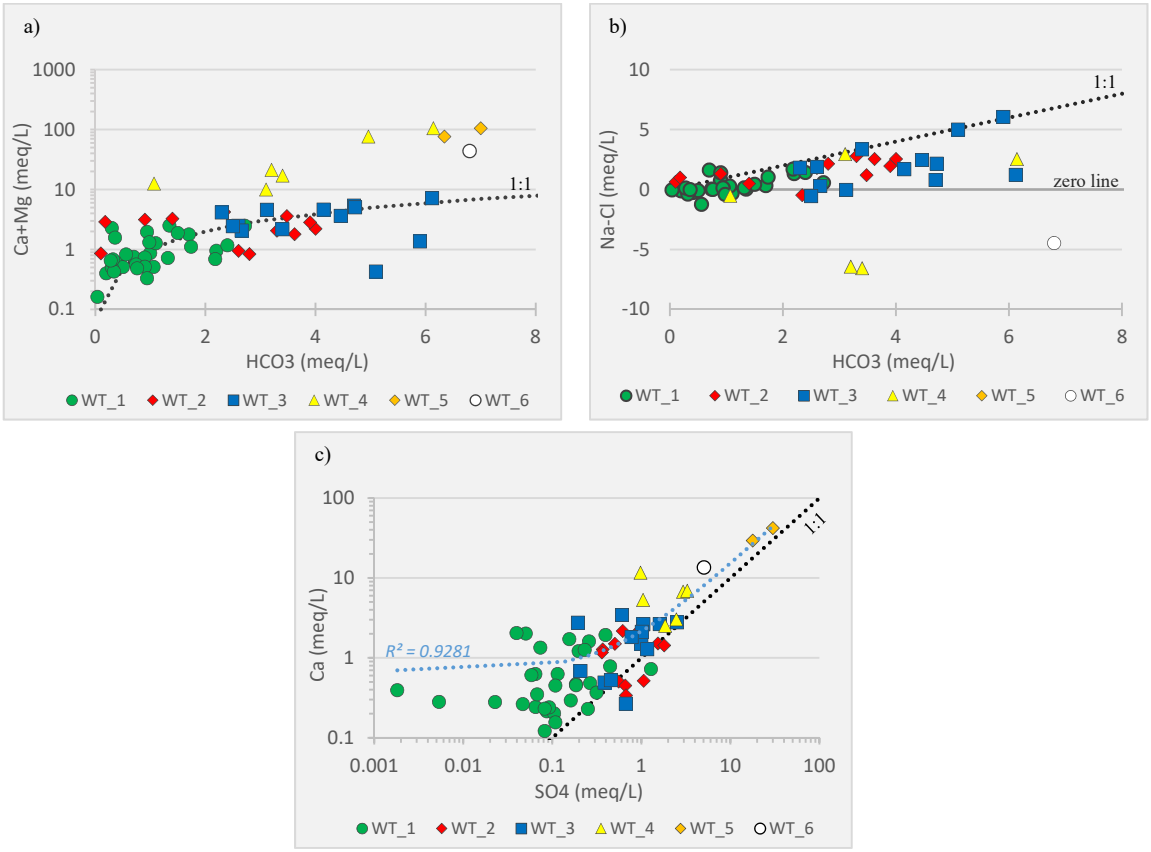

Figure 4-31: a) Ca+Mg vs HCO_3 semi-log plot; b) Na-Cl vs HCO_3 semi-log plot; c) Ca vs SO_4 log-log plot. Values in meq/l. Dotted black line represent ions relations from rock weathering/dissolution.

On the other hand, deviations from the line, expressly great in brackish/salt waters (WT-4, WT-5 and WT-6) can be explained by ion exchange upon mixing resulting in, for example, surplus of Ca in the water. The Figure 5.25b brings the Na-Cl vs HCO_3 plot. Fresh waters as WT-1 plotting near the zero line is likely to be resulting from silicate weathering (Equation 5.3) or freshening, while samples showing a great negative value for Na-Cl (WT-4 and WT-6) can indicate cation exchange upon salinization with uptake of Na by the complex (Appelo and Postma, 2005). Silicate weathering can explain the vast existence of $NaHCO_3$ water types and high Na/Cl ratios, especially true for fresh water groups (WT-1, WT-2 and WT-3), while the low Na/Cl ratios and water types as $CaCl_2$ in WT-4 and WT-6 groups, Table 5.24 and Figure 5.21b can be linked to salinization (e.g. Appelo and Postma, 2005; Han et al., 2013).

Progressive gypsum dissolution with salinity increase is substantiated by the Ca vs SO_4 plot of Figure 5.25c, wherein samples display mutual increase and a good fit with the 1:1 line and R^2 of 0.93, strongly observed in deeper and saline samples, while the surplus of Ca can be linked again to cation exchange processes (Alcala and Custodio, 2008; Appelo and Postma, 2005; Han et al., 2011). However, SO_4/Cl are rather near ocean ratio (Fig 5.17b), which goes up against the hypothesis of gypsum dissolution. This can indicate that, if gypsum dissolution occurs, it occurs in relatively small amounts and it is not the main contributor or process controlling local hydrochemistry. For example, PhreeqC simulations for WT-4 considering small amounts of gypsum dissolution (fresh water + dissolution + mixing) resulted in similar ion concentrations of purely mixing of freshwater and seawater, which will be further discussed in next section.

Nevertheless, low SO_4 concentrations, particularly seen in WT-1 can be linked to sulphate reduction from soil microbiological activities, which is reinforced by high pCO_2 values of these samples (between -2.0 and -0.6g). Sulphate reduction can be also resulted of low aquifer permeability, and/or high organic matter content in the soil, resulting in low O_2 concentrations (Andrade and Stigter, 2011; Appelo and Postma, 2005; Hiscock and Bense, 2014), whereas high SO_4 values, especially observed in WT-2 can be related to minor industrial or agricultural contamination apart of gypsum dissolution. Furthermore, brackish/salt water samples generally display higher deviations in all plots in comparison with fresher waters, which indicates that these waters experiences other processes resulting in high salinity apart of water-rock interaction, as cation exchange and mixing, which is further discussed in next section.

Mixing with seawater

Conservative mixing models are plotted to evaluate mixing of fresh rainwater and possible entrapped seawater remaining from ancient transgression periods. Figure 5.26 present some of selected ions vs Cl concentration, where mixing proportions in the plots result from the mass balance equation for conservative mixing (Equation 2.4) and are expressed as percentage of seawater contribution to the mixture.

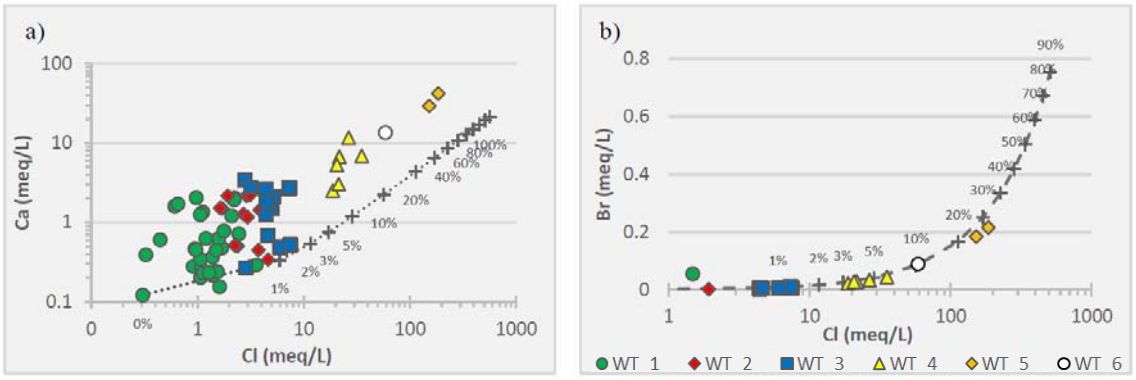

Figure 4-32: Binary plots between selected ions and Cl (meq/L) for water samples labelled as WT groups. Dashed lines indicate conservative mixing between seawater and freshwater endmembers.

From the plot Ca vs Cl, it is clear that brackish/salt water samples (WT-4, WT-5 and WT-6) show higher deviations from pure mixing lines, which can be explained by cation exchange upon mixing. For instance, hydrogeochemical

modelling confirm results of conservative mixing models for brackish/salt waters WT-4, according to the steps: original freshwaters in the aquifer (WT-3) in equilibrium with rock complex, infiltration of seawater from upper aquitard units (3-4%), and subsequent cation exchange to attain the equilibrium back to normality, Table 5.6. Supporting the mixing hypothesis, Br/Cl ratio of brackish/saline water samples plot around ocean ratio, further discussed in next sections.

Table 4-7: Observed and computed parameters of water group WT-4 taking into account mixing and cation exchange. Solutes in mg/L.

	pH	Na	Cl	K	Ca	Mg	SO_4	Na/Cl	Mg/Ca	Br/Cl
Observed	*7.06*	406.0	856.0	16.2	121.0	77.7	100.4	0.73	0.99	1.3E-03
Calculated	*6.62*	404.2	856.6	15.4	128.3	32.7	115.2	0.73	0.43	1.4E-03

Additionally, WT-4 water group represents waters under salinization, which can be explained by leaking of entrapped seawater from ancient transgression periods, yet partly within the thick aquitard units and partly laying on the bottom of phreatic aquifer, and subsequent flushing fresh waters previously in equilibrium with the rock complex (WT-3) – further presented in next sections. This process triggers the release of Ca from the complex and uptake of Na from the infiltrating water, resulting in reduced Na/Cl ratio, as well as in $CaCl_2$ water types as observed in WT-4 group. The high values of Mg can be linked to carbonate dissolution within marls and limestones. Further, isotopically signatures of these water samples indicate a different period of recharge, with a more depleted characteristic than modern rainfall, which supports the different origin and mixing hypothesis.

Source of salinity in groundwater

Different sources of salinity can be expected in Maputo. In this study, Br/Cl ratio supported the investigation together with major cations and environmental stable isotopes analyses. A general linear relationship could be observed in Br and Cl concentrations, with concomitant increase of Br and Cl, Figure 5.26b. This indicates that evaporation plays an important role in saline waters formation in the area, as found in similar studies in semi-arid coastal areas (Bouchaou et al., 2008; Han et al., 2013, 2011).

Figure 5.27 shows that Br/Cl ratio decreases with increasing Cl concentration. The general distribution of Br/Cl ratios near ocean ratio matches the suggestion that ETP, rock weathering/dissolution and/or mixing with seawater, rather than halite dissolution, are most dominant salinization mechanisms in the area (Alcala and Custodio, 2008; Han et al., 2013, 2011; Liu et al., 2015).

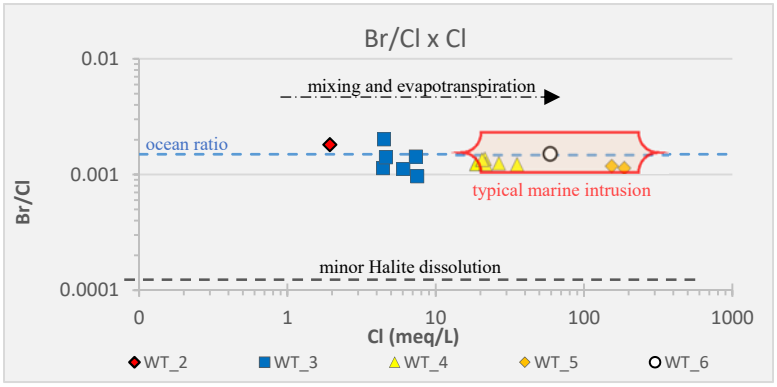

Figure 4-33: Br/Cl vs Cl. Samples fall around marine water formations ratio, as expected for entrapped seawater or seawater formation derived waters. Models show that ETP and mixing can lead to observed values. Reference values according to (Alcala and Custodio, 2008; Han et al., 2013).

Only one sample from phreatic aquifer (PZ14) plotted far above Br/Cl ocean ratio (0.03), which can indicate a secondary input of Br, as industrial waste or agricultural flow. However, the value can be rather interpreted as the ratio of modern rainfall since $NO3^-$ levels in the area are relatively low for analysed samples (max 42.9 mg/L – Appendix D) (Han et al., 2011). Furthermore, brackish/salt samples present SO_4/Cl and Na/Cl ratios near ocean value or below, which suggests a marine origin or marine formation derived waters (Fig 5.17) (Alcala and Custodio, 2008; Appelo and Postma, 2005; Han et al., 2013). High levels of Ca, Mg and SO_4 suggests that gypsum and carbonate dissolution play an important role in groundwater salinization. Although not yet verified in field, presence of halite within Tertiary units can also lead to high EC in groundwater and surface waters inland. If halite is present in the area, Br/Cl ratios close to ocean values can be explained by evaporites formed by residual waters containing low amounts of Br^- relative to Cl, as found and highlighted by other authors (Alcala and Custodio, 2008; Han et al., 2011; Mongelli et al., 2013). Due to these discrepancies, authors as (Leybourne and Goodfellow, 2007; Mongelli et al., 2013) suggest that Br/Cl ratio is not a good discriminator for salinity origin assessment.

Hydrochemical and isotopic approach supported by hydrogeochemical modelling suggest that brackish/salt waters in Maputo can be: 1) resulted from mixing of fresh waters and entrapped seawater, emplaced during previous transgression periods and not yet completely flushed out of the system. These lenses of seawater are laying partly on the bottom of the phreatic aquifer and partly within aquitard units, particularly in locations where this unit is thicker. They can be already somewhat diluted due to mixing with recent recharge waters before discharge in surface water bodies; 2) derived from water-rock interaction with high-soluble carbonate minerals and possibly gypsum within Tertiary units; 3) formed due to high ETP in combination with low precipitation rates, leading to an increased TDS, This is particularly true and strong in semi-arid regions with sparse recharge events. In these cases, secondary soil salinization derived from high ETP leads to an increased TDS in groundwater upon infiltration. Nevertheless, mineral dissolution seems to be very important as an additional source of salts/ions for fresh water groups, isotopic data suggests that high ETP influences in local high salinities, while modelling supports mixing with small fractions of entrapped seawater as additional salinization mechanisms in the area.

Hydrochemical facies analyses and groundwater evolution – conceptual models

Few cross sections were chosen for hydrochemical facies analyses due to their representativeness of the local hydrosystem, comprising mainly all water groups within a groundwater flow line. As previously discussed, the hydrochemical facies is a combination of water type (WT), redox index (RI), base exchange index (BEX), pollution index (PI) and calcite saturation index (CI). These parameters are used to describe evolution of water chemistry and related hydrochemical processes in the direction of groundwater flow. Figures 5.28 and 5.31 present analysed cross sections, followed by a hydrochemical evolution discussion and conceptual flow models. The delineation of geological units considered borehole descriptions and previous geophysical surveys – Vertical Electric Sounding (VES) (ARA-Sul, 2011).

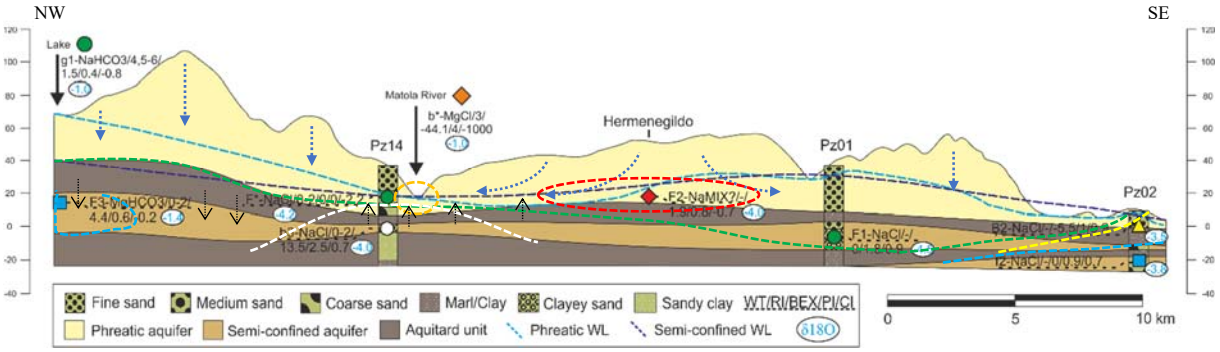

Figure 4-34: Cross section view of hydrochemical facies from "Lake-well" to PZ02. Symbols correspond to defined WT groups. Mind vertical exaggeration of the profile. Dashed coloured lines represent hydrosomes related to each water group. Mind vertical exaggeration of the profile.

From the profile, the complexity and distribution of water group's connection is clearly seen, as some main points and processes can be depicted: The system seems to not have reached yet its hydrochemical maturity since more than one hydrosome is observed within the profile. The anoxic character of surface waters in the lake can be explained by sulphate reduction. In the phreatic aquifer, infiltration of recent fresh waters mainly from precipitation mixes with entrapped seawater from previous transgression periods, laying partly in the bottom of the unit and partly already within the aquitard unit. Previous VES measurements in PZ14 confirms very low resistivity values in the bottom of the phreatic aquifer and within the aquitard units, Figure 5.29.

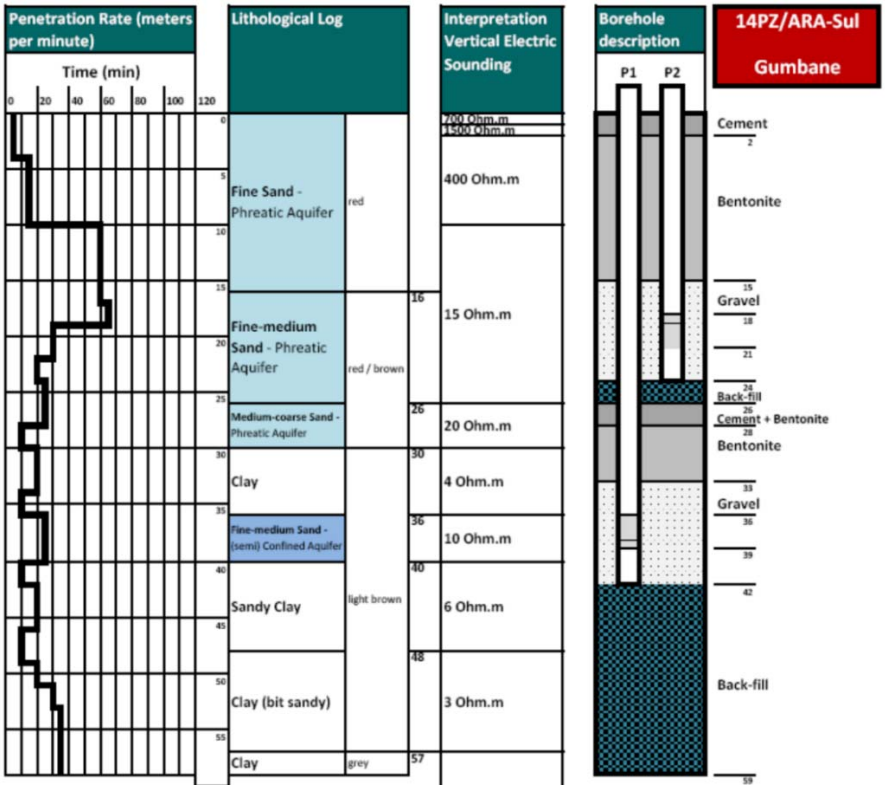

Figure 4-35: Lithological, borehole description and carried out VES measurement. The very low resistivity values derived from VES is a strong indicative of presence of brackish/salt water. (source: (ARA-Sul, 2011)).

Values around 15 *Ohm.m* and between 3-6 *Ohm.m*, are observed in the phreatic and in the aquitard units, respectively. Considering the aquitard unit, if one assumes a formation factor of 2 (clay) the porewater resistivity would result in 2 Ohm.m, according to Archie's law ($\Omega = F \times \Omega_{water}$). That corresponds to an EC of about 5000 µS/cm. This is true not only for the PZ14 but for other piezometers in the area, meaning that the aquitard units seems to be the ones containing the entrapped seawater, probably somewhat diluted in some locations. This can indicate brackish/salt waters presence, also perceived in the semi-confined aquifer Applying the same concept, the semi-confined aquifer reveals the presence of brackish/salt water as well, if one assumes a formation factor of 5, for instance, fine-medium sand, an EC of about 5000 µS/cm is also resulted. The brackish/salt waters in the bottom of phreatic levels of PZ14 can be explained again by upward flows from deeper and saline levels of the system mixing with freshwaters, or remaining seawater yet entrapped in these levels, but somewhat diluted. Furthermore, the high values in shallow levels in PZ14 from the VES measurement however (400 Ohm.m), represents the local unsaturated zone.

The saltwater remaining as lenses in portions of the aquitard unit and slowly infiltrates into the semi-confined aquifer, especially where the aquitard unit is not thick or totally absent. This mixing between previous freshwaters in the semi-confined unit (probably with similar composition of WT-3 group) and the seawater triggers cation exchange under salinization. As expressed before, this explains WT-4 group mean composition, particularly $CaCl_2$ water types. Looking the distribution of WT-4 in the map, almost a line parallel to the actual coast line can be

traced connecting the inland samples, Figure 5.20 Together with geological and structural information, this trend can help in identify where these possible saltwater lenses are located. The use of radioactive isotopes as ^{14}C and ^{3}H can help in assessing dates of sea level changes, transgression periods and inland saltwater entrapment (Lee et al., 2016; Rozanski et al., 2001; Vengosh et al., 2002).

However, although in the water group WT-4, the sample from PZ02F presents different origin from the others, and it can be linked to modern seawater intrusion, hypothetically illustrated for a multilayer coastal aquifer system as the Maputo system, Figure 5.30.

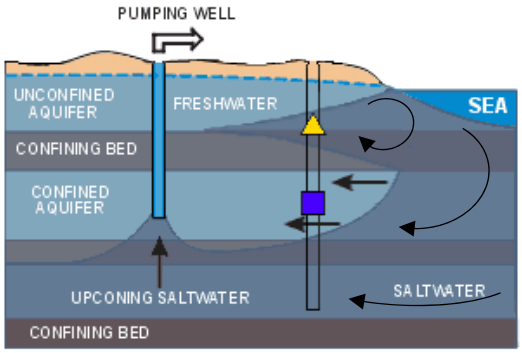

Figure 4-36: Hypothetical scheme elucidating the layering arrangement observed in PZ02 in cross section view of Figure 5.24 (modified from: http://www.hosessa.com/useful-info/).

Yet illustrative, the scheme can represent a scenario taking place in Maputo, where increasing groundwater exploitation can induce seawater intrusion to deeper fresher levels of the aquifer through upconing and lateral flow.

Carbonate dissolution is observed together with increasing alkalinity and Cl concentration as groundwater flows towards East with a small hydraulic gradient. SI in respect to calcite is positive in this portion of the semi-confined aquifer, and mineral dissolutions are substantiated by mutual increasing of Mg and Ca together with SO_4 and Cl concentrations (Appendix E). Presence of gypsum, especially around Matola River in the south was not yet verified but is confirmed through personal communication (Juizo, 2017). WT-6 sample is believed to result from higher seawater contribution mixing (linked to small thickness of aquitard in the region) and/or higher rock-water interactions, laying on deeper levels of the aquifer, as already documented as an issue in the area (DNA, 1988). Although saline, positive BEX of the sample suggests that freshening is taking place. In a water management perspective, this is important to know since excessive pump can disturb the natural layering of the system, bringing these waters to upper levels of the aquifer and inducing salinization.

The enriched isotopic signature of Matola River ($\delta^{18}O$ = -1.0‰) and hydrochemical data suggest mixing of surface waters and groundwater undergoing strong evaporation, which increases $\delta^{18}O$ and hence salinity in the water (Appelo and Postma, 2005; Liu et al., 2015; Rozanski et al., 2001). It is assumed that the river receives different salt mixing contributions coming from the bottom of phreatic aquifer and from the aquitard unit allowing salt groundwater seepage. As previously discussed, upward flow from semi-confined unit can bring up the entrapped

brackish/salt waters, increasing the contribution of saltwaters in the river discharge, explaining the salinization character and negative BEX in the samples. The upward hydraulic gradient however, can be explained by the low groundwater levels in the phreatic, which can be linked to low recharge rates, and the higher total hydraulic head from deeper and more saline groundwater within the aquitard and semi-confined units. Matola River experiencing strong evaporation explains observed high salinity and supersaturation in respect to calcite and dolomite. A PhreeqC model considering mixing of freshwater and seawater (95% and 5%, respectively), and subsequently strong evaporation (80%) resulted in comparable values of observed mean values for WT-5 samples, Table 5.7.

Table 4-8: Observed and computed parameters of water group WT-5 (Matola River waters) taking into account mixing of freshwater and seawater, and subsequently evaporation. Solutes in mg/L.

	pH	Na	Cl	K	Ca	Mg	SO_4	Na/Cl	Mg/Ca	Br/Cl
Observed	*7.33*	1969	5990	33.4	715	670	1146	0.51	1.45	1.19E-03
Calculated	*7.26*	2042	5696	97.4	698	682	816	0.55	1.61	1.47E-03

The big differences in K concentrations can be related to, for example, preferential vegetation uptake for K which was not considered in the simulations, whereas rock weathering/dissolution can explain missing values of SO_4, Ca and the excess of Mg. Also, input of fresh waters from recent recharge can result in diluted solutions and seasonal variations of EC in the river and in groundwater as well. Furthermore, groundwater contribution to Matola River discharges can be computed through hydrograph separation means, utilizing environmental isotopes or other natural or injected tracer (Rozanski et al., 2001), however, this exercise was not carried out during this research.

The centre of the cross section shows a WT-2 sample, understood as a groundwater originated from rainwater under high ETP rates (90%) and somewhat affected by minor silicate weathering. Depleted isotopic values can be explained by different recharge periods or mixing with other waters, while the great recharge potential surrounding PZ01 (interdunes) can explain the presence of freshwaters in deeper levels of the aquifer, also with a depleted isotopic composition. The great thickness of unsaturated zone allows the natural decay and attenuation of main pollution compounds, which results in low PI observed in samples.

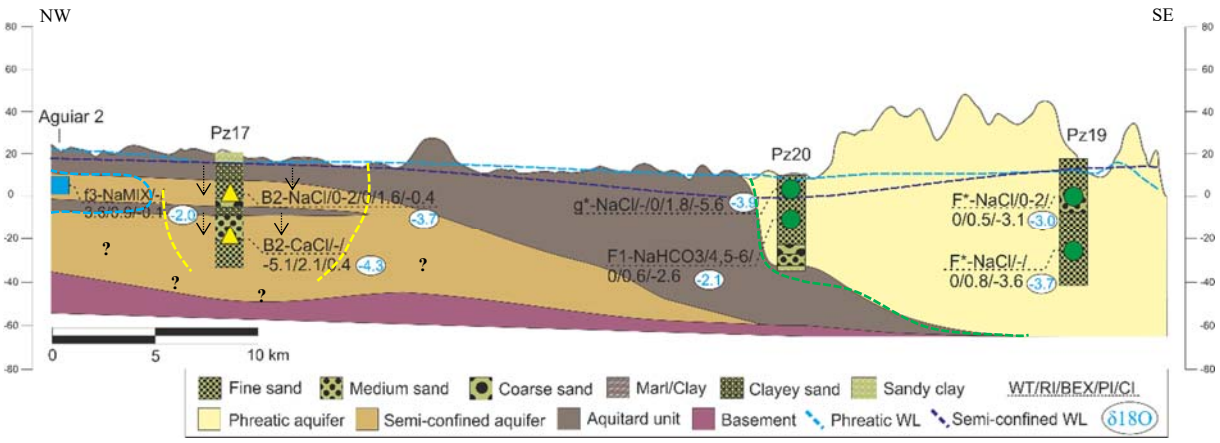

Figure 4-37: Cross section view of hydrochemical facies from "Aguiar 2" to PZ19. Symbols correspond to defined WT groups. Dashed coloured lines represent hydrosomes related to each water group. Mind vertical exaggeration of the profile.

It is observed from the profile of Figure 5.31, that the Northwest region is mainly covered by the local aquitard unit, allowing low recharge as previous confirmed in the recharge potential assessment. The separation of the system in two by the thick aquitard unit is once more clear, as two different hydrosomes can be clearly defined: one with brackish/salt groundwater to the West; and one with fresh groundwater in the dune areas to the East. On the west, infiltration of entrapped seawater, together with low recharge rates, high ETP and mineralization are factors that can explain high salinity of local groundwater in PZ17. The entrapped seawater also explains the high EC observed in the Matecheculi River (4500 µS/cm), which drains the aquitard unit and is partly fed by these brackish/salt groundwaters.

Figure 5.32 shows previous VES measurements carried out in PZ17, together with borehole description and lithological information, where presence of entrapped seawater and brackish/salt waters can be observed from the low resistivity values related to the units.

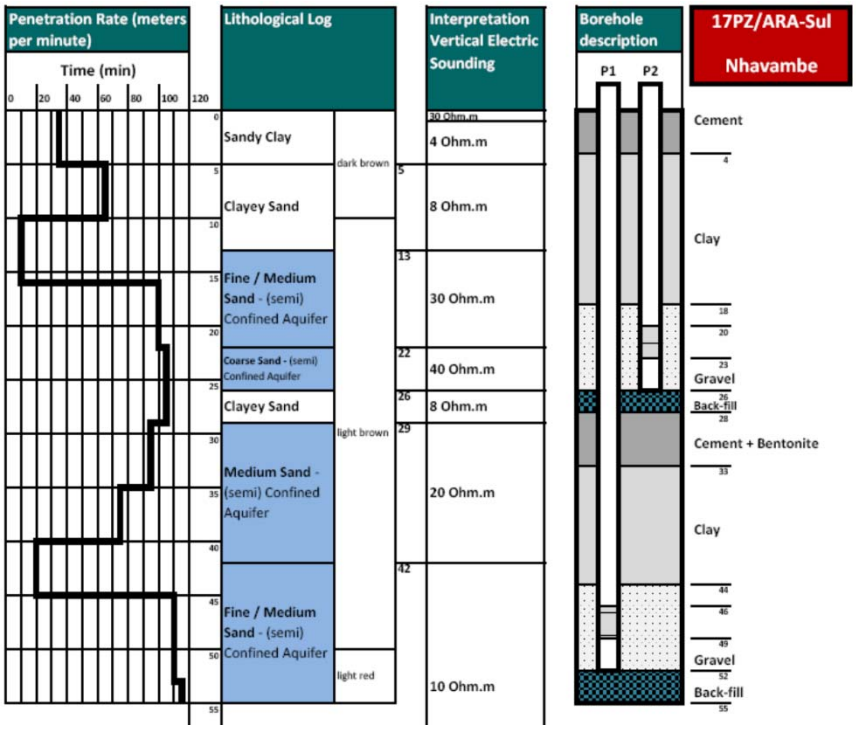

Figure 4-38: Lithological, borehole description and carried out VES measurement. The very low resistivity values derived from VES is a strong indicative of presence of brackish/salt water. (source: (ARA-Sul, 2011)).

From the Figure 5.32, similar interpretation from Figure 5.29 can be done. The semi-confined levels of the aquifer also reveals very low resistivity values from VES, around 10 *Ohm.m*, which would result in a porewater resistivity of 2 *Ohm.m*, or EC of about 5000 µS/cm for a formation factor of 5 (fine-medium sand). Again here, the confining

layers seems to contain entrapped brackish/salt water. The enriched isotopic signature of shallower levels of the piezometer and Aguiar_2 suggest mixing with recent waters, while the depleted signature of deeper and more saline waters can be linked to mixing with older waters. This can indicate an aquitard unit with higher permeability allowing a more rapid flushing of saltwater, or the simply absence of entrapped seawater in this portion of the unit.

The clay layer existing in medium depths in PZ17 (around -10 masl) splits the system in freshening (above the clay) and salinization (below the clay), negative BEX. Therefore, such clay layer is believed to contain yet remaining of seawater flowing downwards into (8 Ohm.m, ~ EC of about 5000 µS/cm). As discussed before, $CaCl_2$ water subtype and negative BEX indicates salinization in the area, while this seawater intrudes the previous fresh semi-confined aquifer trigging cation exchange (Han et al., 2011; Hiscock and Bense, 2014; Mollema et al., 2013). Gypsum dissolution is reinforced by the increase of gypsum SI in deeper levels of the aquifer (Aguiar_2 = -2.36; PZ17F = -1.8, PZ17SC = -1.4). The positive SI in respect to calcite and dolomite in deeper levels of PZ17 indicates precipitation of these minerals, while dissolution can be seen in shallower levels. On the East side of the cross section, coastal dunes present mainly fresh water group WT-1, with low alkalinity and TDS, results of great recharge and rapid infiltration in that area. The depleted isotopic signature can indicate recharge from different periods.

CHAPTER 5

Conclusion and Recommendations

The multi-layered coastal aquifer of Maputo reveals a great complexity regarding behaviour and controls of local hydrochemistry. In this study, a qualitative and quantitative recharge assessment together with a multi hydrochemical facies and isotope analyses approach were carried out to improve the understanding of the coastal hydrosystem. The aquifer system is comprised by unconfined and semi-confined units, separated by an aquitard layer, which is sometimes very thick and sometimes totally absent. While the unconfined aquifer is mainly composed of aeollian sands and sediments from Quaternary, the semi-confined aquifer comprises carbonate rocks from Tertiary. Groundwater flows mainly from West to East, following natural hydraulic gradient of the area, with small local variations within discharge river valleys. Local upward flow from the semi-confined aquifer to the phreatic is also observed.

Recharge assessment through GIS spatial analysis revealed that, natural groundwater recharge is strongly connected to local land use/cover, lithology and geomorphology characteristics, and presents potential ranges varying from very high to very low. High potentials were found in open semi-natural vegetated areas and within inland and coastal dune belts (relatively low ETP and good infiltration). Low recharge potentials were found along clayey river valleys cutting aeollian formations, and in agriculture and urban areas, mainly related to high ETP and runoff components. However, the method only takes into account surface lithology and should, therefore, be accounted as more representative for the unconfined aquifer. Recharge for semi-confined aquifer requires additional investigations, since a connection between aquifers is recognized but not well comprehended. Quantitative recharge valuation through root zone water budget method revealed two main recharge periods according to local seasonal variations and precipitation patterns: a main groundwater recharge period occurring during wet-summer (Nov - Mar), up to 30% of precipitation, and a minor one during dry-winter (Jun - Aug). Extreme daily precipitation events seem to be very important for recharge, especially in the latter case, supporting the importance of daily assessment on recharge calculations. The method is limited by the non-consideration of travel time between root-zone bottom and top of saturated zone, which can result in discrepancies concerning recharge periods front other methods, as Water Table Fluctuation and tracer test analyses.

Subsequent to sampling campaign, six (6) different water groups were classified with the support of multivariate statistical methods (HCA). Samples main physico-chemical parameters, such as EC, $\delta^{18}O$ and major ion concentrations were considered in the classification. Multi hydrochemical facies and isotope analyses revealed water samples varying from fresh ($Cl < 4.2$ meq/L) to brackish/saline ($28 < Cl < 282$ meq/L) main types with respect to Stuyfzand classes, and showing a great isotopic range ($\delta^{2}H$ between -26.5‰ and +4.4‰, and $\delta^{18}O$ between -4.6‰ and +0.2‰). Samples plot around GMWL and LWML, with groundwater been more depleted than surface and rainwater samples, which indicates meteoric origin for both cases but a stronger evaporation in the

isotopic enriched samples, also indicated by groundwater samples deriving a regression line with slope of 5.4, smaller than both global and local meteoric lines.

Concerning water types distribution, the unconfined aquifer shows mostly fresh water types (WT-1, WT-2 and WT-3) experiencing different ETP rates (75-90%) and mostly silicate weathering as controlling hydrochemistry; whereas the semi-confined aquifer displays great of its West inland sectors with brackish/salt waters (WT-4, WT-5 and WT-6) under salinization due to leaking of entrapped seawater from transgression periods remaining mainly within aquitard units. Moreover, fresher water types as WT-1 were found in areas of great recharge potential as dune belts, resulting from relatively rapid infiltration and minor mineralization/evaporation processes. In these areas, a great connectivity between aquifers is expected since water types from different depths show similar composition, like low HCO_3, low TDS and similar $\delta^{18}O$ values. Matola River samples (WT-5) revealed high salinity (14700 ~ 17680 µS/cm), being related to brackish/salt groundwater seepage and subsequent evaporation. Incomati River samples have a fresher composition (500 ~ 800 µS/cm), although high EC was registered in upstream effluents (Matecheculi River - 4500 µS/cm, near PZ17), which indicates different surface waters contributing more than groundwater for its discharge.

With regard to local salinization mechanisms, hydrochemical and isotopic data, supported by conservative mixing and hydrogeochemical models suggest that, inland brackish/salt waters are formed due to mixing with small fractions of entrapped seawater from ancient transgression periods remaining as lenses and yet infiltrating the semi-confined aquifer. Presence of $CaCl_2$ water subtypes implies cation exchange upon salinization due to infiltration of entrapped seawater into the Tertiary aquifer. While $NaHCO_3$ water types suggest cation exchange upon freshening in many parts of the unconfined aquifer, especially true for regions where a thick aquitard unit is observed. Furthermore, Br/Cl ratios analysed to distinguish possible different salinity origins supports the defined conceptual model. Brackish/salt water samples Br/Cl ratios plotted around ocean ratio, which relate their salinity origin to seawater or seawater formation derived water, rather than halite dissolution. High Na/Cl ratios suggest strong silicate weathering in fresher water types, while low Na/Cl ratios in brackish/salt waters are explained by cation exchange processes upon mixing with seawater. SO_4/Cl of brackish/salt waters are rather near ocean ratio, which do not give a conclusive prove about gypsum dissolution in the area as a contributor factor increasing salinity.

Nonetheless, further studies are recommended since the present research has its own limitations. Groundwater monitoring campaign is being currently carried out in Maputo under the SALINPROVE project, with Divers for level, temperature and EC monitoring. Together with flow and mass transport numerical models, that will provide a better view of seasonal variations and comportments of local hydrosystem concerning recharge and hydrochemical processes; Groundwater sampling should be constantly carried out for improving recognition of trends and fluctuations of water quality; Purging of wells/boreholes (appx 3x its volume) before sampling is highly recommended for more representative groundwater samples, while sampling for major ions analyses with a two months interval is suggested; Sampling of different rain events is also fundamental for achieve a more representative LMWL (considering seasonal variations of isotopic composition of precipitation), as well as for Cl mass balance meanings; Groundwater dating using radioactive environmental isotopes, such as ^{14}C and/or ^{3}H, should be performed to evaluate seawater entrapment and transgression periods, and improve conceptual models

of salinization; Surface seawater incursion becomes also important on assessing salinization effects of local deltas/rivers, especially with the threat of sea level rise, and should be evaluated mutually with tidal variations assessment and river EC profiles analyses (especially in Matola River); Field verification of halite/gypsum occurrence is important to support the findings of this study in what concerns salinization mechanisms of Maputo area.

CHAPTER 6

References

- Adelana, S.M., Allinson, G., Kitching, M., Ii, H., Salzman, S., Mcnamara, E., Taniguchi, M., Croatto, G., Shelley, B., 2015. Flow, Recharge and Mixing Processes in the Werribee Basin (Australia) Using Natural Environmental Isotope Geochemistry: Implications for Water Resources Management.
- Adonis, S., 2007. The Hydrochemical Characteristics of Groundwater in the Incomati Estuary.
- Aghil, Y.S.T.B., Oliver, D.H., Nair, C.N., 2017. Hydrochemical characteristics and quality assessment of groundwater along the Manavalakurichi coast , Tamil Nadu , India. Appl. Water Sci. 7, 1429–1438. doi:10.1007/s13201-015-0325-8
- Alcala, F.J., Custodio, E., 2008. Using the Cl / Br ratio as a tracer to identify the origin of salinity in aquifers in Spain and Portugal 189–207. doi:10.1016/j.jhydrol.2008.06.028
- AlSuhaimi, A.O., AlMohaimidi, K.M., Momani, K.A., 2016. Preliminary assessment for physicochemical quality parameters of groundwater in Oqdus Area, Saudi Arabia. J. Saudi Soc. Agric. Sci. doi:10.1016/j.jssas.2016.12.002
- Andrade, A.I.A.S.S., Stigter, T.Y., 2011. Hydrogeochemical controls on shallow alluvial groundwater under agricultural land: Case study in central Portugal. Environ. Earth Sci. 63, 809–825. doi:10.1007/s12665-010-0752-7
- Andrade, A.I.A.S.S., Stigter, T.Y., 2009. Multi-method assessment of nitrate and pesticide contamination in shallow alluvial groundwater as a function of hydrogeological setting and land use. Agric. Water Manag. 96, 1751–1765. doi:10.1016/j.agwat.2009.07.014
- Appelo, C.A.J., Postma, D., 2005. Geochemistry, Groundwater and Pollution - 2nd Edition. Amsterdam.
- ARA-Sul, 2011. Monitoring MMA Aquifer – Quantative and Qualitative Aspects. Maputo.
- Bonilla Valverde, J., Blank, C., Roidt, M., Schneider, L., Stefan, C., 2016. Application of a GIS Multi-Criteria Decision Analysis for the Identification of Intrinsic Suitable Sites in Costa Rica for the Application of Managed Aquifer Recharge (MAR) through Spreading Methods. Water 8, 391. doi:10.3390/w8090391
- Bouchaou, L., Michelot, J.L., Vengosh, A., Hsissou, Y., Qurtobi, M., Gaye, C.B., Bullen, T.D., Zuppi, G.M., 2008. Application of multiple isotopic and geochemical tracers for investigation of recharge , salinization , and residence time of water in the Souss – Massa aquifer , southwest of Morocco 267–287. doi:10.1016/j.jhydrol.2008.01.022
- Chairuca, L., 2016. Hydrogeology of Mozambique. Earthwise.
- Chairuca, L., 1997. Hydro-geological Assessment of the Marracuene-Manhiça Region.
- Clark, I.D., Fritz, P., 1997. Environmental isotopes in hydrogeology. CRC Press, Boca Raton.
- DNA, 1988. Groundwater Management in Grande Maputo. Maputo.
- Drever, J., 1997. The Geochemistry of Natural Waters: Surface and Groundwater Environments, 3rd ed.

Prentice Hall, New Jersey, USA.

- Edmunds, W.M., 1996. Bromine geochemistry of British groundwaters 60, 275–284.
- Edmunds, W.M., Ma, J., Aeschbach-Hertig, W., Kipfer, R., Darbyshire, D.P.F., 2006. Groundwater recharge history and hydrogeochemical evolution in the Minqin Basin, North West China. Appl. Geochemistry 21, 2148–2170. doi:10.1016/j.apgeochem.2006.07.016
- Eriksson, E., Khunakasem, V., 1969. Chloride Concentration in Groundwater, Recharge Rate and Rate of Deposition of Chloride in the Israel Coastal Plain. J. Hydrol. 7, 178–197.
- Ferguson, G., Gleeson, T., 2012. Vulnerability of coastal aquifers to groundwater use and climate change. Nat. Clim. Chang. 2, 342–345. doi:10.1038/NCLIMATE1413
- FIPAG, 2012. Estudos Ambientais e Sociais para o Sistema de Abastecimento de Água do Grande Maputo. Maputo.
- García-Menéndez, O., Morell, I., Ballesteros, B.J., Renau-Prunõnosa, A., Renau-Llorens, A., Esteller, M. V., 2016. Spatial characterization of the seawater upconing process in a coastal Mediterranean aquifer (Plana de Castellón, Spain): evolution and controls. Environ. Earth Sci. 75, 18. doi:10.1007/s12665-016-5531-7
- Ghesquière, O., Walter, J., Chesnaux, R., Rouleau, A., 2015. Scenarios of groundwater chemical evolution in a region of the Canadian Shield based on multivariate statistical analysis. J. Hydrol. Reg. Stud. 4, 246–266. doi:10.1016/j.ejrh.2015.06.004
- Güler, C., Thyne, G., 2004. Hydrologic and geologic factors controlling surface and groundwater chemistry in Indian Wells-Owens Valley area , southeastern California , USA 285, 177–198. doi:10.1016/j.jhydrol.2003.08.019
- Han, D., Kohfahl, C., Song, X., Xiao, G., Yang, J., 2011. Geochemical and isotopic evidence for palaeo-seawater intrusion into the south coast aquifer of Laizhou Bay, China. Appl. Geochemistry 26, 863–883. doi:10.1016/j.apgeochem.2011.02.007
- Han, D., Post, V.E.A., Song, X., 2015. Groundwater salinization processes and reversibility of seawater intrusion in coastal carbonate aquifers. J. Hydrol. 531, 1067–1080. doi:10.1016/j.jhydrol.2015.11.013
- Han, D., Song, X.F., Currell, M.J., Yang, J.L., Xiao, G.Q., 2013. Chemical and isotopic constraints on evolution of groundwater salinization in the coastal plain aquifer of Laizhou Bay, China. J. Hydrol. 508, 12–27. doi:10.1016/j.jhydrol.2013.10.040
- Hiscock, K.M., Bense, V.F., 2014. Hydrogeology: principles and Practice, 2nd editio. ed. Wiley Blackwell.
- IWACO, 1986. Study of Groundwater to Supply Maputo – Summary of the Hydrogeology of the Study Area. Maputo.
- Johnson, T., 2007. Battling Seawater Intrusion in 13, 1–2.
- Juizo, D., 1995. Modelação Geohidrológica do Sistema Aquifero da Zona Norte de Maputo.
- Kansas Geological Survey, 1995. KGS Pub. Inf. Circ. 2--Part 3 of 5 [WWW Document]. Public Inf. Circ. 2. URL http://www.kgs.ku.edu/Publications/pic2/pic2_3.html (accessed 5.5.17).
- Lee, S., Currell, M., Cend??n, D.I., 2016. Marine water from mid-Holocene sea level highstand trapped in a coastal aquifer: Evidence from groundwater isotopes, and environmental significance. Sci. Total Environ. 544, 995–1007. doi:10.1016/j.scitotenv.2015.12.014
- Leybourne, M.I., Goodfellow, W.D., 2007. Br / Cl ratios and O , H , C , and B isotopic constraints on the origin of saline waters from eastern Canada Br / Cl ratios and O , H , C , and B isotopic constraints.

doi:10.1016/j.gca.2007.02.011

- Liu, F., Song, X., Yang, L., Zhang, Y., Han, D., Ma, Y., Bu, H., 2015. Identifying the origin and geochemical evolution of groundwater using hydrochemistry and stable isotopes in the Subei Lake basin , Ordos energy base , Northwestern China 551–565. doi:10.5194/hess-19-551-2015
- Magesh, N.S., Chandrasekar, N., Soundranayagam, J.P., 2012. Delineation of groundwater potential zones in Theni district, Tamil Nadu, using remote sensing, GIS and MIF techniques. Geosci. Front. 3, 189–196. doi:10.1016/j.gsf.2011.10.007
- Mahmoud, S.H., Alazba, A.A., 2015. Hydrological response to land cover changes and human activities in arid regions using a geographic information system and remote sensing. PLoS One 10, 1–19. doi:10.1371/journal.pone.0125805
- Matsinhe, N.P., Juízo, D., Rietveld, L.C., Persson, K.M., 2008. Water services with independent providers in peri-urban Maputo: Challenges and opportunities for long-term development. Water SA 34, 411–420.
- Mollema, P.N., Antonellini, M., Dinelli, E., Gabbianelli, G., Greggio, N., Stuyfzand, P.J., 2013. Hydrochemical and physical processes influencing salinization and freshening in Mediterranean low-lying coastal environments. Appl. Geochemistry 34, 207–221. doi:10.1016/j.apgeochem.2013.03.017
- Mongelli, G., Monni, S., Oggiano, G., Paternoster, M., Sinisi, R., 2013. Tracing groundwater salinization processes in coastal aquifers: a hydrogeochemical and isotopic approach in the Na-Cl brackish waters of northwestern Sardinia, Italy. Hydrol. Earth Syst. Sci. 17, 2917–2928. doi:10.5194/hess-17-2917-2013
- Mook, W.G., 2001. Environmental Isotopes in the Hydrological Cycle Principles and Applications Environmental Isotopes in the Hydrological Cycle Principles and Applications.
- Mozambique, T.G. of, 2005. Projecto de Reabilitação das Redes de Água Potável da Aglomeração de Maputo. Maputo.
- Muiuane, E., 2007. The Quality of Groundwater in and around Maputo city, Mozambique, Department of Geology, Eduardo Mondlane University. Maputo.
- Narany, T.S., Ramli, M.F., Aris, A.Z., Nor, W., Sulaiman, A., Juahir, H., Fakharian, K., 2014. Identification of the Hydrogeochemical Processes in Groundwater Using Classic Integrated Geochemical Methods and Geostatistical Techniques , in Amol-Babol Plain , Iran 2014. doi:10.1155/2014/419058
- Neumann, B., Vafeidis, A.T., Zimmermann, J., Nicholls, R.J., 2015. Future coastal population growth and exposure to sea-level rise and coastal flooding - A global assessment. PLoS One 10. doi:10.1371/journal.pone.0118571
- Nonner, J.C., 2015. Introduction to Hydrogeology, Third Edition: Unesco-IHE Delft Lecture Note Series. CRC Press/Balkeman.
- Parkhurst, D.L., Appelo, C.A.J., 2013. Description of Input and Examples for PHREEQC Version 3—A Computer Program for Speciation, Batch-Reaction, One-Dimensional Transport, and Inverse Geochemical Calculations, in: Groundwater Book 6, Modeling Techniques. U.S. Geological Survey Techniques and Methods, Amsterdam, p. 497.
- Rosário Dias, L.A.X., 2016. IMPACTO DA PROLIFERAÇÃO DE FUROS NA REGIÃO DO MAPUTO. Universidade Eduardo Mondlane.
- Rozanski, K., Fröhlich, K., Mook, W., 2001. Environmental Isotopes in the Hydrological Cycle Principles and Applications.

- Sajil Kumar, P.J., 2013. Interpretation of groundwater chemistry using piper and chadhas diagrams: a comparative study from perambalur taluk. Elixirpublishers.Com 54, 12208–12211.
- Senanayake, I.P., Dissanayake, D.M.D.O.K., Mayadunna, B.B., Weerasekera, W.L., 2016. An approach to delineate groundwater recharge potential sites in Ambalantota, Sri Lanka using GIS techniques. Geosci. Front. 7, 115–124. doi:10.1016/j.gsf.2015.03.002
- Shaban, A., Khawlie, M., Abdallah, C., 2006. Use of remote sensing and GIS to determine recharge potential zones: The case of Occidental Lebanon. Hydrogeol. J. 14, 433–443. doi:10.1007/s10040-005-0437-6
- Shah, N., Nachabe, M., Ross, M., 2007. Extinction depth and evapotranspiration from ground water under selected land covers. Ground Water 45, 329–338. doi:10.1111/j.1745-6584.2007.00302.x
- Smidt, E.H., 1990. Gestão da Água Subterrânea na Ilha do Grande Maputo, Águas SubterrÂneas. Maputo.
- Steinbruch, F., Weise, S.M., 2016. Characterization of the Rainfall of Central Mozambique Based on Isotopes of Water, in: Raju, N.J. (Ed.), Geostatistical and Geospatial Approaches for the Characterization of Natural Resources in the Environment: Challenges, Processes and Strategies. Springer International Publishing, Cham, pp. 321–325. doi:10.1007/978-3-319-18663-4_49
- Stigter, T.Y., Van Ooijen, S.P.J., Post, V.E.A., Appelo, C.A.J., Carvalho Dill, A.M.M., 1998. A hydrogeological and hydrochemical explanation of the groundwater composition under irrigated land in a Mediterranean environment, Algarve, Portugal. J. Hydrol. 208, 262–279. doi:10.1016/S0022-1694(98)00168-1
- Stuyfzand, P.J., 1993. Hydrochemistry and Hydrology of the Coastal Dune Area of the Western Netherlands. Free University of Amsterdam.
- Stuyfzand, P.J., 1989. A new hydrochemical classification of watertypes. IAHS Publ. 182, 89–98.
- Swanson, S., Bahr, J., Schwar, M., Potter, K., 2001. Two-way cluster analysis of geochemical data to constrain spring source waters. Chem Geol 179, 73–91. doi:10.1016/S0009-2541(01)00316-3
- Tekleab, S., Wenninger, J., Uhlenbrook, S., 2014. Characterisation of stable isotopes to identify residence times and runoff components in two meso-scale catchments in the Abay / Upper Blue Nile basin , Ethiopia 2415–2431. doi:10.5194/hess-18-2415-2014
- Vengosh, A., Gill, J., Davisson, M.L., Hudson, G.B., 2002. A multi-isotope (B , Sr , O , H , and C) and age dating (3 H – 3 He and C) study of groundwater from Salinas Valley , California : Hydrochemistry , dynamics , and contamination processes 38.
- Vengosh, A., Spivack, A.J., Artzi, Y., Ayalon, A., 1999. Geochemical and boron, strontium, and oxygen isotopic constraints on the origin of the salinity in groundwater from the Mediterranean coast of Israel 35, 1877–1894.
- Werner, A.D., Bakker, M., Post, V.E.A., Vandenbohede, A., Lu, C., Ataie-Ashtiani, B., Simmons, C.T., Barry, D.A., 2013. Seawater intrusion processes, investigation and management: Recent advances and future challenges. Adv. Water Resour. 51, 3–26. doi:10.1016/j.advwatres.2012.03.004
- WHO, 2011. Guidelines for Drinking-water Quality, World Health Organization. WHO Press.
- Wood, W.W., 1999. Use and Misuse of Chloride-Mass Balance Method in Estimating Groundwater Recharge. Ground Water 37, 1–3.
- Yeh, H.-F., Cheng, Y.-S., Lin, H.-I., Lee, C.-H., 2016. Mapping groundwater recharge potential zone using a GIS approach in Hualian River, Taiwan. Sustain. Environ. Res. 26, 33–43. doi:10.1016/j.serj.2015.09.005

Appendices

Appendix A - **Study area information.**

A.01 – Electrical conductivity (EC) contour map (ARA-Sul, 2011).

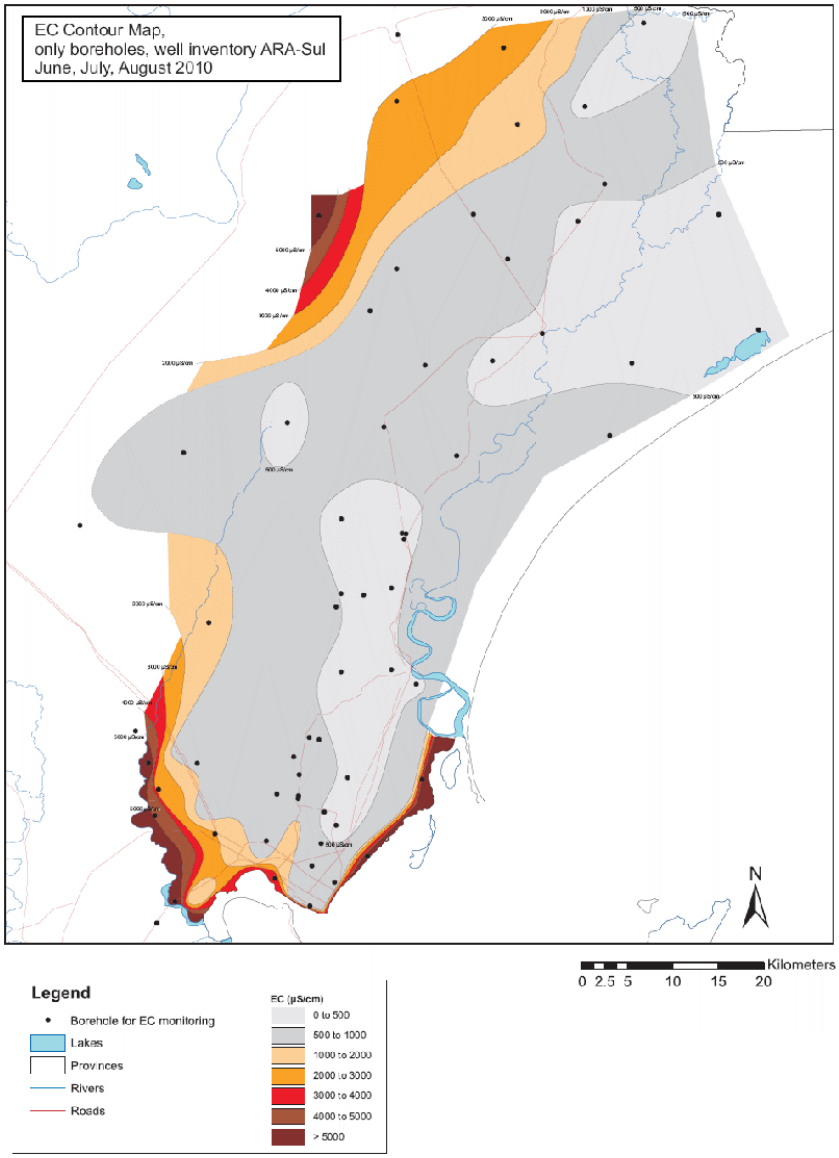

Map with EC values distribution according to hydrochemistry data and geophysical survey. High values inland are recognized in western portions in the north and south, while fresh water bodies are seen in the centre of the study area.

A.02 – Precipitation stations location together with average annual precipitation distribution (in mm/y).

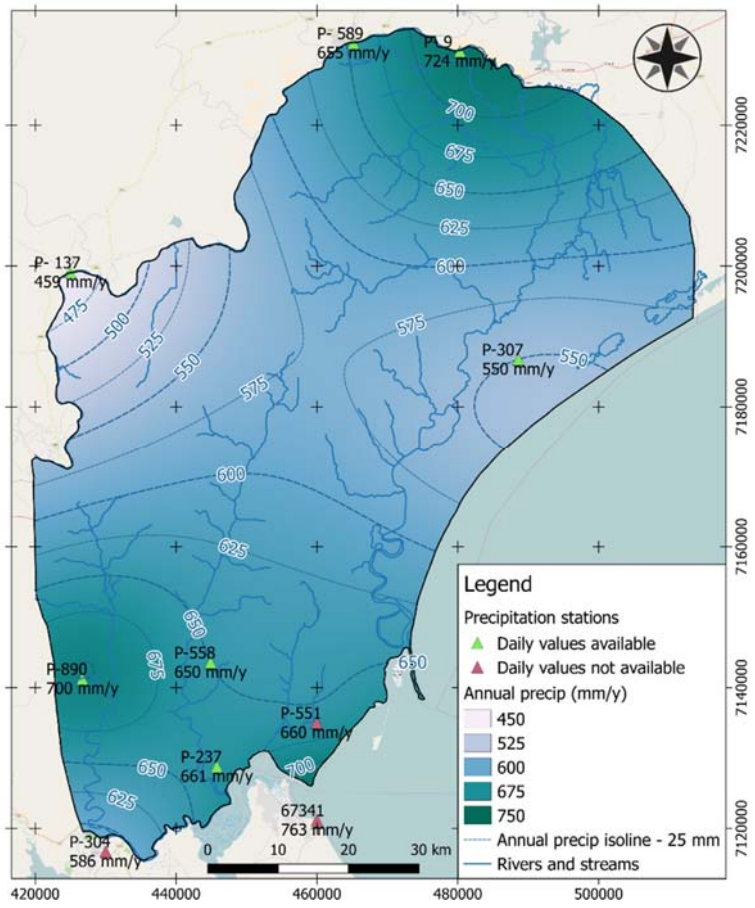

Stations are presented with their codes and average annual precipitation data. Stations containing daily precipitation values are presented in green, while in red those without daily values available.

A.03 – Daily data availability of precipitation stations.

Number of days with data per year for each precipitation station.

Year	P-558	P-137	P-237	P-307	P-890	P-9
2000	366	366	366	0	0	366
2001	365	365	335	365	92	365
2002	365	365	365	365	365	365
2003	365	365	365	365	365	365
2004	366	305	366	366	366	366
2005	365	335	365	365	365	365
2006	365	334	365	301	365	365
2007	365	303	365	181	304	350
2008	366	366	335	0	366	366

2009	365	365	364	0	334	365
2010	365	365	304	0	365	273

- Data > 300 days in a year
- Data < 300 days in a year
- No data in the year

Stations P-237, P-558 and P-890 present data from about 1960. The stations not presented here did not contain daily precipitation data and could not be used for recharge calculations.

A.04– Annual precipitation of different stations in the study area, and monthly temperature averages, together with year average temperature 1910-2016 (KNMI Climate Explorer, 2016).

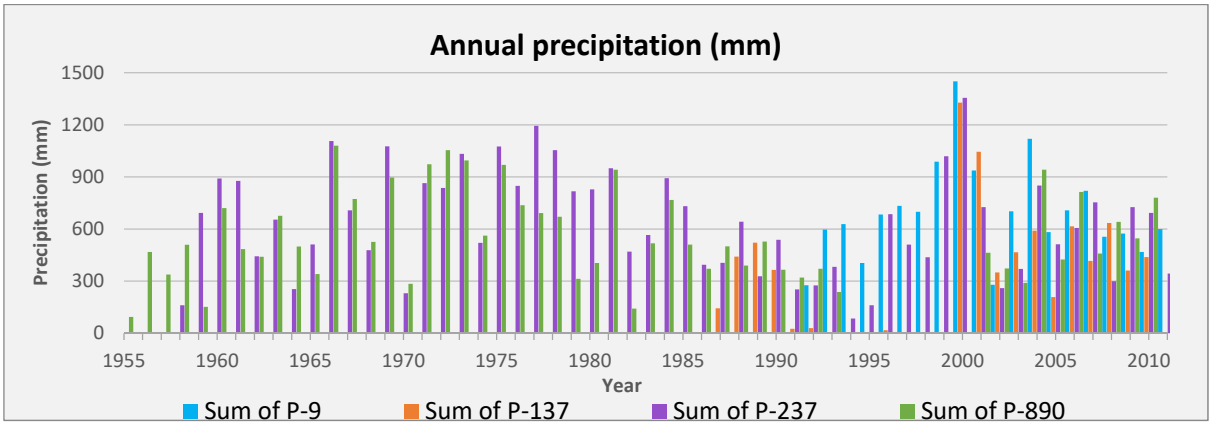

Annual precipitation of different precipitation stations in the study area. Each colour represents a different meteorological station. It is observed a variation of dry and wet years with high variability in the precipitation rates. It is seems to exist climate cycles of about 25 years when years with high precipitation rates tend to occur.

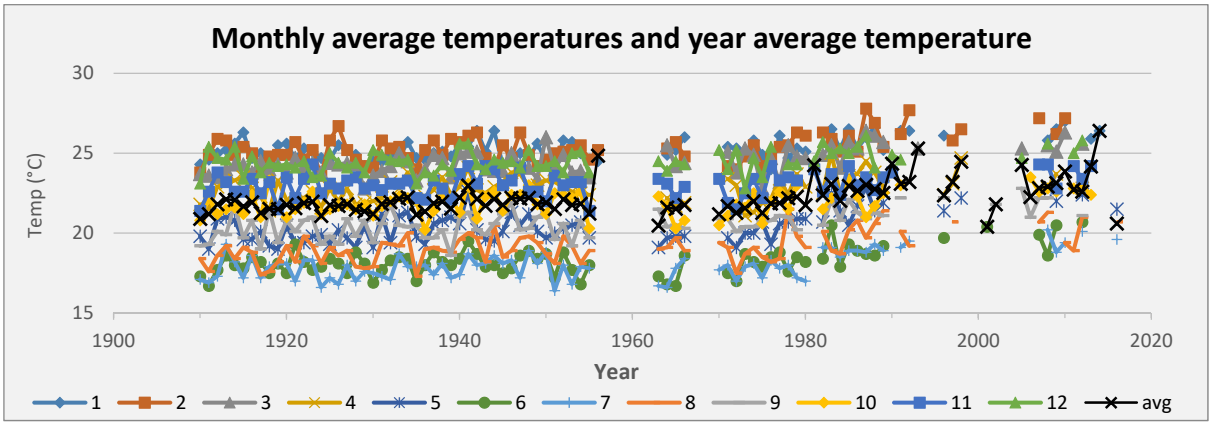

Month temperature averages, as well as year average temperature 1910-2016. Each colour represents a month in the year. Black line represents the year average. Even with gaps and missing data, a general increase of temperatures is easily observed (source: KNMI Climate Explorer).

Appendix B - **Recharge calculation data and information.**

B.01 – Equations used in GIS for WLC under Recharge Potential assessment.

Slope	(("slope@" < 3)*100) + ((("slope@" >= 3) and ("slope@" < 5))* (-5*"slope@"+115)) + ((("slope@">= 5) and ("slope@" < 10))*(-8*"slope@"+130)) + ((("slope@">= 10) and ("slope@" < 20))*(-5*"slope@"+100)) + (("slope@" >= 20)*0)
Drainage Frequency	(("DF@" <= 50)*100) + (("DF@" > 50)*(-.667*"DF@"+133.334)) + (("DF@" > 200)*0)

B.02 – Crop information for different crop types of the area, FAO (1998).

Crop type	Crop Factor	Root Zone (m)
Open shrubland	0.7	1.0
Close shrubland	0.9	1.0
Herbaceous	1	1.5
Broadleaved trees	0.9	1.9
Rainfed crops	1	1.0

B.03 – Available moisture at field capacity for different soil textures (Fetter, 1994).

Soil type	Available moisture at field capacity (*Filed capacity minus wilting point*)
Sand	0.05
Fine Sand	0.1
Sandy loam	0.15
Fine sandy loam	0.18
Loam	0.23
Silt loam	0.2
Light clay loam	0.2
Heavy clay loam	0.18
Clay	0.13

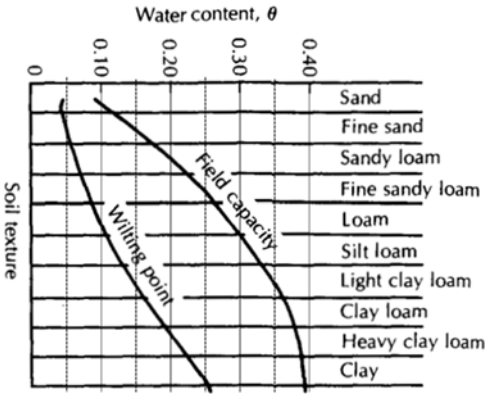

Available soil moisture relation with water content and soil textures (Fetter, 1994)

B.04 – Thornthwaite evapotranspiration formula and method

Given that Thornthwaite formula (Thornthwaite, 1948) is based on monthly values, a factor was used according to each season of the year to achieve daily ETP for each month. Factor values were obtained through a comparison process using two different sets of monthly average temperatures (KNMI Climate Explorer, 2016; and Klimatafel von Maputo-Mavalane (Flugh.)/Mosambik, 2016). From the different temperatures dataset, monthly ETPs were obtained through the formula. The total monthly evaporation from open pan was then multiplied for the factor to result in the monthly ETP for the different temperature sets.

The two set of temperatures resulted in similar conversion factors and the obtained values were in accordance with values from the literature for ETP from evaporation from an open pan through the Penman-Monteith equation (FAO, 1998). So that, the days within each month received the same multiplication factor to convert daily evaporation to daily ETP for the recharge calculation spreadsheet. Values of **0.75** for hot and wet season (Dec-Apr) and **0.55** for drying cold season (May-Nov) were applied.

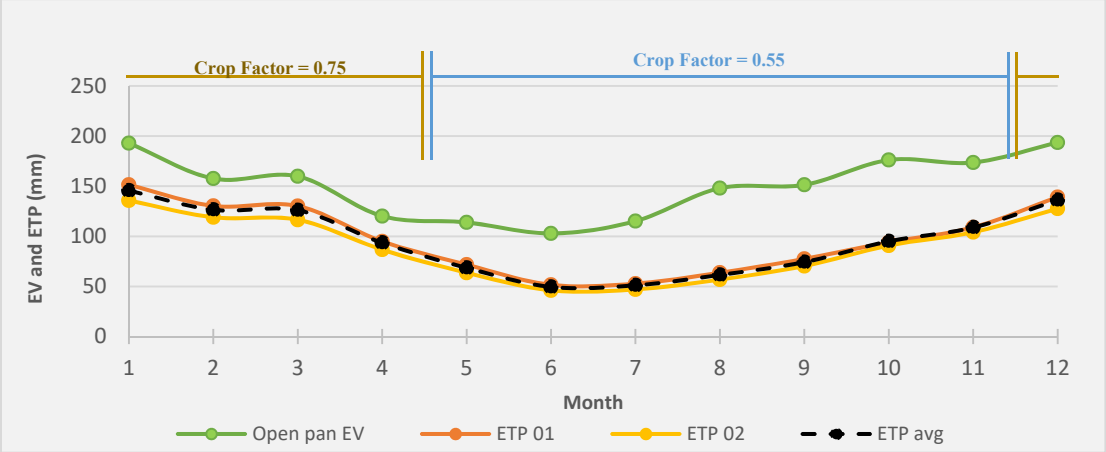

Evaporation from an open pan (green line) and ETP values obtained through combination of Thornthwaite formula and conversion factor from two different temperature sets.

B.05 – Monthly average values of water balance from different piezometers for simulated years (2000-2010). Values expressed in mm (Legend at the bottom and similar for all charts).

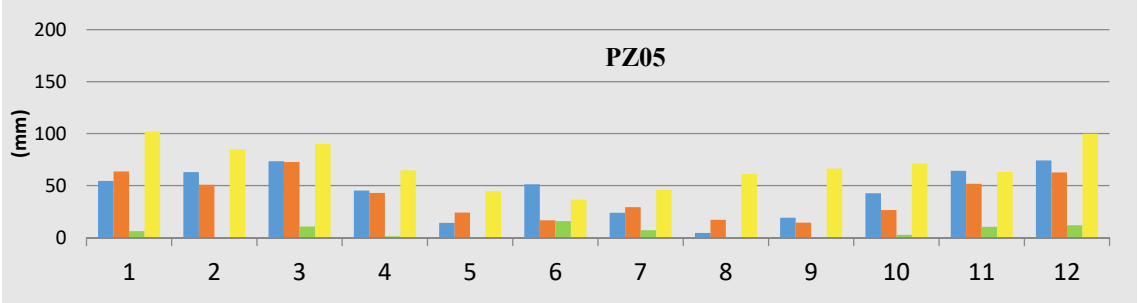

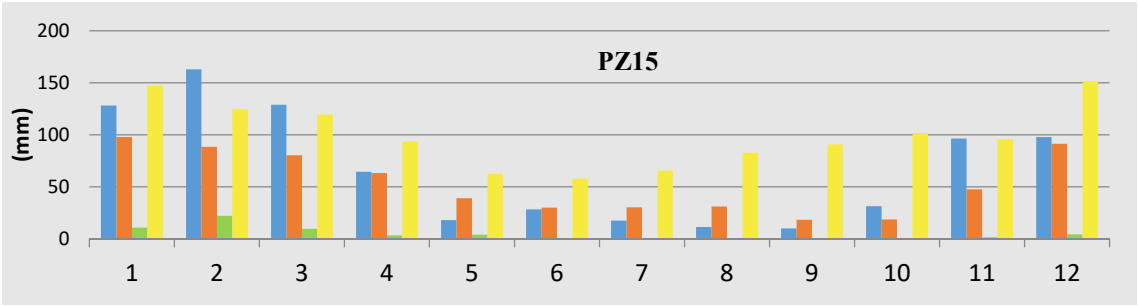

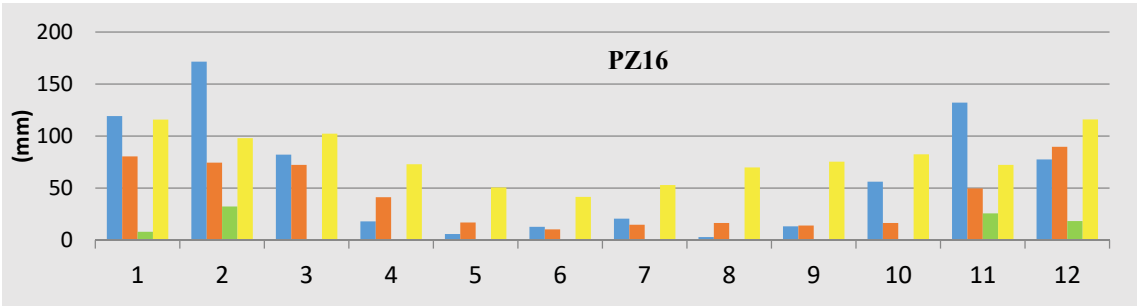

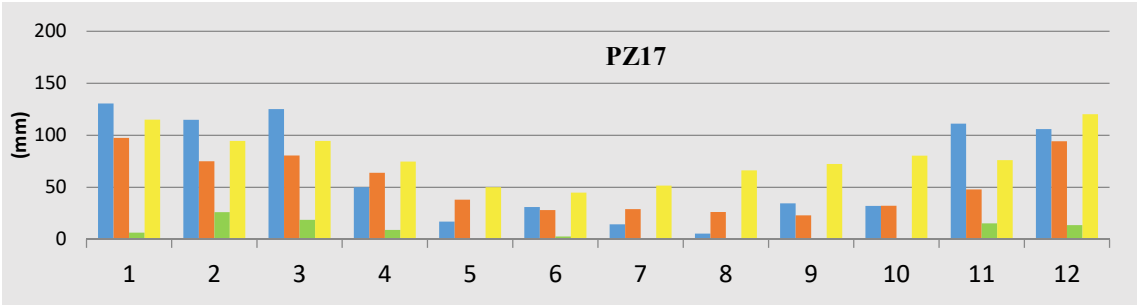

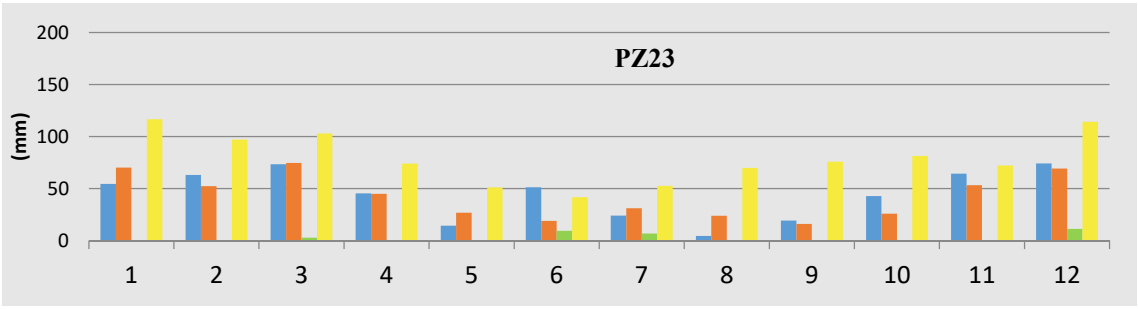
PZ23
(mm)
200
150
100
50
0
1
2
3
4
5
6
7
8
9
10
11
12

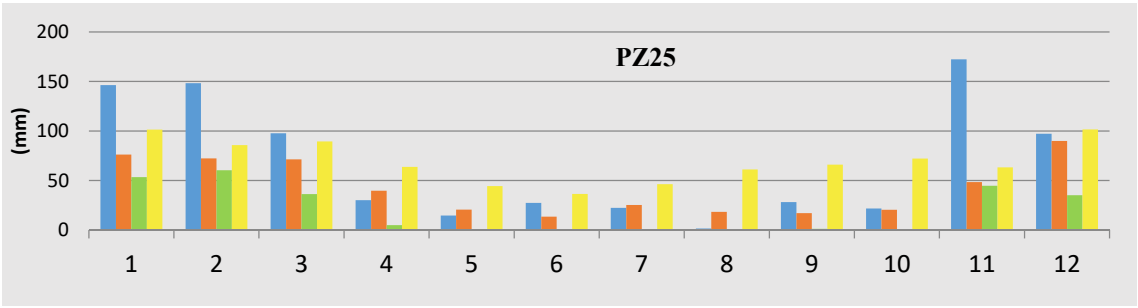
PZ25
(mm)
200
150
100
50
0
1
2
3
4
5
6
7
8
9
10
11
12

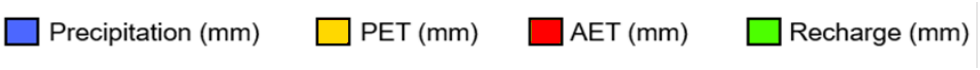
Precipitation (mm)
PET (mm)
AET (mm)
Recharge (mm)

Appendix C - Chemical parameters and field measurements

C.01 – Redox Index classification criteria, based on Stumm (1984).

		Sensitive components (mg/L)			
Level	**Environment**	**NO_3^-**	**Mn^{2+}**	**Fe^{2+}**	**SO_4^{2-}**
0-2	**(sub)oxic**	≥ 1	< 0.1	< 0.1	
3-4	**anoxic**	< 0.5		≥ 0.1	≥ 0.9 $(SO4)_o$
5-6	**deep anoxic**	< 0.5			
ACBT		All Concentrations Below Threshold			

*H2S and CH4 were not measured nor considered in the classification, therefore omitted in the table.

Element	Threshold (mg/L)
NO_3^-	1
Mn^{2+}	0.5
Fe^{2+}	0.25
SO_4^{2-}	3

C.02 – Calibration curve for ARA-Sul EC probe.

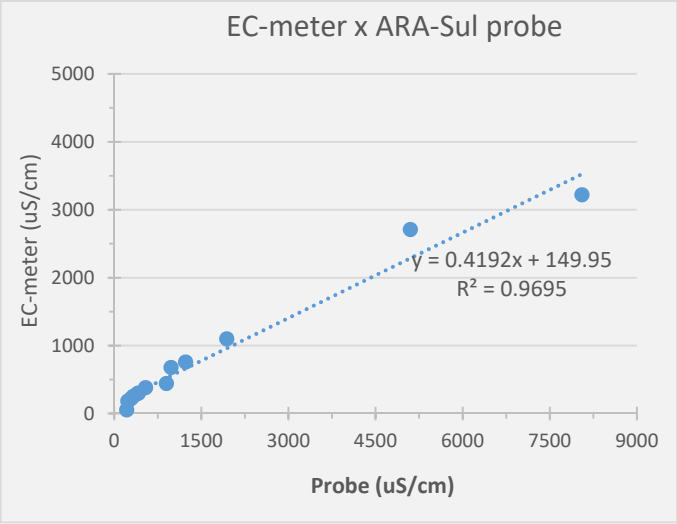

Calibration curve for ARA-Sul Probe using hand EC-meter.

From the curve it is clear that high EC values present higher deviation.

Appendix D - **Water types grouping, water samples results, and statistical results of physicochemical parameters.**

D.01 – Dendrogram obtained from HCA, and defined water type groups.

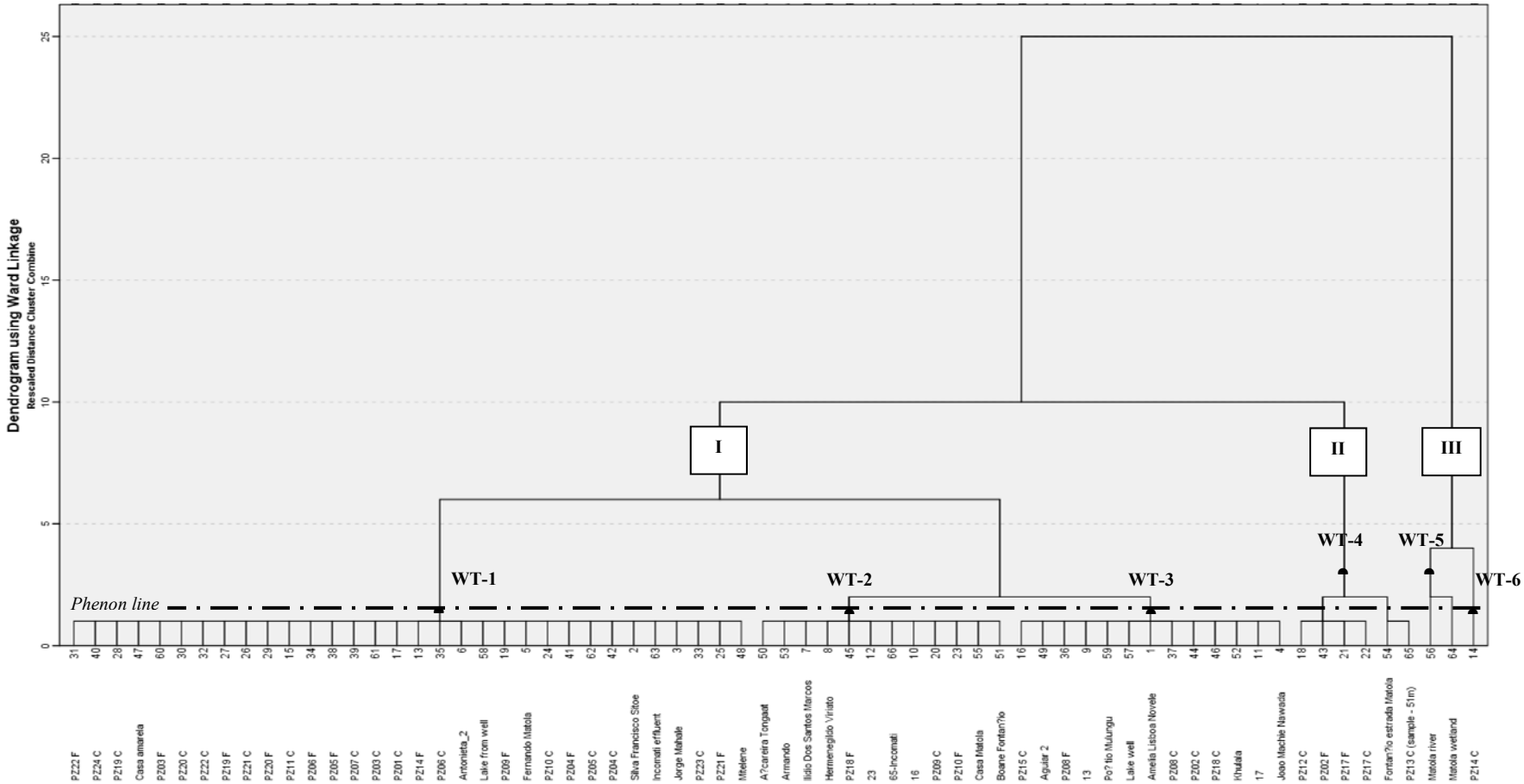

Water samples within hierarchical cluster analysis and defined water groups. Fresh water types (WT-1, WT-2 and WT-3) form a bigger cluster (I), as well as brackish/saline water samples (WT-4 (II) and WT-5 and WT-6(III)). WT-4 and WT-5 were defined slightly above phenon line, instead of two sub-groups, due to similarities of samples.

D.02 – Descriptive statistics of physicochemical parameters and variables of each water type group. Elements in meq/l.

WT	N	Parameter	EC (µS/cm)	Na	K	Mg	Ca	Cl	HCO3	SO4	NO3	Sr	Br	*Na/Cl*	*Mg/Cl*	*Mg/Ca*	*SO4/Cl*	*Ca/SO4*	*SO4/Na*	*Ca/HCO3*	*Cl/HCO3*	*Br/Cl*	*Sr/Cl*	D2	18O
		std.d.	116	0.730	0.042	0.128	0.591	0.735	1.355	0.228	0.060	0.000	0.000	0.576	0.186	0.469	0.119	38.748	0.146	1.215	2.428	0.000	0.001	5.252	0.755
		min	54	0.210	0.019	0.040	0.122	0.300	0.000	0.000	0.000	0.000	0.056	0.511	0.024	0.042	0.006	0.564	0.005	0.032	0.192	0.038	0.000	-26.50	-4.630
1	32	***avg***	299	**1.457**	**0.107**	**0.292**	**0.696**	**1.409**	**1.213**	**0.184**	**0.022**	**0.001**	**0.056**	**1.137**	**0.252**	**0.678**	**0.132**	**15.532**	**0.133**	**0.995**	**2.497**	**0.038**	**0.001**	**-14.99**	**-3.532**
		max	545	3.071	0.197	0.586	2.045	3.600	7.700	1.300	0.300	0.002	0.056	3.155	1.115	1.797	0.522	218.20	0.760	6.361	9.849	0.038	0.003	-4.500	-1.040
		std.d.	51	0.991	0.101	0.672	0.665	0.893	1.382	0.419	0.227	0.001	0.000	0.441	0.321	1.093	0.222	1.180	0.169	1.011	12.416	0.000	0.000	6.273	0.958
		min	636	2.213	0.024	0.389	0.341	1.600	0.100	0.400	0.000	0.001	0.004	0.712	0.104	0.305	0.122	0.487	0.071	0.158	0.510	0.002	0.000	-22.40	-4.500
2	12	***avg***	742	**3.925**	**0.204**	**1.121**	**1.271**	**2.817**	**2.425**	**0.850**	**0.100**	**0.002**	**0.004**	**1.479**	**0.454**	**1.146**	**0.334**	**1.836**	**0.251**	**1.030**	**5.766**	**0.002**	**0.001**	**-13.85**	**-3.343**
		max	824	5.374	0.397	2.375	2.195	4.600	4.100	1.800	0.700	0.003	0.004	2.491	1.058	4.594	0.935	3.514	0.561	3.354	45.620	0.002	0.002	-0.500	-1.580
		std.d.	133	1.488	0.398	0.940	1.017	1.576	1.286	0.603	0.080	0.002	0.002	0.503	0.311	0.959	0.190	3.493	0.131	0.301	0.715	0.000	0.001	5.612	1.088
		min	933	3.613	0.035	0.160	0.268	2.800	2.300	0.200	0.000	0.000	0.005	0.785	0.056	0.478	0.027	0.398	0.021	0.052	0.449	0.001	0.000	-20.90	-4.490
3	13	***avg***	1122	**6.322**	**0.334**	**1.720**	**1.771**	**5.015**	**4.038**	**0.908**	**0.023**	**0.003**	**0.008**	**1.368**	**0.377**	**1.233**	**0.214**	**2.948**	**0.157**	**0.471**	**1.423**	**0.001**	**0.001**	**-13.64**	**-3.142**
		max	1460	10.017	1.233	3.687	3.450	7.500	6.200	2.500	0.300	0.006	0.011	2.615	1.321	3.604	0.788	14.198	0.552	1.193	2.952	0.002	0.002	0.200	-0.980
		std.d.	908.4	7.646	0.112	2.503	3.032	9.808	5.568	1.589	0.880	0.132	7.550	0.206	0.054	0.318	0.034	3.779	0.055	0.547	4.304	0.000	0.000	3.199	0.421
		min	2600.0	11.304	0.312	4.000	2.530	21.983	18.805	1.065	0.978	0.000	21.779	0.466	0.196	0.816	0.037	1.233	0.079	0.982	5.377	0.001	0.000	-20.70	-4.590
4	6	***avg***	3450.0	17.649	0.414	6.394	6.052	30.509	24.113	3.644	2.091	0.084	29.931	0.722	0.258	1.163	0.088	4.018	0.124	1.750	8.093	0.001	0.000	-17.02	-3.913
		max	5250.0	32.957	0.653	10.123	11.700	50.422	35.366	6.139	3.269	0.371	45.145	0.997	0.358	1.581	0.135	11.964	0.243	2.375	17.651	0.001	0.001	-11.30	-3.440
		std.d.	1490	4.696	0.139	8.107	6.400	16.450	0.000	6.050	0.000	0.010	0.016	0.022	0.016	0.051	0.022	0.121	0.055	0.000	0.000	0.000	0.000	0.650	0.635
		min	14700	80.913	0.714	46.996	29.350	152.300	6.400	17.800	0.000	0.056	0.185	0.488	0.309	1.500	0.117	1.408	0.220	4.553	23.629	0.001	0.000	3.100	-1.030
5	2	***avg***	16190	**85.609**	**0.853**	**55.103**	**35.750**	**168.75**	**6.400**	**23.850**	**0.000**	**0.066**	**0.201**	**0.510**	**0.325**	**1.550**	**0.140**	**1.529**	**0.276**	**4.553**	**23.629**	**0.001**	**0.000**	**3.750**	**-0.395**
		max	17680	90.304	0.992	63.210	42.150	185.200	6.400	29.900	0.000	0.076	0.217	0.531	0.341	1.601	0.162	1.649	0.331	4.553	23.629	0.001	0.000	4.400	0.240
6	1		9200	**46.261**	**0.456**	**30.123**	**13.550**	**59.000**	**6.900**	**5.000**	**0.400**	**0.032**	**0.090**	**0.784**	**0.511**	**2.223**	**0.086**	**2.685**	**0.109**	**1.960**	**8.534**	**0.002**	**0.001**	**-14.70**	**-4.040**

D.03 – Boxplot for pH together with major ion concentrations, and main ratios divided according to each water type.

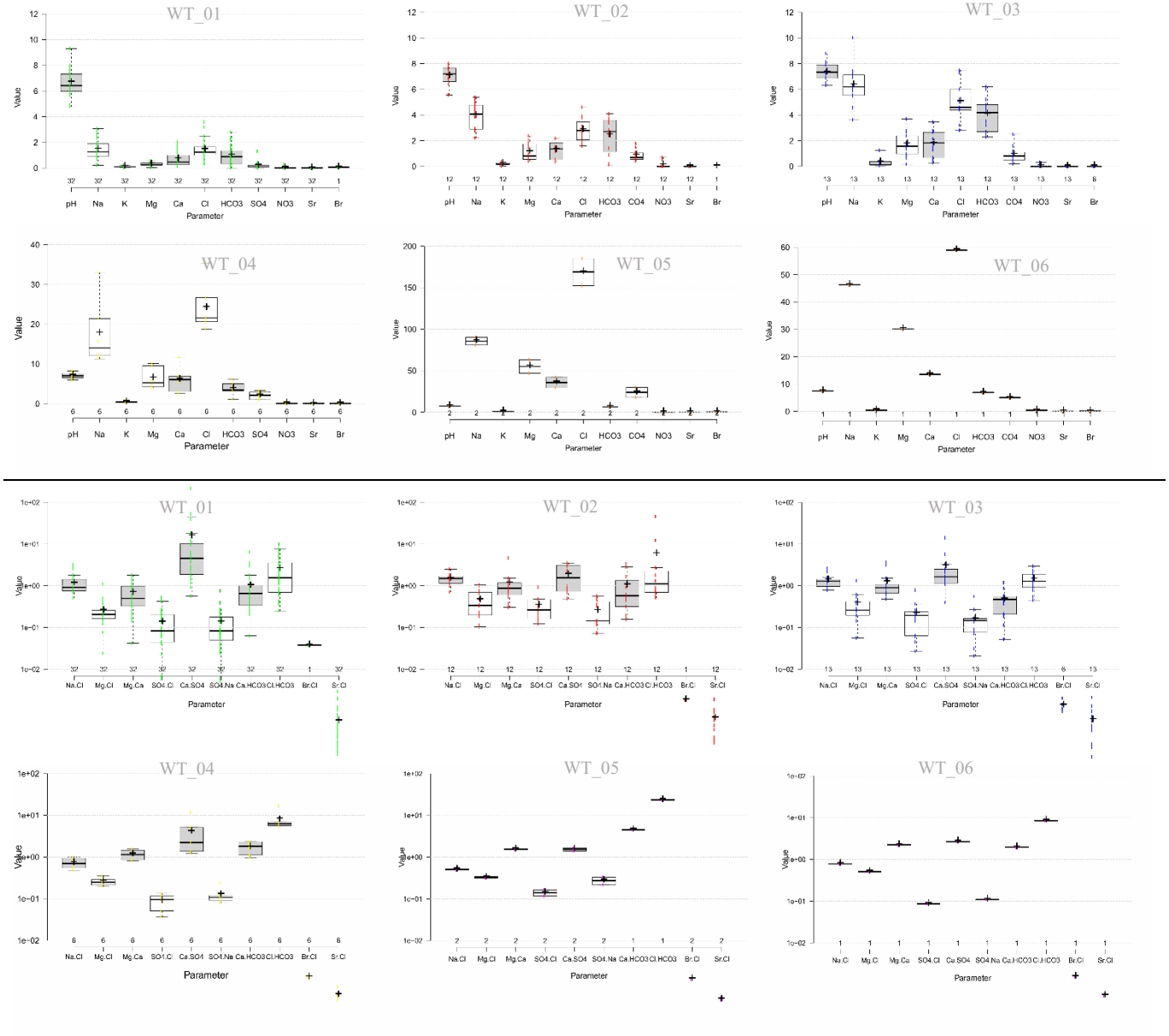

D.04 – Schöeller-Berkaloff and SAR diagrams with mean values of each water group. WT-5 does not appear in SAR diagram due to relatively high EC value for the scale.

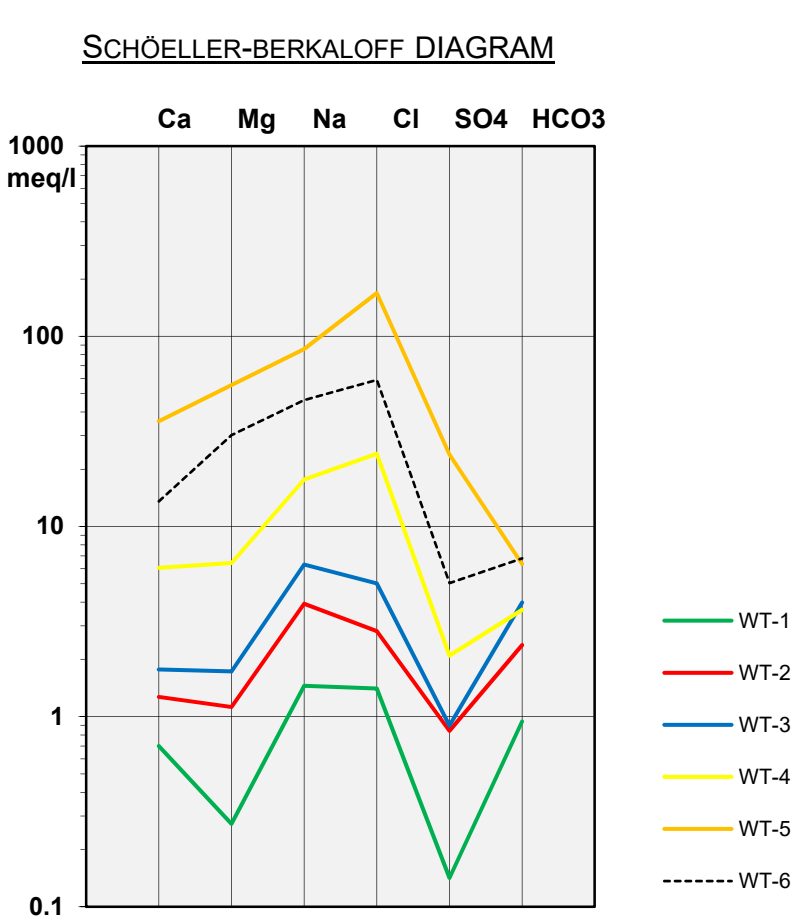

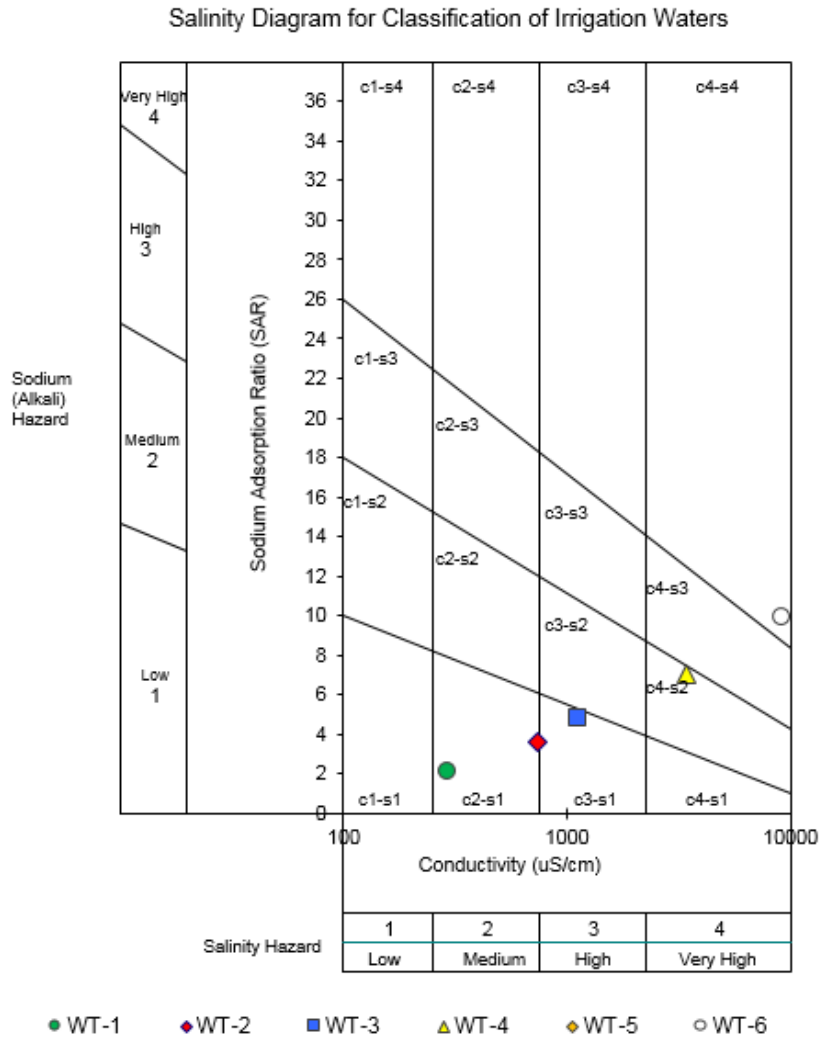

D.05 – Physicochemical parameters from water samples of Maputo area divided by WT groups.

N	NAME	TYPE	WT	Facies (WT/R/BEX/PI/SI)	EC	TDS	pH	T.	IE	Na	K	Mg	Ca	Cl	HCO3	SO4	NO3	Sr	Br	δ 2H	δ 18O	SI Calcite	SI Gypsum	SI Dolomite	SI pCO2	SI Halite
2	Silva Francisco Sitoe	SGW	1	F1-CaCl2/0-2/0/1.5/0	545.0	778.6	7.84	26.3	8.6	1.94	0.20	0.47	2.02	2.23	1.35	0.05	0.27	0.00109		-13.9	-3.4	-0.05	-3.35	-0.58	-2.93	-7.00
3	Jorge Mahale	SGW	1	F0-NaCl/0-2/1.6/0.8/-1.4	468.0	668.6	7.3	27.6	16.3	3.07	0.07	0.27	0.48	1.70	0.70	0.27	0.14	0.00044		-18.4	-4.5	-1.44	-3.17	-2.98	-2.65	-6.91
5	Fernando Matola	SGW	1	F1-CaHCO3/0-2/0/0.8/0.1	355.0	507.1	8	26.6	3.8	1.28	0.13	0.43	1.35	1.13	1.70	0.07	0.06	0.00072		-17.6	-3.9	0.06	-3.32	-0.22	-2.98	-7.47
6	Antonieta_2	SGW	1	F0-NaCl/0-2/0/0/-1.5	268.0	382.9	6.97	28.0	3.0	1.14	0.20	0.24	0.63	1.20	1.00	0.12	0.03	0.00046		-17.7	-3.9	-1.47	-3.39	-3.19	-2.16	-7.48
13	PZ14 F	SGW	1	F*-NaCl/0-2/0/0/-2.2	240.0	342.9	7.05	26.2	7.5	1.02	0.12	0.35	0.24	1.49	0.41	0.06	0.05	0.00026	5.59E-02	-16.5	-4.2	-2.20	-4.02	-4.10	-2.63	-7.43
16	PZ11 C	DGW	1	F0-NaCl/4-6/0.9/0.7/-2.7	302.0	431.4	6.08	25.4	6.6	1.97	0.07	0.37	0.37	1.38	0.90	0.31	0.00	0.00041		-17.5	-4.0	-2.70	-3.21	-5.26	-1.33	-7.19
18	PZ01 C	DGW	1	F1-NaCl/ACBT/0/1.8/0.9	317.0	452.9	9.3	25.3	9.1	1.47	0.13	0.05	1.22	2.10	1.10	0.20	0.01	0.0022		-18.6	-4.5	0.95	-2.94	0.67	-4.61	-7.14
20	PZ09 F	SGW	1	g1-CaHCO3/ACBT/0.6/0.6/-0.1	255.0	364.3	7.77	27.8	9.7	0.94	0.06	0.27	1.61	0.61	1.50	0.26	0.00	0.00179		-26.5	-4.6	-0.12	-2.68	-0.86	-2.79	-7.87
25	PZ10 C	DGW	1	F*-CaCl2/4-6/0/0.8/-2.5	350.0	500.0	6.05	25.2	18.1	1.76	0.06	0.34	1.94	2.22	0.30	0.40	0.00	0.00021		-17.9	-3.7	-2.51	-2.45	-5.64	-1.79	-7.04
26	PZ21 F	SGW	1	F2-NaHCO3/4-6/1.4/0/-1.1	442.0	631.4	7.04	25.8	0.8	2.67	0.12	0.32	0.63	1.59	2.20	0.06	0.01	0.00124		-10.2	-3.4	-1.12	-3.69	-2.40	-1.91	-7.00
27	PZ21 C	DGW	1	g0-CaHCO3/4,5-6/0/0.9/-2.9	118.3	169.0	5.84	25.3	0.6	0.29	0.07	0.16	0.40	0.33	0.74	0.00	0.00	0.00039		-6.6	-2.7	-2.94	-5.33	-6.12	-1.17	-8.62
28	PZ19 F	SGW	1	F*-NaCl/0-2/0/0.5/-3.1	220.0	314.3	6.37	25.5	4.6	1.12	0.09	0.25	0.22	1.39	0.30	0.09	0.06	0.00032		-7	-3.0	-3.08	-3.94	-5.94	-2.09	-7.42
29	PZ19 C	DGW	1	F*-NaCl/ACBT/0/0.8/-3.6	162.5	232.1	6.02	25.4	3.5	0.79	0.10	0.20	0.20	1.07	0.20	0.11	0.01	0.00025		-12.9	-3.7	-3.62	-3.86	-7.11	-1.91	-7.68
30	PZ20 F	SGW	1	g*-NaCl/ACBT/0/1.8/-5.6	53.7	76.7	4.78	25.3	4.1	0.21	0.02	0.04	0.12	0.31	0.04	0.08	0.00	5.5E-05		-17.1	-3.9	-5.59	-4.12	-11.52	-1.21	-8.78
31	PZ20 C	DGW	1	F1-NaHCO3/4,5-6/0/0.6/-2.6	200.0	285.7	6.2	24.3	8.1	1.05	0.07	0.23	0.28	0.91	1.06	0.01	0.00	0.00059		-4.9	-2.1	-2.60	-5.04	-5.17	-1.38	-7.63
32	PZ22 F	SGW	1	F*-NaCl/4,5-6/0/0.5/-2.7	184.5	263.6	6.43	26.7	5.9	0.83	0.09	0.24	0.26	1.09	0.50	0.05	0.01	0.00051		-5.5	-2.5	-2.68	-4.12	-5.25	-1.92	-7.65
33	PZ22 C	DGW	1	F*-NaCl/4-6/0/0.9/-3.5	204.0	291.4	5.91	25.3	3.8	0.92	0.10	0.27	0.23	1.13	0.30	0.25	0.01	0.00041		-14	-3.9	-3.51	-3.46	-6.82	-1.63	-7.60
34	PZ23 C	DGW	1	F2-NaHCO3/ACBT/1.5/0.2/-1.1	469.0	670.0	7	24.8	4.5	2.94	0.12	0.39	0.79	1.78	2.40	0.45	0.01	0.00111		-21.3	-4.0	-1.06	-2.79	-2.31	-1.84	-6.92
35	PZ06 F	SGW	1	F0-NaCl/4-6/1.5/0.5/-2.6	297.0	424.3	6.37	25.3	16.5	2.71	0.20	0.27	0.24	1.54	0.90	0.09	0.01	0.00021		-21.3	-3.9	-2.58	-3.92	-4.98	-1.62	-7.00
36	PZ06 C	DGW	1	F*-NaCl/4-6/0/0.9/-3.7	241.0	344.3	5.86	24.9	6.1	1.20	0.15	0.27	0.16	1.62	0.34	0.11	0.01	0.00018		-19	-4.2	-3.68	-3.99	-7.00	-1.53	-7.33
39	PZ05 F	SGW	1	g0-CaHCO3/0-2/0/0.3/-0.7	301.0	430.0	7.33	27.1	21.8	0.69	0.09	0.24	1.72	0.66	0.94	0.16	0.02	0.00054		-13.1	-3.1	-0.73	-2.86	-2.15	-2.56	-7.97
41	PZ07 C	DGW	1	F1-NaCl/0-2/0/0.4/-2.1	285.0	407.1	6.44	25.9	12.9	1.41	0.14	0.27	0.45	1.50	1.32	0.11	0.02	0.00058		-17.8	-4.0	-2.06	-3.57	-4.21	-1.52	-7.30
42	PZ24 C	DGW	1	F0-NaCl/0-2/0/0.5/-2.5	187.2	267.4	6.37	26.3	11.5	0.91	0.13	0.13	0.35	1.07	0.76	0.07	0.02	0.00034		-18	-3.5	-2.45	-3.84	-5.17	-1.68	-7.63
43	PZ04 F	SGW	1	F2-NaHCO3/0-2/1.8/0.5/-0.7	381.0	544.3	7.61	27.1	0.2	2.50	0.14	0.22	0.47	0.95	2.18	0.18	0.03	0.00044		-18.6	-3.5	-0.67	-3.35	-1.50	-2.47	-7.25
44	PZ04 C	DGW	1	F2-CaHCO3/ACBT/0.9/0.7/0.3	403.0	575.7	7.91	26.7	2.9	1.39	0.09	0.42	2.05	0.98	2.72	0.04	0.00	0.00121		-17.9	-3.1	0.34	-3.44	0.15	-2.69	-7.50

N	NAME	TYPE	WT	Facies (WT/R/BEX/PI/SI)	EC	TDS	pH	T.	IE	Na	K	Mg	Ca	Cl	HCO3	SO4	NO3	Sr	Br	δ 2H	δ 18O	SI Calcite	SI Gypsum	SI Dolomite	SI pCO2	SI Halite
49	Casa amarela	SGW	1	F0-NaCl/ACBT/0/1.1/-3.3	210.0	300.0	5.65	25.4	16.5	1.23	0.10	0.10	0.23	1.29	0.94	0.08	0.01	0.00022		-15.1	-4.1	-3.27	-3.94	-6.78	-0.88	-7.41
50	Mitelene	SGW	1	F*-NaCl/4,5-6/0/1.7/-4.4	446.0	637.1	4.92	25.9	2.9	2.37	0.04	0.40	0.28	3.20	0.32	0.02	0.00	0.00073		-21	-4.2	-4.40	-4.48	-8.50	-0.61	-6.75
60	Lake	SW	1	g1-NaHCO3/4,5-6/1.5/0.4/-0.8	270.0	385.7	7.44	29.4	7.8	1.40	0.09	0.50	0.61	0.45	1.74	0.06	0.00	0.00088		-4.5	-1.0	-0.77	-3.72	-1.44	-2.38	-7.83
62	PZ03 F	SGW	1	F*-NaCl/ACBT/0/0.8/-3.2	209.0	298.6	5.94	27.6	7.7	0.94	0.09	0.20	0.46	0.97	0.28	0.18	0.01	0.00026		-11.6	-3.3	-3.18	-3.29	-6.57	-1.68	-7.65
63	PZ03 C	DGW	1	F*-CaCl2/4-6/0/0.2/-1.9	291.0	415.7	6.71	27.3	22.5	0.90	0.11	0.31	1.26	1.07	0.36	0.23	0.00	0.00044		-16.3	-3.9	-1.89	-2.81	-4.23	-2.35	-7.64
64	PZ05 C	DGW	1	F0-NaCl/4-6/-1.4/0.9/-3.2	367.0	524.3	5.85	25.0	19.4	1.84	0.11	0.53	0.29	3.59	0.56	0.16	0.00	0.0005		-10.3	-2.6	-3.24	-3.62	-6.10	-1.31	-6.81
66	Incomati eff	SW	1	F0-NaCl/ACBT/0/1.3/-1.7	537.0	767.1	6.82	24.0	21.4	1.69	0.09	0.59	0.73	2.46	0.98	1.28	0.01	0.00107		-11.1	-2.8	-1.69	-2.37	-3.35	-2.05	-7.02
7	Ilidio	SGW	2	F2-NaHCO3/ACBT/3.3/0.9/0	708.0	1011.4	7.67	28.6	9.0	4.27	0.27	0.55	1.50	1.71	3.30	0.50	0.01	0.0012		-16.7	-4.5	0.04	-2.52	-0.18	-2.36	-6.79
8	Hermenegildo	SGW	2	F2-NaMIX/ACBT/1.9/0.8/-0.7	636.0	908.6	7.5	28.3	6.0	3.85	0.13	0.44	0.51	2.39	2.60	0.56	0.01	0.00085		-17.8	-4.0	-0.69	-2.90	-1.26	-2.28	-6.68
10	16	SGW	2	F2-NaHCO3/ACBT/3.1/0.8/0.4	771.0	1101.4	8.02	27.7	1.1	4.88	0.14	0.94	1.28	2.72	4.00	0.37	0.00	0.00162		-16.6	-4.2	0.37	-2.75	0.78	-2.64	-6.53
12	23	SGW	2	F2-NaHCO3/ACBT/2.3/1.1/0.4	824.0	1177.1	7.87	27.8	0.8	4.44	0.25	0.66	2.17	2.89	3.90	0.62	0.00	0.00129		-19.1	-3.6	0.43	-2.31	0.52	-2.50	-6.55
21	PZ09 C	DGW	2	F2-NaCl/4-6/1.9/0.6/-1.4	778.0	1111.4	6.78	27.8	5.7	5.37	0.14	0.39	0.45	3.75	2.80	0.66	0.00	0.00076		-18.8	-3.9	-1.45	-2.91	-2.80	-1.54	-6.35
24	PZ10 F	SGW	2	f*-NaCl/ACBT/0/1.5/-4.2	759.0	1084.3	5.57	25.8	2.7	4.63	0.22	0.52	0.34	4.64	0.10	0.67	0.00	0.0008		-18	-4.2	-4.22	-2.99	-8.11	-1.77	-6.31
47	PZ18 F	SGW	2	F2-CaHCO3/0-2/2.5/1.5/0.1	679.0	970.0	7.6	28.1	2.9	2.86	0.28	1.45	2.17	1.93	3.48	0.93	0.05	0.00205	3.50E-03	-4.7	-1.7	0.13	-2.14	0.24	-2.27	-6.92
52	Açuc Tongaat	SGW	2	F2-CaMIX/3/0/1.1/-0.4	718.0	1025.7	7.21	27.4	0.7	2.21	0.12	2.02	2.20	3.11	2.34	1.04	0.00	0.00285		-11.5	-3.0	-0.44	-2.10	-0.75	-2.06	-6.82
53	Boane Fontanário	SGW	2	F2-NaHCO3/0-2/2.6/0.3/-0.6	745.0	1064.3	7.17	25.4	0.5	5.10	0.02	0.63	1.17	2.96	3.62	0.36	0.04	0.00069		-22.4	-4.1	-0.57	-2.78	-1.27	-1.83	-6.47
55	Armando	SGW	2	F0-MgMIX/0-2/3/2.5/-1.9	715.0	1021.4	6.4	23.2	16.2	2.73	0.40	1.63	1.52	1.64	0.90	1.53	0.52	0.00312		-8.9	-2.6	-1.87	-2.05	-3.59	-1.68	-7.00
57	Casa Matola	SGW	2	F*-NaCl/0-2/3.2/3.2/-3.8	767.0	1095.7	5.56	25.8	19.6	2.93	0.33	2.38	0.52	2.25	0.18	1.06	0.69	0.00169		-11.3	-2.7	-3.81	-2.67	-6.82	-1.51	-6.83
70	65-Incomati	SW	2	F1-NaCl/4-6/1.7/1.6/-0.5	808.0	1154.3	6.85	25.4	1.3	3.82	0.15	1.84	1.44	3.87	1.40	1.80	0.00	0.00249		-0.5	-1.6	-0.50	-1.97	-0.82	-1.48	-6.54
1	Amelia	SGW	3	F3-NaHCO3/0-2/4.7/2.1/0.5	933.0	1332.9	8.79	26.2	3.9	7.45	0.13	0.16	0.27	2.85	5.10	0.67	0.03	0.00023		-17.6	-4.2	0.46	-3.20	0.86	-3.34	-6.33
4	João Machie	SGW	3	f3-NaCl/0-2/2.1/1.2/0.1	1460.0	2085.7	7.42	26.7	2.3	7.11	0.12	2.71	2.66	7.35	4.70	1.06	0.04	0.00418		-16.9	-4.1	0.09	-2.11	0.33	-1.98	-5.96
9	13	SGW	3	f2-NaCl/ACBT/2/1.1/-0.4	1002.0	1431.4	7.34	29.0	1.4	6.19	0.19	0.97	1.51	5.01	2.60	1.00	0.00	0.002		-16.5	-4.1	-0.41	-2.27	-0.85	-2.13	-6.17
11	17	SGW	3	f3-NaMIX/ACBT/3/1.6/0.5	1150.0	1642.9	7.9	28.2	0.1	6.95	0.13	1.50	2.12	5.23	4.46	1.02	0.01	0.00231		-17.2	-3.7	0.48	-2.18	0.97	-2.47	-6.11
17	PZ15 C	DGW	3	f2-NaMIX/ACBT/3.4/1.1/-0.9	1050.0	1500.0	6.87	24.4	2.3	7.18	0.12	0.87	1.29	4.47	3.40	1.17	0.00	0.00152	9.01E-03	-20.9	-4.5	-0.91	-2.28	-1.86	-1.57	-6.16
37	PZ08 F	SGW	3	f2-NaCl/ACBT/1.8/0.4/-1.8	1100.0	1571.4	6.47	27.9	1.8	5.48	1.23	1.56	0.49	6.04	2.66	0.39	0.00	0.00015	6.76E-03	-15.6	-3.4	-1.76	-3.16	-2.85	-1.25	-6.14
38	PZ08 C	DGW	3	f2-NaCl/4-6/0/0.5/-1.9	1213.0	1732.9	6.37	26.6	4.5	5.89	1.23	1.90	0.53	7.50	2.50	0.46	0.00	0.00121	7.26E-03	-13.9	-3.4	-1.89	-3.08	-3.07	-1.19	-6.02

N	NAME	TYPE	WT	Facies (WT/R/BEX/PI/SI)	EC	TDS	pH	T.	IE	Na	K	Mg	Ca	Cl	HCO3	SO4	NO3	Sr	Br	δ 2H	δ 18O	SI Calcite	SI Gypsum	SI Dolomite	SI pCO2	SI Halite
46	PZ02 C	DGW	3	f2-NaCl/ACBT/0/0.9/0.7	1230.0	1757.1	8.15	26.7	2.7	6.27	0.38	1.83	2.77	7.34	3.12	0.19	0.00	0.00429	1.05E-02	-17.4	-3.8	0.67	-2.78	1.31	-2.90	-6.01
48	PZ18 C	DGW	3	f3-NaMIX/0-2/4/2.2/0.7	1182.0	1688.6	8.03	27.8	2.8	5.94	0.40	2.38	2.66	4.41	4.72	1.61	0.04	0.00328	5.01E-03	0.2	-1.0	0.70	-1.92	1.52	-2.59	-6.26
51	Aguiar 2	SGW	3	f3-NaMIX/ACBT/3.6/0.9/-0.1	1064.0	1520.0	7.4	26.7	4.1	5.53	0.04	2.78	1.83	4.48	4.15	0.78	0.00	0.00442		-9.5	-2.0	-0.12	-2.36	0.09	-2.01	-6.27
54	Khulala	SGW	3	f3-NaHCO3/0-2/5.8/0.2/-0.6	1193.0	1704.3	7.22	25.4	3.1	10.02	0.05	0.67	0.69	4.61	5.90	0.21	0.02	0.00063	6.51E-03	-16.8	-3.2	-0.58	-3.31	-1.03	-1.68	-6.00
59	Well (lake)	SGW	3	F3-MgHCO3/0-2/4.4/0.6/-0.2	1000.0	1428.6	6.93	25.8	6.4	3.61	0.06	3.69	3.45	2.79	6.12	0.61	0.03	0.00588		-8.4	-1.4	-0.17	-2.24	-0.17	-1.38	-6.67
61	Poço tio Mulungu	SGW	3	F2-NaMIX/0-2/2.7/2.6/-1.3	1005.0	1435.7	6.3	24.3	3.9	4.56	0.28	1.33	2.79	3.19	2.30	2.52	0.31	0.002		-6.9	-2.2	-1.33	-1.65	-2.86	-1.18	-6.50
19	PZ12 C	DGW	4	B1-NaCl/0-2/0/2/-2.1	2600.0	3714.3	5.97	25.8	1.8	15.65	0.40	4.00	2.53	18.81	1.07	1.85	0.06	0.00768	2.38E-02	-20.7	-3.9	-2.09	-1.98	-3.84	-1.19	-5.23
22	PZ17 F	SGW	4	B2-NaCl/0-2/0/1.6/-0.4	3220.0	4600.0	7.15	27.3	3.5	21.43	0.40	4.22	3.05	21.49	3.10	2.47	0.07	0.00793	3.00E-02	-11.3	-3.7	-0.38	-1.84	-0.47	-1.91	-5.05
23	PZ17 C	DGW	4	B2-CaCl2/ACBT/-5.1/2.1/0.4	3020.0	4314.3	7.58	27.0	6.1	12.11	0.31	5.78	6.75	21.72	3.40	2.94	0.00	0.01712	2.75E-02	-19.3	-4.3	0.41	-1.46	0.91	-2.31	-5.30
45	PZ02 F	SGW	4	B2-NaCl/ACBT/-5.5/1/0.9	2710.0	3871.4	8.2	27.4	6.4	11.30	0.65	4.69	5.34	20.63	3.20	1.04	0.00	0.01048	2.84E-02	-15.8	-3.5	0.91	-1.96	1.94	-2.97	-5.34
56	Fontanário estrada Matola	DGW	4	b3-NaCl/0-2/5.5/2.3/-0.5	5250.0	7500.0	6.54	25.3	5.6	32.96	0.39	10.12	6.95	35.37	6.14	3.27	0.37	0.01427	4.46E-02	-15.5	-3.4	-0.45	-1.54	-0.60	-1.04	-4.68
68	PZ13 C	DGW	4	B3-CaCl2/4-6/-6.3/0/0.1	3900.0	5571.4	6.95	24.0	2.2	12.43	0.33	9.55	11.70	26.66	4.96	0.98	0.00	0.01279	3.42E-02	-19.5	-4.6	0.11	-1.79	0.27	-1.55	-5.21
58	Matola river	SW	5	b*-MgCl/3/-44.1/4/-1000	17680.0	25257.1	7.35	24.8	4.9	90.30	0.99	63.21	42.15	185.16	**7.00**	29.93	0.00	0.07557	2.17E-01	4.4	0.2	-1000.00	-0.33	-1000.00	-1000.00	-3.63
67	Matola wetland	SW	5	b3-NaCl/ACBT/-34.8/3.3/0.7	14700.0	21000.0	7.3	25.0	5.9	80.91	0.71	47.00	29.35	152.3	6.34	17.80	0.00	0.05616	1.85E-01	3.1	-1.0	0.69	-0.63	1.73	-1.87	-3.75
14	PZ14 C	DGW	6	b3-NaCl/0-2/13.5/2.5/0.7	9200.0	13142.9	7.43	25.5	12.2	46.26	0.46	30.12	13.55	59.0	6.80	5.05	0.40	0.03208	9.04E-02	-14.7	-4.0	0.66	-1.29	1.81	-1.93	-4.35

Abbreviations:

N – sample number

SGW – shallow groundwater (phreatic aquifer); DPG – deep groundwater (semi-confined aquifer); SW – surface water

WT – Water group number

EC – Electrical conductivity in *µS/cm*

TDS – Total dissolved salts in *mg/L*

T. – Temperature in *°C*

IE – Ionic balance error in *%*

Ion concentrations in *meq/L*

Isotope values in *‰* referent to Vienna VSMOW

Lower detection limits for major ion analyses (*mg/L*):

Cl^- = 2.0

NO_3^- = 0.3

SO_4^{2-} = 2.0

PO_4^{2-} = 0.3

Na^+ = 4.0 E-03

K^+ = 1.9 E-03

Ca^{2+} = 89.0 E-03

Mg^{2+} = 0.6 E-03

D.06 – Nitrate ($NO3^-$) distribution in both aquifers.

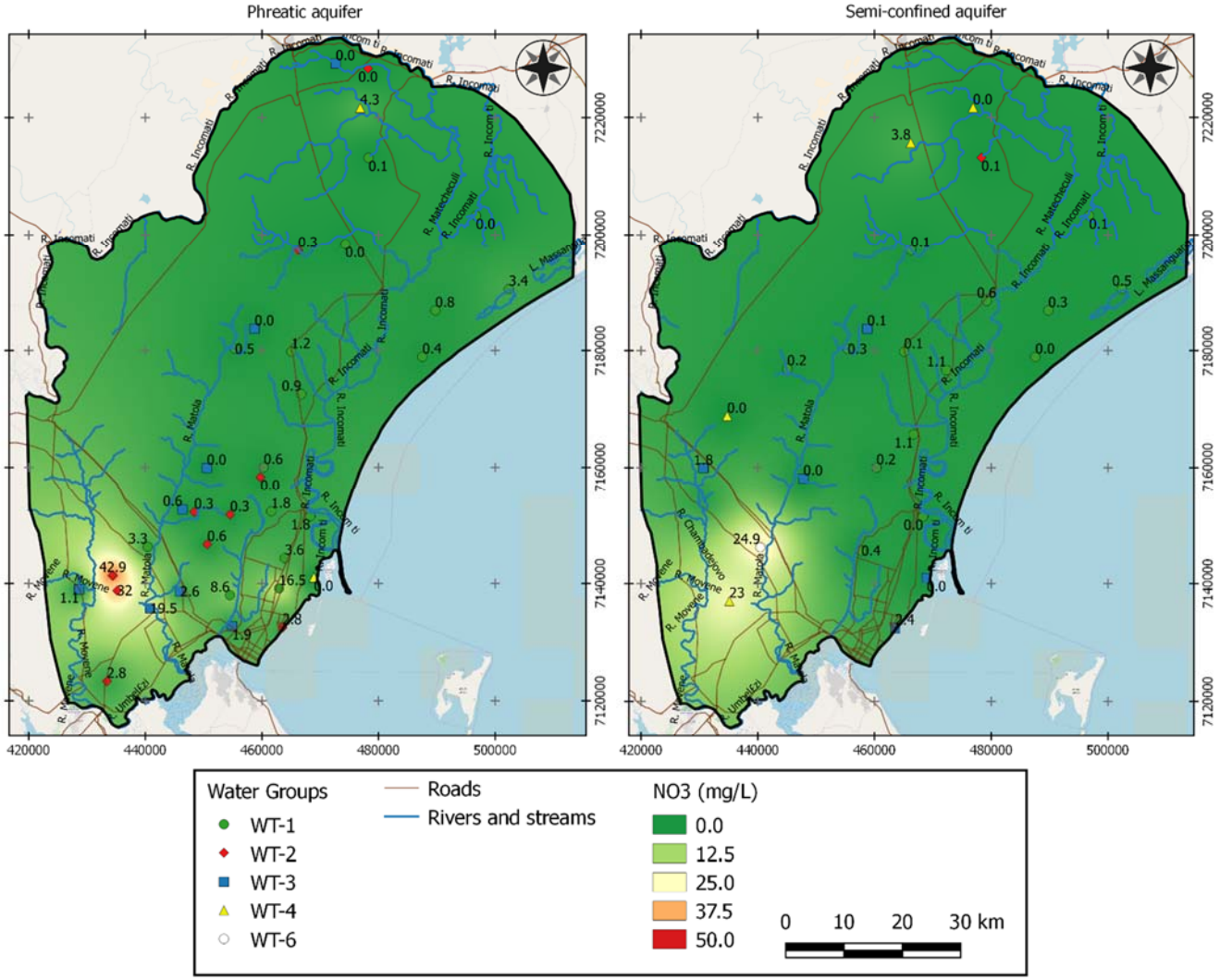

High values of NO_3^- concentrations are observed especially in peri-urban areas of Matola, probably linked to the poor sanitation system.. Although, general values are far below WHO limit for potable water (50 mg/L), which can be explained by thick unsaturated zone in the area allowing time enough for natural decay of NO_3^- (denitrification).

Appendix E **- Cross sections and related plots**

E.01 – Cross section 01 – "Lake - PZ02": Blue lines represent main direction of groundwater flow and hydrochemical evolution from recharge to discharge areas; green lines represent flow from PZ14F to PZ14C (from phreatic to semi-confined levels).

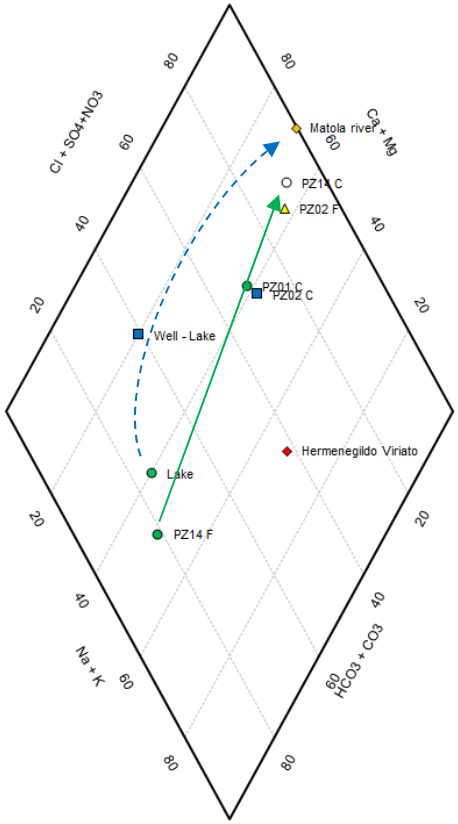

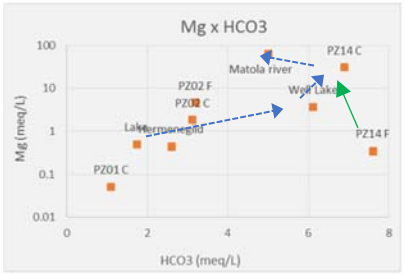

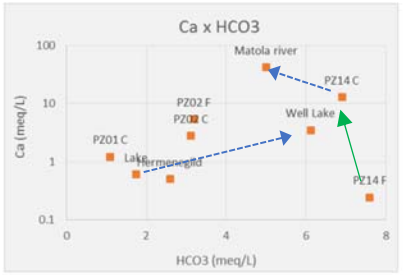

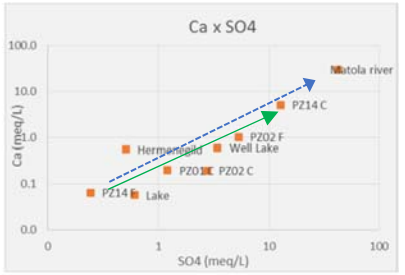

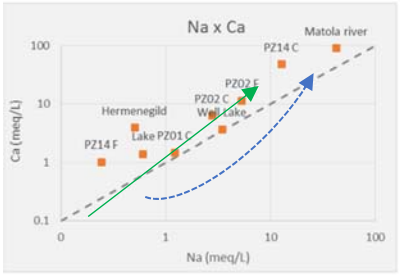

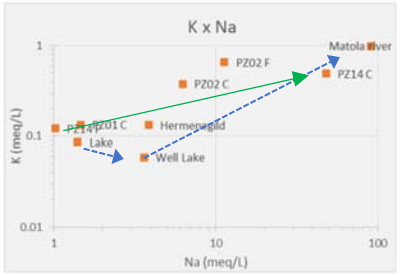

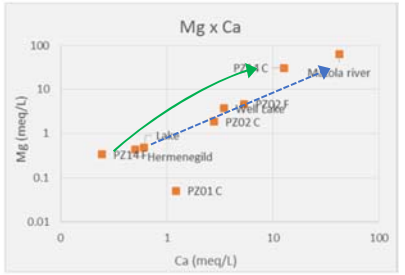

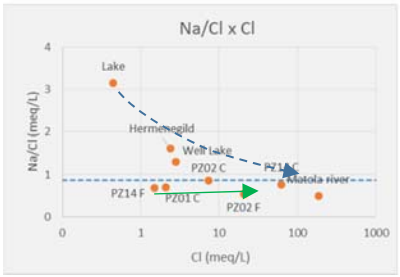

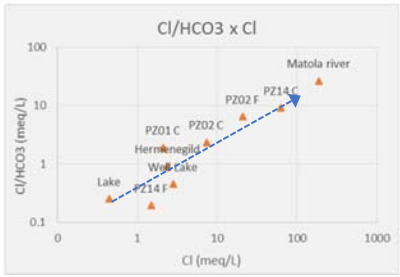

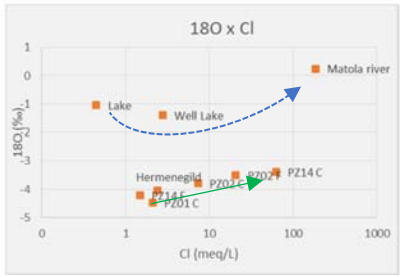

E.02 – Cross section 02 – "Aguiar 2 – PZ19": Blue dashed lines represent main directions of groundwater flow and hydrochemical evolution from recharge to discharge areas; green lines represent flow from PZ17F to PZ17C (from phreatic to semi-confined levels).